Methodologies for Seismic Assessment of Concrete Gravity Dam-Foundation Systems

Gurinderbir Singh Sooch

A Thesis

in

The Department

of

Building, Civil & Environmental Engineering

Presented in Partial Fulfillment of the Requirements
for the Degree of Master of Applied Science (Civil Engineering) at
Concordia University
Montreal, Quebec, Canada

December 2011

CONCORDIA UNIVERSITY
School of Graduate Studies

This is to certify that the thesis prepared

By: Gurinderbir Singh Sooch

Entitled: Methodologies for Seismic Assessment of Concrete Gravity Dam-Foundation Systems

and submitted in partial fulfillment of the requirements for the degree of

Master of Applied Science (Civil Engineering)

complies with the regulations of the University and meets the accepted standards with respect to originality and quality.

Signed by the final examining committee:

Dr. O. Pekau Chair

Dr. R. Sedaghati Examiner

Dr. L. Tirca Examiner

Dr. A. Bagchi Supervisor

Approved by _____
Chair of Department or Graduate Program Director

_____
Dean of Faculty

Date December 19, 2011

ABSTRACT

Seismic performance evaluation of Concrete Gravity Dams

Gurinderbir Singh Sooch

The number and size of hydroelectric dams have increased greatly across the Canadian landscape since 1910. The concrete gravity dams should perform satisfactorily during a seismic event as in case of failure, the release of impounded reservoir water can cause catastrophic damage in the downstream communities. Traditionally the foundation in a dam is modeled by a sub-structuring approach for the purpose of seismic performance analysis. The main disadvantage of sub-structuring approach is that it cannot be used for solving nonlinear dynamic problems. Therefore, in that case seismic response analysis must be carried out in time domain as it allows inclusion of nonlinear behavior in a system. In this study, different earthquake input mechanisms has been studied considering the following models A) massless foundation , B) free-field earthquake input at dam foundation interface and C) deconvolved earthquake input model. Deconvolution is a mathematical process which allows the adjustment of the amplitude and frequency contents of an earthquake ground motion applied at the base of the foundation to achieve the desired output at the dam-foundation interface. It has been observed that the existing procedures of deconvolution are inadequate for the high frequency earthquake records. A Modified deconvolution procedure has been proposed here for efficient deconvolution of high frequency earthquake records. The above discussed input mechanisms are studied in more detail with two different geometrical models. It has been found that model C is the most rational and accurate one compared to the other models.

In the second part of this study elastic and inelastic analysis of dams with different geometries has been performed to study the existing guidelines for the seismic assessment of dams. The performance of the dam models has been assessed using both the high frequency and low frequency earthquake records scaled at 0.35g. Based on the study it can be concluded that the different numerical models induce slight differences in the results relating to the tensile damage in dam foundation system. However, the results are consistent with each other. Also, the results from the linear elastic analysis provided valuable insight about seismic performance of concrete gravity dams but they fail to account for the existing deterioration in the dam.

ACKNOWLEDGMENTS

I am very deeply grateful to Dr. Ashutosh Bagchi for the guidance, support, patience and instruction throughout my dissertation.

I would also like to thank Dr. L. Tirca , Dr. A. Zsaki, Dr. Kinh H. Ha and Dr. Oscar A. Pekau from Concordia University for their valuable advice during the course of my master's.

Finally I am deeply grateful of my family and friends. Their support and motivation helped me to finish my master's.

To My Parents

Nirmal Singh and Tajinder Kaur

TABLE OF CONTENTS

LIST OF FIGURES

LIST OF TABLES

LIST OF EQUATIONS

CHAPTER 1 INTRODUCTION

1.1 Overview

According to the Canadian Dam Association (CDA, 2003) there are around 933 dams in Canada. Till now very few dams around the world have been shaken by strong earthquakes (USSD, 2000). Concrete gravity dams have shown satisfactory performance during the earthquake. However, Shih-Kang Dam in Taiwan suffered the complete loss of reservoir during Chi-Chi earthquake in September 1999 (JSCE, 1999). Hsifengkiang dam in China and Koyna dam in India also suffered considerable damage in 1962 and 1967 earthquakes, respectively (Bolt et al., 1974), (Hall, 1988). Therefore it is necessary that the evaluation of the gravity dam should be performed realistically by incorporating the effects of the interaction among dam, foundation and reservoir. In many earlier studies (e.g., Chakrabarti and Chopra, 1974; Fenves and Chopra, 1985) dam-foundation interaction effect have been modeled using a sub-structuring approach. However, this approach is insufficient for modeling the nonlinear and non-homogenous geometrical and material properties of the foundation. Therefore, analysis must be carried out in time domain using finite element analysis to account for non-homogeneous soil properties and non-linearity in the governing equations.

Many studies have been carried out in past to understand the earthquake input mechanism for time domain analysis. The following four models are generally considered to simulate the different earthquake input mechanism: rigid base model, massless foundation model, free field acceleration input model, deconvolved earthquake records (Figure 3.1). It is found that the rigid base model produces unnecessary amplification in

the model. Therefore for all practical purposes the rigid-base model may not be useful (Leger and Boughoufalah, 1989).

The massless foundation input model however, recommended by various researchers and also employed by in current design practices, is also not an efficient input model. Dam-foundation interaction is absent in this model as the foundation in considered massless. Tan and Chopra (1995), and Chopra (2008) reported that by employing the massless foundation, the stresses in a dam may be overestimated by a factor of two or three.

In the case of the free-field foundation input model, the acceleration history is directly applied at the interface of the dam and foundation. However, this model ignores spatial variation of ground motions. This may lead to significant error in the level of stresses and their location in the estimated response (Chopra and Wang, 2010).

In the case of the deconvolved ground motion input model, the analysis is conducted in the following two steps: first, a deconvolution analysis is performed to generate the foundation-base level ground motion which is compatible to the free-field ground motion, and then the response of the dam-foundation system is determined by the time-history analysis. Deconvolution is a mathematical process which allows the adjustment of the amplitude and frequency contents of an earthquake ground motion to achieve the desired output. A computer program namely, SHAKE developed by Schnabel et al.(1972) for deconvolution has been used in previous studies (Leger and Boughoufalah, 1989; Luk et al., 2005; and Polam et al., 2007). However, the deconvolution process using SHAKE computer program is quite cumbersome as the

response obtained using this program is very sensitive to the values of the parameters such as, the shear modulus, and the equivalent viscous damping ratio in case of flexible foundations (Boughoufalah, 1988).

Satisfactory performance of concrete gravity dams during a seismic event is necessary because the release of the impounded water can cause considerable amount of devastation in the downstream populated areas. The importance of structural reassessment of existing dams has been well recognized. There are existing guidelines developed by several dam managing and owner agencies, dam associations, federal authorities in several countries for seismic evaluation of concrete gravity dams (e.g., (CDA, 2007), (FERC, 2002), (FERC, 1999) , (USACE, 2007), (FEMA-65, 2005), (BRE, 1991)). Generally the existing guidelines recommend the linear elastic analysis for the seismic response evaluation of dams under moderate level seismic hazard and when there is only a limited damage under the maximum credible earthquake without the release of impounded water. As the inelastic analysis is time consuming and computationally expensive such analysis is recommended only in case of severe damage under a strong earthquake. The performance indicators used for the evaluation in case of linear elastic analysis are percentage of area overstressed as compared to the capacity, the cumulative inelastic duration of stresses beyond the capacity of concrete and the sliding safety factor (USACE, 2007).

The evaluation procedure suggested in (Ghanaat, 2004), (USACE, 2003), (USACE, 2007) does not rely on the stress checks alone. The performance evaluation is based on the displacement time histories, spatial variation of stresses, stress demand to capacity ratios, and the accumulated duration of overstress excursions. If the results

obtained are within the specified limits, there is no need to perform nonlinear analysis; otherwise, the nonlinear analysis would be recommended.

Understanding of the behavior of cracked dams during a seismic event is essential for implementation of various rehabilitation schemes. Earlier researchers have used linear elastic analysis (Chakrabarti, 1974a; and Chopra and Gupta, 1982), smeared crack model (Bhattacharjee, 1993), discrete crack approach based on elastic fracture mechanics (Ayari and Saouma, 1990) and boundary elements model (Pekau et al. , 1995; Batta et al., 1996). In the present study, the analysis has been performed using a commercial finite element software ABAQUS (Version 6.11). The tensile damage in concrete have been simulated using concrete damage plasticity model as proposed by Lubliner et al. (1989) and Lee and Fenves (1998), and extended finite element methods as proposed by Belytschko and Black (1999) with cohesive damage material model.

1.2 Objectives

The objectives of this thesis are the followings

1. To develop an appropriate input mechanism for ground motion applied to dam foundation systems.
2. Study the existing guidelines on seismic evaluation of concrete gravity dams.

1.3 Organization of thesis

This thesis is organized in five chapters. The first chapter provides an introduction to the subject. Chapter 2 presents the literature review relevant to the objective of thesis.

Chapters 3 and 4 are composed in manuscript format intended for submission to peer reviewed journals. As these chapters are self contained, there is some repetition of

texts in the introductory sections. However, the references are merged to a single list of references provided at the end of the thesis.

Chapter 3 focuses on the different earthquake input models for the analysis in time domain. Also, the proposed modified deconvolution procedure has been presented in this chapter along with the evaluation of different earthquake input models.

Chapter 4 presents the elastic and inelastic analysis of dams with different numerical models. Various analyses have been performed to study the existing guidelines for the seismic assessment of dams.

Finally, Chapter 5 presents the summary of this study and provides general conclusions along with the work for further studies.

CHAPTER 2 LITERATURE REVIEW

2.1 Introduction

A large volume of literature exists in areas of dam engineering including the studies related to structural performance, seismic performance evaluation, and safety assessment. Only a summary of relevant literature in the following areas has been provided here in the context of the present thesis.

1. Response of dams during earthquakes
2. Seismic wave scattering in dam-foundation-reservoir systems
3. Guidelines for evaluating the seismic safety of existing dams
4. Nonlinear dynamic analysis of dams

2.2 Response of dams during earthquakes

The number and size of hydroelectric dams have increased greatly across the Canadian landscape since 1910. Despite the benefits, dams are innately hazardous structures and failure or miss-operation can result in devastation of the downstream areas. Concrete gravity dams have shown satisfactory performance during earthquake, while only very few dams around the world have been shaken by strong earthquakes (USSD, 2000). Shih-Kang Dam, Taiwan was struck by M_w 7.6 Chi-Chi Earthquake in September 1999. The dam experienced a PGA (Peak Ground Acceleration) of 0.5*g*, where *g* is the acceleration due to gravity, and was located 50 km away from the epicenter. A large portion of the dam was moved due the foundation offset during the earthquake measuring around 10 m vertically and 2 m horizontally. During the same event, Suei-Sheh dam and Chi Chi Weir exhibited minor damage (JSCE, 1999).

The 105 m high concrete buttress Hsinfengkiang dam, China experienced an earthquake of magnitude M_w 6.1 in March, 1962. Formations of cracks in dam were reported. At the top of dam, 108 m long crack was formed which linked both the downstream and upstream faces (Bolt et al., 1974; Hall, 1988).

The Pacoima Dam, a 113 m high arch dam in California was built in 1928 in a narrow canyon. The arch dam was shaken twice by earthquakes, first by the M_w 6.6 San Fernando earthquake on February 9, 1971, and later by the M_w 6.7 Northridge earthquake on January 17, 1994. In both the earthquakes, the damage was localized at the contraction joint at the left thrust block (Hall, 1988; Mojtahedi and Fenves, 2000).

The 103 m high gravity dam, Koyna Dam located in India, experienced probably a reservoir induced earthquake of magnitude M_w 6.5 on December 11, 1967. Significant damage was observed to Koyna dam in the form of cracks on both upstream and downstream faces of a number of non-overflow monoliths. Some cracks were also observed in the lower elevations inside the operation and foundation galleries (Hall, 1988).

2.3 Seismic wave scattering in dam-foundation-reservoir systems

To realistically evaluate the response of gravity dam subjected to a seismic event, it is important to incorporate the effects of interaction among dam, foundation and reservoir in the analysis. Chakrabarti and Chopra (1974) and Fenves and Chopra (1985) studied the dam-foundation interaction effect in the frequency domain using visco-elastic half space solutions to model the foundation and quantified effects of various parameters on linear elastic dam. The half-space assumption for modeling the foundation permits

only an approximate modeling for a dam site with similar geological conditions to a great depth. Considering the ground reality at the dam sites, the analytical models based on frequency domain analysis are insufficient as the foundation model is simply represented only by foundation stiffness matrix (foundation impedance) and a loading function in the form of kinematic motion that cannot be used to model nonlinear and non-homogenous geometrical and material foundation properties. Therefore, the analysis must be carried out in the time domain using the finite element analysis to account for non-homogeneous soil properties and non-linearity in the governing equations.

To understand the earthquake input mechanism many studies have been carried out in the past. Clough et al. (1985), and Leger and Boughoufalah (1989) studied various models to simulate different earthquake input mechanisms. These models include rigid base, massless foundation, deconvolved earthquake records, and free field input. In the case of the rigid base model, the free-field acceleration time history was applied at the base of the foundation. The Model showed considerable amount of amplification in the response quantities of interest as the finite foundation model without transmitting boundaries acted as a box in which the applied the earthquake time history at the base amplified because of the reflection of the seismic waves at the boundaries of the model.

The massless model is among the most commonly used one in the current practice. In this case, only the flexibility of the foundation is considered and foundation-dam interaction is ignored. The seismic wave scattering is also absent in this model, and thus it eliminates the artificial dynamic amplification of the base free-field earthquake ground motion (Clough, 1980). However, Tan and Chopra (1995), and Chopra (2008) reported that by employing the massless foundation, the stresses in a dam may be

overestimated by a factor of two or three. This overestimation of stresses can result from the fact that the radiation damping and foundation material are completely ignored in this model. Radiation damping accounts for the spatial dissipation of energy in a soil medium. In other words, the soil near the base of a structure tends have cyclic movement that causes the energy to be radiated away from the structure (Booth and Key, 2006). This effect cannot be considered as an inherent material property of the foundation.

In case of deconvolved earthquake records (Reimer, 1973), a deconvolution analysis is carried out to determine the base acceleration for a specified free field acceleration history at the base of a dam. Deconvolution is a mathematical process which allows the adjustment of the amplitude and frequency content of an earthquake ground motion applied at the foundation-base to achieve the desired output at the free ground surface at the dam-base. Another alternative is to use the free-field input directly at the foundation dam interface. In that case, the spatial variation of ground motion along the base of the dam is ignored (Clough and Chopra, 1977; Chuhan et al., 1995). However, ignoring the spatial variation of ground motion could have significant impact on the stresses in the dam (Chopra and Wang, 2010). However, the influence would differ for different earthquakes depending on the location of the source with respect to the dam site.

Lysmer (1969) developed the non-reflecting transmitting boundaries. Cohen (1980), and Wolf (1986) further worked on validating the effectiveness of these non-reflecting boundaries (i.e., artificial boundaries) which are also commonly used to represent to the unbounded extent of the foundation in the finite sized foundation rock. The seismic waves are not allowed to be reflected or refracted at the boundaries but they

can propagate through them towards infinity. However, absorption of the seismic waves is not modeled correctly for all incident angles.

2.4 Guidelines for evaluating the seismic safety of existing dams

Seismic safety of existing dams is currently assessed based on the guidelines developed by Several dam managing and owner agencies, dam associations, and government agencies in several countries have developed guidelines for seismic evaluation of concrete gravity dams (e.g., (CDA, 2007), (FERC, 2002), (FERC, 1999) , (USACE, 2007), (FEMA-65, 2005), (BRE, 1991)). In the case of a moderate level of seismic hazard and when there is only a limited damage under the maximum credible earthquake without the release of impounded water, the existing guidelines recommend the linear elastic analysis for the seismic response evaluation of dams. As the inelastic analysis is time consuming and computationally expensive such analysis is recommended only in the case of severe damage under a strong earthquake. The performance indicators used for the evaluation of a dam are percentage of area overstressed as compared to the capacity, the cumulative inelastic duration of stresses beyond the capacity of concrete, and the sliding safety factor (USACE, 2007).

The methodology recommended by Ghrib et al. (1995) suggested a progressive analysis methodology for evaluating the seismic safety of concrete gravity dams which involves five analysis levels comprising preliminary screening, pseudo-static, pseudo-dynamic, linear time history and nonlinear history with increasing complexity.

The evaluation procedure provided in Ghanaat (2004), USACE (2003), and USACE, (2007) does not rely on examining the stress distribution alone. In this case, the

performance evaluation is based on the displacement time histories, the spatial variation of stresses, the demand capacity ratios for stresses, and the accumulated duration of overstress excursions. Figure 2.2 illustrates the accumulated duration of overstress excursions. Figure 2.3 and Figure 2.4 illustrate the performance threshold curves for arch dams and concrete gravity dams. In case the performance indicators cross the threshold values as shown in Figure 2.3 and Figure 2.4, nonlinear analysis is required to further investigate the performance of the dam. The maximum design earthquake (MDE) is used to formulate the performance. The following three performance levels are considered in this case:

a) Minor or no Damage: The response of dam is assumed to be elastic if the Demand Capacity Ratio (DCR) ≤ 1. The dam is considered to behave in the elastic range with no possibility of damage.

b) Acceptable Level of Damage: If the DCR ≥ 1 the cracking in a dam can be considered with no possibility of failure; if the estimated DCR < 2, the overstressed regions are limited to 15 percent of cross sectional area of dam, and the cumulative duration of stress excursion also fall below the performance line as shown in Figure 2.3 and Figure 2.4.

c) Severe Damage: If the DCR >2 for a region more than 15 percent of cross section area of dam and the cumulative overstress duration for all DCR values between 1 and 2 are above the performance curves as shown in Figure 2.3 and Figure 2.4, the damage is considered as severe. It is recommended that the

nonlinear time history analysis be performed to further assess the condition of the dam.

2.5 Nonlinear dynamic analysis of dams

Understanding of the behavior of a cracked dam during a seismic event is essential for the implementation of various rehabilitation schemes. Earlier, researchers have used linear elastic analysis (Chakrabarti, 1974a; Chopra and Gupta, 1982), smeared crack model (Bhattacharjee, 1993), discrete crack approach based on elastic fracture mechanics (Ayari and Saouma, 1990), and boundary elements model (Pekau et al., 1995; Batta et al., 1996). In this study, the analysis is performed using a commercial finite element software ABAQUS (Version 6.11). The tensile damage in concrete have been simulated using concrete damaged plasticity model proposed by Lubliner et al. (1989) and Lee and Fenves (1998), and extended finite element methods proposed by Belytschko et al. (1999) with cohesive damage material model.

2.6 Summary

From the literature review it has been found that there is a need to develop appropriate input mechanism for ground motions applied to dam foundation systems. Also there is a need to develop a modified procedure for deconvolution of free-field ground motions as the existing deconvolution process as implemented in relevant computer programs such as, SHAKE (Schnabel et al., 1972) is quite cumbersome, and computationally inefficient. Also, there is a need to study the existing guidelines on seismic evaluation of concrete gravity dams with elastic and inelastic analysis to evaluate the response of dam under different type of earthquakes and with different numerical models in order to assess the sensitivity to different types of ground motions and modeling techniques (e.g., elastic and

inelastic models) to the response of dam-foundation systems, Some of these issues are addressed here to achieve the objectives of the present thesis.

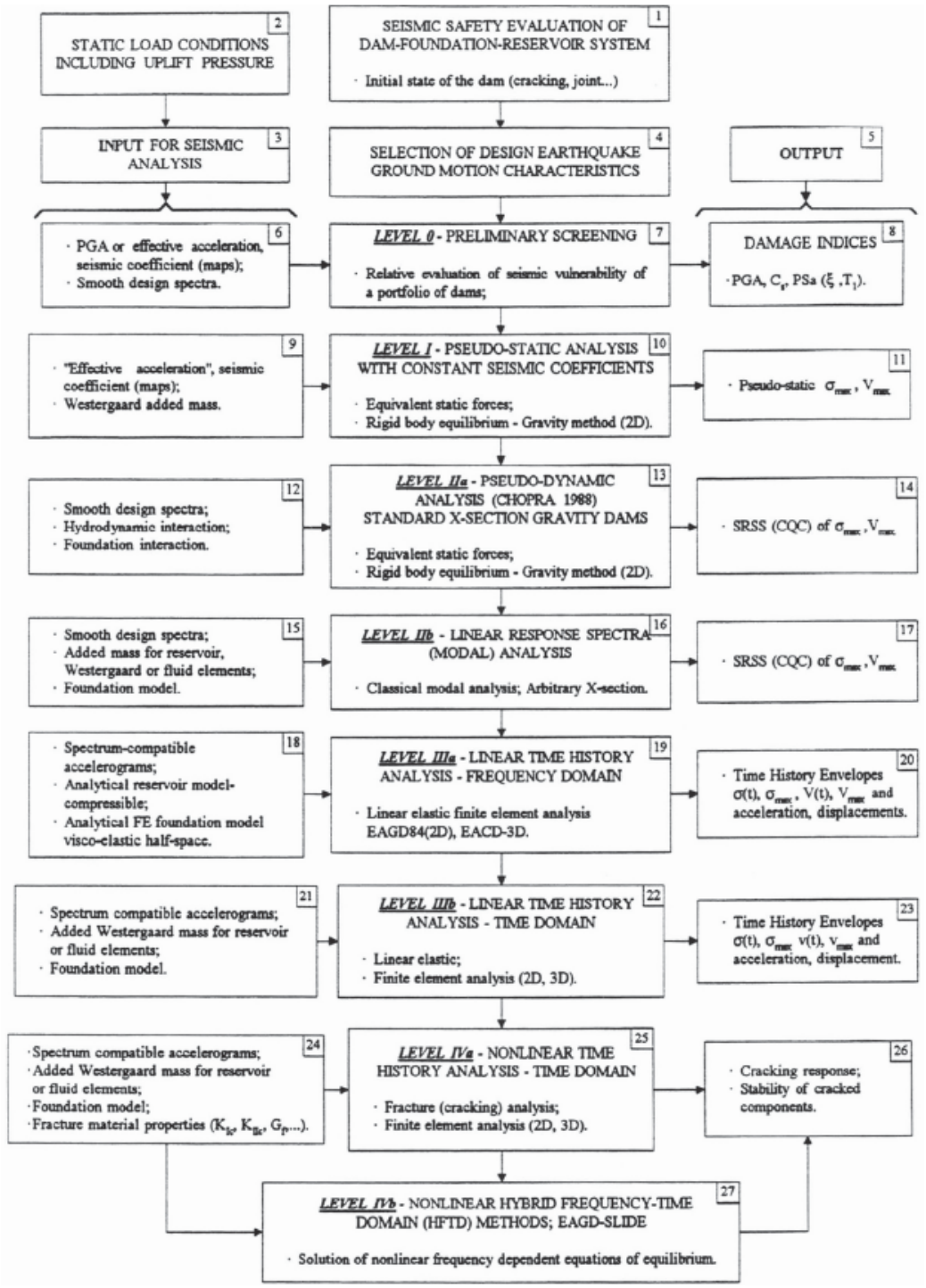

Figure 2.1 A progressive methodology for seismic safety evaluation of dams (Ghrib, 1995)

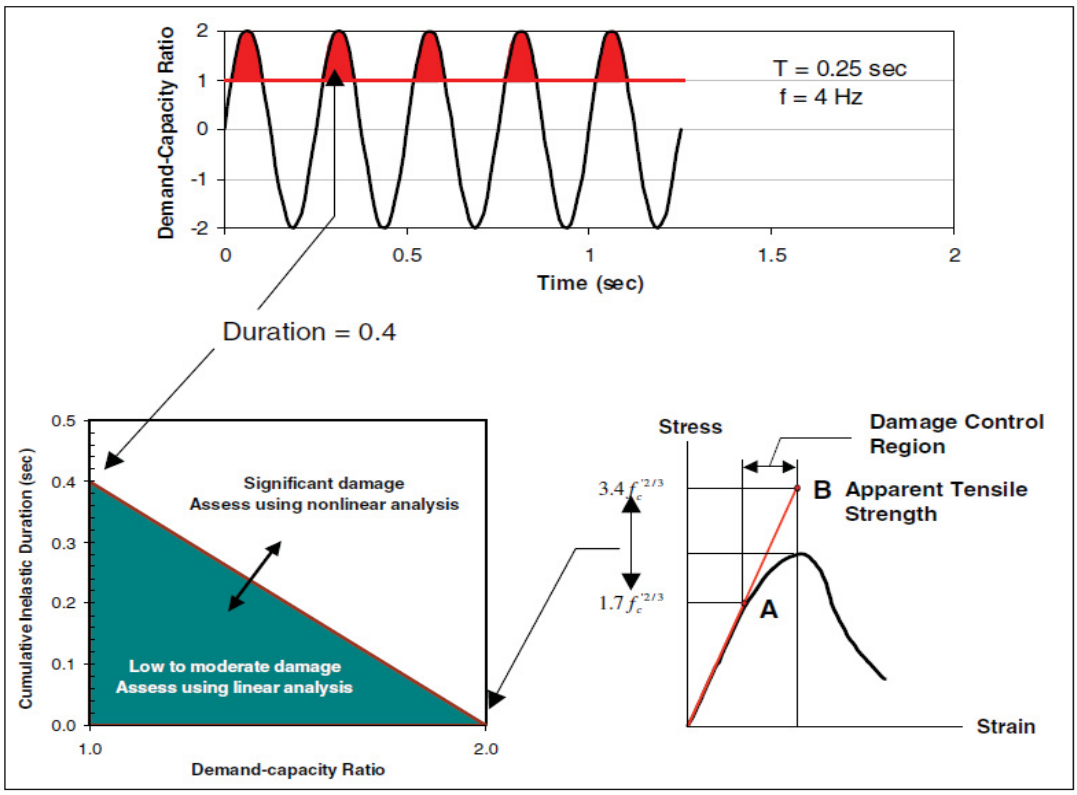

Figure 2.2 Seismic Performance and damage criteria (Ghanaat, 2004)

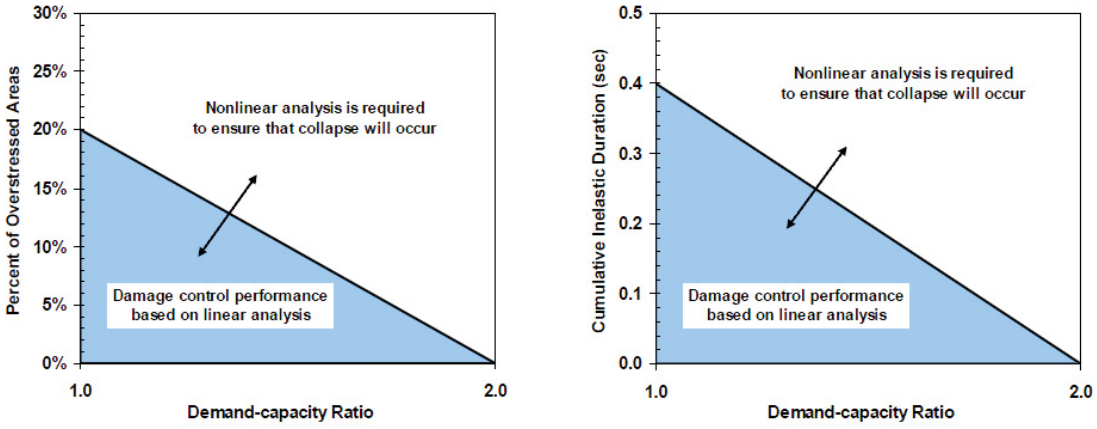

Figure 2.3 Seismic Performance threshold curves for arch dams (Ghanaat, 2004)

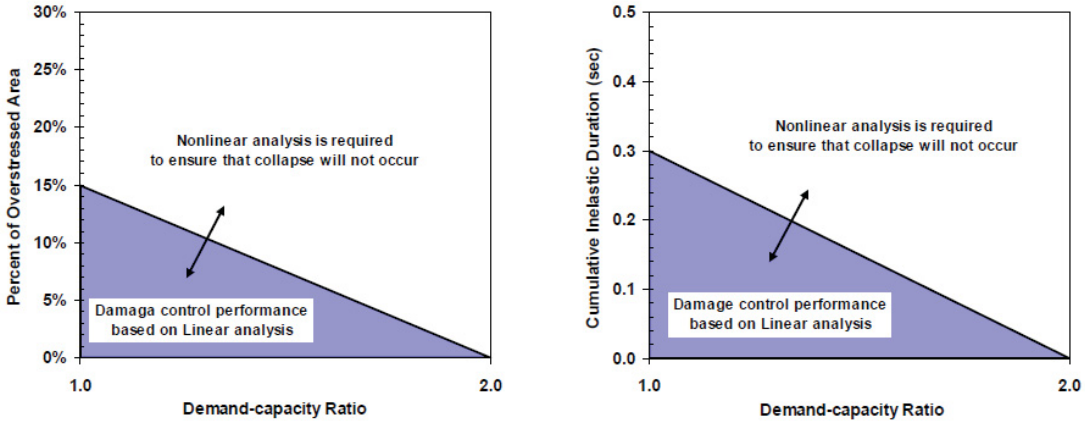

Figure 2.4 Seismic Performance threshold curves for gravity dams (Ghanaat, 2004)

CHAPTER 3 SEISMIC WAVE SCATERING IN DAM-FOUNDATION SYSTEM

3.1 Abstract

The number and size of hydroelectric dams have increased greatly across the Canadian landscape since 1910. The concrete gravity dams should perform satisfactorily during a seismic event as in case of failure, the release of impounded reservoir water can cause catastrophic damage in the downstream communities. Traditionally the foundation in a dam is modeled by a sub-structuring approach for the purpose of seismic performance analysis. The main disadvantage of sub-structuring approach is that it cannot be used for solving nonlinear dynamic problems. Therefore, in that case seismic response analysis must be carried out in time domain as it allows inclusion of nonlinear behavior in a system. In this study, different earthquake input mechanisms has been studied considering the following models A) massless foundation , B) free-field earthquake input at dam foundation interface and C) deconvolved earthquake input model. Deconvolution is a mathematical process which allows the adjustment of the amplitude and frequency contents of an earthquake ground motion applied at the base of the foundation to achieve the desired output at the dam-foundation interface. It has been observed that the existing procedures of deconvolution are inadequate for the high frequency earthquake records. A Modified deconvolution procedure has been proposed here for efficient deconvolution of high frequency earthquake records. The above discussed input mechanisms are studied in more detail with two different geometrical models. It has been found that model C is the most rational and accurate one compared to the other models.

3.2 Introduction

The number and size of hydroelectric dams have increase greatly across the Canada since 1910 (CDA, 2007). Concrete gravity dams have shown satisfactory performance during the earthquake, there are a few dams around the world that have been shaken by strong earthquake (USSD, 2000). Shih-Kang Dam suffered complete loss of reservoir during Chi-Chi earthquake in September 1999 (JSCE, 1999). Hsifengkiang dam in China and Koyna dam in India, respectively also suffered considerable damage in 1962 and 1967 earthquakes, respectively (Bolt and Cloud, 1974), (Hall, 1988). Therefore, it is necessary that the evaluation of the gravity dams should be done realistically by incorporating the effects of interaction among dam, foundation and reservoir. Chakrabarti and Chopra (1974), and Fenves and Chopra (1985) studied the dam-foundation interaction effect in the frequency domain using visco-elastic half space solutions to model the foundation. Considering the ground reality at the dam sites, the analytical models based on frequency domain analysis are insufficient as the foundation model cannot be used to model nonlinear and non-homogenous geometrical and material foundation properties. Therefore, analysis must be carried out in time domain using finite element analysis to account for non-homogeneous soil properties and non-linearity in the governing equations.

To understand the earthquake input mechanism for time domain analysis many studies have been carried out in the past. Clough et al. (1985), and Leger and Boughoufalah (1989) studied a set of four models to simulate different earthquake input mechanisms. These models used in those studies include rigid base, massless foundation, deconvolved earthquake records, and free field input. In case of free-field input model,

the free field acceleration is applied directly at the foundation dam interface. In that case, the spatial variation of ground motion along the base of the dam is ignored (Clough and Chopra, 1977), (Chuhan et al., 1995). Alves (2004) investigated the Pacoima Dam response for the spatial variation in ground motion where the foundation was considered massless and water incompressible. Chopra and Wang (2010) investigated Mauvoisin dam and Pacoima Dam for spatial variation in ground motion. It was concluded that the spatial variation could have significant effect on the stresses in the dam induced during an earthquake. However, the influence would differ for different earthquakes depending on the location of the source with respect to the dam site.

In case of deconvolved input model (Reimer, 1973), a deconvolution analysis is carried out to determine the base acceleration for a specified free field acceleration history at the base of a dam. Deconvolution is a mathematical process which allows the adjustment of the amplitude and frequency content of an earthquake ground motion to achieve the desired output. Computer program SHAKE developed by Schnabel et al.(1972) for deconvolution has been used in previous studies (Leger and Boughoufalah, 1989), (Luk et al., 2005), (Polam et al., 2007). However, the deconvolution process using the procedure used in SHAKE computer program is very cumbersome as the response obtained through this program is very sensitive to the values of the controlling parameters such as the shears modulus, and the equivalent viscous damping ratio in case of flexible foundations (Boughoufalah, 1988).

Non-reflecting boundaries (i.e., artificial boundaries) as developd by Lysmer (1969) are also commonly used to represent to the unbounded extent of the foundation in the finite sized foundation rock. In the numerical model the artificial boundaries do not

allow the seismic waves to be reflected or refracted at the boundaries but in turn they mimic a behavior in which the seismic waves are allowed to propagate through them towards infinity. However, in that case, absorption of waves is not modeled correctly for the overall domain and for various incident angles in a given model. Furthermore, non-reflecting boundaries allow the foundation to bend, and thus it fails to represent the concept of one dimensional foundation column that is consistent with the mode of shear waves propagation. To overcome the limitation in the existing procedure as adopted in SHAKE (Schnabel et al., 1972) and enforce the one dimensional shear column mode for the foundation. Luk et al. (2005) and Polam et al. (2007) performed a series of analysis with different constraint models to represent foundation models, which are found to yield encouraging results. In the present study a similar approach has been undertaken and implemented using a commercial software ABAQUS (Abaqus Inc, 2011).

The purpose of this paper is to propose a modification in the existing procedure in the deconvolution procedure to improve its efficiency for deconvolution of high frequency ground motions. Numerical study has also been performed with dam models with two different geometries and a set of different earthquake free field acceleration time histories to evaluate various earthquake input mechanisms.

3.3 Seismic wave scattering in dam foundation system

To evaluate the response of a dam during a seismic event, it is necessary that the numerical model should represent the physical model as closely as possible. Therefore, the foundation should also be included in the finite element model of a dam. The earthquake acceleration is applied at the base of the foundation and it propagates vertically by an elastic wave propagation mechanism until it reaches the top of the

foundation. The size of foundation in the numerical model is finite compared to the semi-infinite foundation in the physical model. The seismic waves are reflected from the boundaries of the numerical model. This seismic wave scattering due to artificial boundaries in the numerical model results in altering the frequency content of the input seismic and amplitude ground motion as the wave propagates through the deformable foundation rock. A numerical model to evaluate the seismic performance must account for such wave scattering effect to obtain a reliable response.

3.3.1 *Massless foundation input model, Model A*

The foundation is considered massless in this model as shown in Figure 3.1. Therefore, only the flexibility of the foundation is considered and the dam-foundation interaction is ignored. In the absence of dam-foundation interaction, no dynamic amplification and alteration in the acceleration history will be observed at the top of the foundation if the free field acceleration history is applied at the base of the foundation. Since the foundation mass density is zero, the input motion propagates instantaneously through the foundation. However it is important to note that since the foundation mass is not included here, the system's vibration modes may be affected. The change in the system frequencies can alter the response of a dam. Also, this model does not capture the dam-foundation interaction effects.

3.3.2 *Free field earthquake input model at dam foundation interface model, Model B*

In this model the free field ground acceleration history is applied at the interface of dam and foundation (Figure 3.1). The spatial variation of ground motion along the base of the dam is ignored. Therefore, it is assumed that the input motion along the base of the dam remains unaltered in amplitude and phase. In other words earthquake motions are not

affected by the presence of the dam or by the local topology. The effect of this assumption will differ for different earthquakes depending on the location of the source with respect to the dam site and local topology of the dam site. Chopra and Wang (2010) conducted a study to show that the spatial variation can have significant effect on the stresses and the distribution patterns of stresses induced in the dam during a seismic event. However, if the non- uniform ground motions along the dam-foundations interface are available for a particular dam, or derived through mathematical modeling or experimental testing, the results produced through free field acceleration histories will yield accurate results (Alves, 2004). As in most cases when the non-uniform ground motions records along the dam-foundation interface are not available, Model C should be preferred.

3.3.3 ***Deconvolved earthquake input model, Model C***

In this method, the analysis is carried out in two steps. First a deconvolution analysis is performed to determine the acceleration time history that can be applied to the base of the foundation to reproduce the specified free field acceleration time history at the base of a dam (Figure 3.1). The calibrated base acceleration history is then applied to the base of the foundation to perform the seismic analysis. Deconvolution analysis can be performed using a mathematical process as described in Figure 3.2 (Reimer, 1973) which is explained below.

Deconvolution analysis allows the adjustment of the amplitude and frequency content of an earthquake ground motion applied at the base of the foundation to achieve the desired output ground acceleration at the dam-foundation interface. A step-by-step iterative procedure for deconvolution is shown in Figure 3.2. Initially, the ground

acceleration applied at the base of the foundation is assumed to be the same as the specified one i.e. the original free filed ground acceleration time history at the dam-foundation interface. The acceleration time history at the top surface (i.e., dam-foundation interface) is the estimated by solving the wave propagation problem of the dam-foundation system using the finite element analyses techniques. This estimated or reproduced ground acceleration at the dam-foundation interface is then compared to the original free field ground acceleration after transforming both the signals into the frequency domain using Fourier analysis. The Fourier transform a pair for continuous signals can be written as show in Equation 3.1 and 3.2.

$$X(f) = \int_{-\infty}^{\infty} x(t) e^{-i2\pi ft} dt \qquad \text{Equation 3.1}$$

$$x(t) = \int_{-\infty}^{\infty} X(f) e^{i2\pi ft} df \qquad \text{Equation 3.2}$$

where, the lowercase x(t) represents the time-domain function, the uppercase X(f) represents the frequency-domain function and $i = \sqrt{-1}$. The response of the system is expressed as an integration of the superimposed responses can written in Equation 3.3.

$$u(t) = \int_{-\infty}^{\infty} [A(f)X(f)] e^{i2\pi ft} df \qquad \text{Equation 3.3}$$

where A(f) is the transfer function. Therefore, Equation 3.3 can be rewritten as

$$x(t) = \int_{-\infty}^{\infty} [A(f)^{-1} u(f)] e^{i2\pi ft} df \qquad \text{Equation 3.4}$$

where, U(f) is the Fourier transform of u(t). The numerical evaluation of Fourier integral is time consuming and difficult. Therefore, for numerical evaluation purposes, the Fourier

integral is evaluated using discrete transform. The analogous discrete Fourier transform (DFT) pair can be written as shown in Equation 3.5 and 3.6

$$X(j) = \frac{1}{N}\sum_{k=0}^{N-1} x(k)W_n^{-jk} \qquad \text{Equation 3.5}$$

$$x(k) = \sum_{k=0}^{N-1} X(j)W_N^{+jk} \qquad \text{Equation 3.6}$$

where, X(j) and x(k) are, in general, complex series and $W_n = e^{2\pi i/N}$. Numerical evaluation of Equation 3.5 and Equation 3.6 is performed by employing the fast Fourier transform (FFT) and inverse Fast Fourier transform (IFFT) algorithms developed by (Cooley & Tukey, 1965). FFT yields complex Fourier amplitude values for a set of discrete frequencies (Equation 3.5). The complex Fourier amplitudes are then converted into absolute values. IFFT of set of Fourier amplitudes for a set of discrete frequencies yields a time domain signal (Equation 3.6). A correction factor for each frequency is computed using the ratio of the amplitude of the target signal to that of the recorded acceleration history obtained by the deconvolution process in a given iterations. This correction factor is applied to the acceleration history applied at the base of the foundation in frequency domain. The modified acceleration history is then transformed back into time domain acceleration signal by employing IFFT and the analysis of the foundation system is carried with the modified time history of the ground acceleration applied at the base of the foundation. The procedure is repeated until the original ground motion at the base of the dam closely matches the reproduced ground motion record generated by using the modified ground motion applied at the base of the foundation. The

resulting ground motion at the foundation-base would be called the deconvolved ground motion that should be used in the analysis of the dam-foundation system.

The main advantage of this procedure is that the foundation dam interaction can be included in the analysis. Deconvolution is carried using a reference point or node at the top of the foundation. Therefore, the finite element model will automatically induce variation in the acceleration history along the interface nodes due to geometry of model and presence of the dam. Thus the results obtained from the deconvolution procedure are more realistic. However, the efficiency of the deconvolution analysis affects the quality of the results obtained.

3.3.4 *Modified Deconvolution procedure*

The existing procedure for deconvolution as discussed in Section 3.3.3 does not produce appropriate results for high frequency ground motion records. However, it works very well for the low frequency ground motion records. To overcome such limitation, a modified procedure has been proposed in this section. Figure 3.3 shows the detailed flow chart for the modified deconvolution procedure. Similar to the existing procedure, here the reproduced acceleration history at the top of foundation is compared to the original one, both converted to frequency domain using Fourier analysis. However the correction factors to adjust the deconvolved signal are determined differently. Instead of adjusting the Fourier amplitudes at different frequencies, the spectral density at different frequency are adjusted. The response spectra of the reproduced acceleration history and the input ground motion (i.e. original free field accelearion) are computed for the discrete set of frequencies obtained using FFT. The correction factors are calculated for each frequency

by the ratio of the target response spectrum amplitude TSa(j) and the response spectrum amplitude RSa(j) of reproduced acceleration history.

$$CF(j) = {}^{TSa(j)}\Big/_{RSa(j)} \qquad \text{Equation 3.7}$$

This correction factor is then applied to the acceleration history applied at the base of the foundation in frequency domain (both the real a(j), and the imaginary b(j) coefficients].

$$a(j)_{modified} = a(j) * CF(j) \qquad \text{Equation 3.8}$$

$$b(j)_{modified} = b(j) * CF(j) \qquad \text{Equation 3.9}$$

The modified acceleration history is then transformed back to a time domain acceleration history by performing IFFT using the modified coefficients [$a(j)_{modified}$ and $b(j)_{modified}$]. The analysis of the dam-foundation system is carried with the modified time history of ground acceleration applied at the base of the foundation. The procedure is iteratively repeated until the recorded ground motion at the base of the dam matches with the original free-field ground motion record. The response spectrum of the reproduced ground motion at the top of the foundation should match the target response spectrum by less than 10% difference at every frequency and by less than 5% difference at the range of frequencies close to fundamental frequency. To determine the closeness of the response spectrum of reproduced ground motion at the top surface with the original ground motion coefficient of determination (R^2) has been utilized.

$$S_t = \sum_i (y - \bar{y})^2 \qquad \text{Equation 3.10}$$

$$S_r = \sum_i (y - \bar{y}_r)^2 \qquad \text{Equation 3.11}$$

where, y is the amplitude of the response spectrum for original ground motion, $\bar{y}_r$ is the amplitude of the response spectrum for reproduced ground motion at the top of foundation, $\bar{y}$ is the mean, S_t and S_r are the total sum of squares and of residuals for the original and reproduced ground motions, respectively. The difference of S_t and S_r are normalized to obtain R^2.

$$R^2 = {(S_t - S_r)}/{S_t} \qquad \text{Equation 3.12}$$

A value of 1 for R^2 represents a perfect fit of the two data series which are represented here by the response spectra of the original and reproduced ground acceleration, respectively. The proposed modified deconvolution procedure is found to work very well for both high frequency ground motions and low frequency ground motions.

3.4 Finite element model and constraints

Two geometrically different monoliths of concrete gravity dams have been considered here to study the seismic wave scattering in dam foundation system. Figure 3.4 and Figure 3.5 show the geometry of both the models G-1 and G-2 respectively. Model G-1 represents a geometrical configuration which is commonly used for dams. However, Model G-2 has an irregular foundation. These kinds of irregular foundations are popular in large surface toe hydroelectric projects (Liang et al., 2011; Gupta et al., 2009) located on good quality foundation rock. In case of surface toe hydroelectric projects with this type of geometric configuration higher than usual machine head can be achieved with

less excavation. The assumed material properties are summarized in Table 3.1. Five percent material damping is considered in the analysis with Rayleigh damping assumptions. The hydrodynamic interaction is modeled by added mass model considering incompressible water.

The dam and foundation system is modeled using four noded bilinear plain strain finite elements. Figure 3.6 and Figure 3.7 represent the finite element mesh for dam-foundation system G-1 and G-2 respectively. To perform the deconvolution procedure, the soil must act as a one dimensional soil column. To simulate the one dimensional soil column behavior, a set of constraints needs to be applied on the boundaries Figure 3.8 and Figure 3.9 show the representation of constraints in the foundation. These constraints allow the shear deformations in foundation to simulate the propagation of waves but they do not allow the foundation to deform in bending mode. This includes constraining the boundaries nodes of two sides at same level to have the same displacement. In case the other side cannot be constrained in the same manner as in case of inclined slope, two adjustment nodes are constrained on the same side such that they act as shear column. If the dam is removed from the model all the nodes on the same layer will have same displacements. Foundation size should be sufficiently large to accommodate the local displacements near the dam. The size of the foundation is assumed three times the height of the dam or 3H, which is almost equal to 300 m on each side of the dam in this case which can be considered as sufficiently large size to accommodate the local displacements near the dam. The assumption the foundation size of 3H on each side of dam is based on the study by Bayraktar et al. (2009). During the meshing of the foundation the nodes along the boundaries of different layers are kept at the same level so

that no unnecessary stresses are induced due to different displacement induced by the non-aligned constriants. If the nodes along the boundaries of different layers are at different levels the constraints will try to impose the same displacement at these levels which may produce unnecessary stress along the boundaries Figure 3.10 and Figure 3.11 represent the finite element mesh for dam-foundation system G-1 and G-2 for Model B. The silent boundaries are modeled using infinite elements (Lysmer and Kuhlemeyer, 1969).

3.5 Selection of seismic ground motions

Two different ensembles of ground motions containing high frequency and low frequency ground motions have been considered here. The first ensemble of high frequency ground motion includes two simulated ground motions for the Montreal region which are: M6 recorded a 30 km and M7 at 70 km. In addition, the ensemble includes the San Fernando 1971 earthquake. These ground motion records are referred here as M #1, M #2 and M #3, respectively. The horizontal and vertical components of the ground motions are denoted here by H and V, respectively (Figure 3.12).The second ensemble of low frequency ground motions include Friuli 1976, Livermore 1980 and simulated ground motion for Victoria region which is M6.5 recorded at 30 km. These ground motion records are referred here as V #1, V #2 and V #3 respectively (Figure 3.13). All the selected ground motions correspond to rock site condition. The horizontal component of high frequency ground motions have been scaled accordingly for Montreal level of seismic hazard. The horizontal component of low frequency ground motions have been scaled accordingly for Vancouver level of seismic hazard. The vertical component of all ground motions were scaled to the two third of the respective horizontal components.

Figure 3.12 and Figure 3.13 show the scaled response spectra of the ground motions for each ensemble. The time periods of Model A for the dam-foundation systems for geometry G-1 and G-2 are 0.412 sec, 0.295 sec respectively, while that of Model B foundation system are 0.628 sec, 0.67 sec respectively. Figure 3.14 and Figure 3.15 show response spectra for M #3 and V #2, respectively.

3.6 Efficiency of Modified Deconvolution procedure

Figure 3.16 through Figure 3.21 presents the results of the different deconvolved free-field acceleration history by modified (MDP) and existing deconvolution procedures (EDP) for dam-foundation system, G-1. It can be concluded from the results that the MDP works very well for both high frequency and low frequency ground motion. However, EDP produces acceptable results only in the cases of V#1 and V #2. Figure 3.22 shows the values of the coefficient of Determination (R^2) for different iterations for MDP and EDP in the case of M #3 ground motion. The values R^2 values for the selected iterations for M #3(H) and M #3(V) for MDP are 0.984 and 0.898, respectively and for EDP they are 0.982 and 0.958, respectively. It can be observed that for MDP that R^2 approaches relatively more smoothly and converging well in both cases. However, the R^2 values for EDP fluctuate at different iterations and the convergence is poor in both cases. R^2 value of 0.984 can be simply interpreted as 98.4 % of variance between the original and reproduced ground motion.

Figure 3.23 and Figure 3.24 present R^2 values for ground motions V #2 and V #3 respectively. The values of R^2 for the selected iteration for V #2(H) and V #2(V) with MDP are 0.993 and 0.995, respectively and for EDP, they are 0.999 and 0.999, respectively. In the case of V #2 ground motion the results obtained for both MDP and

EDP are satisfactory. However, in case of V #3 ground motion the results obtained from EDP are not satisfactory. The values of R^2 for selected iterations for V #3(H) and V #3(V) with MDP are 0.958 and 0.889, respectively and for EDP, they are 0.966 and 0.822, respectively. Therefore, it can be concluded that the performance of EDP in the cases of low frequency ground motions is better than its performance in the cases of high frequency ground motions. However, the performance of EDP is not acceptable even in case of low frequency ground motions as evident from the results obtained for V#3. MDP showns a satisfactory performance in the cases of all types of ground motions. Figure 3.25 and Figure 3.26 present the deconvolved ground motions in the case of M #1 and V #1, respectively for the dam-foundation system, G-2 with MDP and EDP along with the original ground motions It is important here to note that the quality of the deconvolution process effects the response results of dam-foundation system.

3.7 Dynamic Response of the Dam-Foundation systems

The response of the dam foundation system subjected to an earthquake has been determined in terms of the response parameters such as the dam crest displacement with respect to the dam-foundation interface, dam crest acceleration, element stress and factor of safety. Root mean square (RMS) and the maximum values have been used to represent the response quantities. In comparison to the maximum values for a given time history, the RMS values provide better representation of the response quantities.

$$\mathrm{RMSD(U1)} = \left(\sum_{i=1}^{n} u1_i^2 \right)^{1/2} \qquad \text{Equation 3.13}$$

$$\text{RMSD(U2)} = \left(\sum_{i=1}^{n} u2_i^2\right)^{1/2} \quad \text{Equation 3.14}$$

$$\text{RMSD} = ((RMSD(U1))^2 + (RMSD(U2))^2)^{1/2} \quad \text{Equation 3.15}$$

where, RMSD(U1) and RMSD(U2) are the root mean square displacement in the horizontal and vertical directions respectively. RMSD is the root mean square of RMSD(U1) and RMSD(U2). Table 3.2, 3.3 and 3.4 present the RMSD, RMSD(U1),RMSD(U2), U1max and U2max values of dam-foundation system, G-1 for Model B and C for all the ground motions. Figure 3.27 present the RMSD, ratio R1 of dam-foundation system, G-1 for Model B and C.

$$\text{RMSD, ratio R1} = \frac{(RMSD)_{Model\ B,G-1}}{(RMSD)_{Model\ C,G-1}} \quad \text{Equation 3.16}$$

As the value of ratio R1 for different ground motions is almost equal to 1, it can be concluded that the response obtained from both the models B and C are sufficiently close to each other. Figure 3.28 present the RMSD, ratio R2 of dam-foundation system, G-2 for Model B and C.

$$\text{RMSD, ratio R2} = \frac{(RMSD)_{Model\ B,G-2}}{(RMSD)_{Model\ C,G-2}} \quad \text{Equation 3.17}$$

Comparing to the results of dam-foundation system G-1 the results of dam-foundation system G-2 are quite different for some ground motions. The values obtained for Model B are almost half of values obtained for Model C. The variation in the results for dam-foundation system, G-1 and G-2 can be explained easily. The irregularity in the foundation of dam-foundation system G-2 induces spatial variation in the ground

motions. In case of Model C, the ground accelerations are deconvoluted with respect to a single node at the heel of the dam. Therefore a variation is induced automatically with the change in the geometry. On the other hand, in case of Model B, all the nodes are assumed to have the same acceleration as ground motions are applied at the interface of dam-foundation system. Figure 3.29 presents the distribution of the peak acceleration of ground motion for M #3 applied along the top of the foundation for Model B and C. The sharp rise in the peak ground motion acceleration can be observed near the irregular section of foundation. Therefore, in the absence of non-uniform free-field ground motions, the results obtained from Model C will be more accurate than the results obtained from Model B.

Figure 3.30 and Figure 3.31 present the RMSD, ratio R3 and ratio R4, respectively. Variations in these ratios are expected as the Model A does not consider dam-foundation interaction and radiation damping as foundation is massless in this model.

$$\text{RMSD, ratio R3} = \frac{(RMSD)_{Model\ A,G-1}}{(RMSD)_{Model\ C,G-1}} \qquad \text{Equation 3.18}$$

$$\text{RMSD, ratio R4} = \frac{(RMSD)_{Model\ A,G-2}}{(RMSD)_{Model\ C,G-2}} \qquad \text{Equation 3.19}$$

Figure 3.32 and Figure 3.33 present dam crest displacement of dam-foundation system G-1 for ground motions M #3 and V #1. As discussed earlier, Model B and C produce similar results for dam-foundation system, G-1 where as some variation are observed in case of Model A. Figure 3.34 and Figure 3.35 present the dam crest displacement for dam-foundation system, G-2 for ground motions M #3 and V #1. In this case, a variation

is observed between all the models. The main reason for the difference in results between Model B and C is due to the fact that the spatial variation in ground motions is accounted for in case of Model C, while that is neglected in the other model.

3.8 Conclusions

The study presents a modified deconvolution procedure for the deconvolution of input ground motions for the use in the seismic response analysis of dam-foundation systems. The modified deconvolution procedure performs well for both high frequency and low frequency ground motions. Also the relative performance of earthquake input mechanisms namely A) massless foundation input model, B) free-field earthquake input at dam foundation interface model, C) deconvolved earthquake input model have been studied. It is concluded that the Model C is the most accurate one compared to the other models as it provides a rational and accurate model where spatial variation in ground motion can be easily accounted for. Model B does not yield appropriate results for irregular geometries as the spatial variation of ground motion cannot be accounted for in this model. Model A, where the foundation mass is ignored may not produce realistic response unless special care is taken to artificially adjust other parameters like foundation damping. It is important here to note that the modified deconvolution procedure proposed in study is expected to be effective for both two and three dimensional studies. However, in the present study, only two dimensional models are considered.

Table 3.1 Material properties

Material	Concrete	Rock
Elastic Modulus (MPa)	3.45×10^4	2.76×10^4
Poisson's ratio	0.2	0.33
Unit weight (kN/m3)	23.5	25.9

Table 3.2 Results for Model A in G-1 (mm)

	M#1	M#2	M#3	V#1	V#2	V#3
RMSD	473.8	432.3	229.3	549.3	532.8	254.6
RMSD(U1)	414.1	404.2	209.2	511.9	497.8	237.4
RMSD(U2)	230.2	153.3	93.9	199.1	189.7	92.0
U1max	15.3	29.2	22.1	32.9	30.6	27.3
U2max	5.9	8.0	7.2	11.3	9.4	7.9

Table 3.3 Results for Model B in G-1 (mm)

	M#1	M#2	M#3	V#1	V#2	V#3
RMSD	297.3	552.3	235.7	415.3	449.1	249.1
RMSD(U1)	202.6	514.8	211.4	367.2	405.3	228.2
RMSD(U2)	217.6	200.0	104.2	193.9	193.5	99.8
U1max	10.4	32.3	26.1	31.7	24.8	29.8
U2max	5.6	14.2	10.3	12.0	10.7	11.7

Table 3.4 Results for Model C in G-1 (mm)

	M#1	M#2	M#3	V#1	V#2	V#3
RMSD	309.8	539.0	242.6	420.4	438.1	248.4
RMSD(U1)	219.2	501.8	218.3	372.3	393.9	227.4
RMSD(U2)	218.9	196.7	105.8	195.5	192.0	99.9
U1max	11.0	32.1	26.7	30.0	24.6	30.1
U2max	5.5	14.2	10.5	11.5	10.6	11.7

Table 3.5 Results for Model A in G-2 (mm)

	M#1	M#2	M#3	V#1	V#2	V#3
RMSD	274.9	190.0	111.8	172.5	210.2	97.4
RMSD(U1)	220.5	165.7	96.8	135.1	179.6	82.7
RMSD(U2)	164.2	92.9	56.0	107.3	109.3	51.5
U1max	9.0	11.3	14.9	13.1	17.1	9.8
U2max	3.8	5.2	4.9	4.7	5.3	3.7

Table 3.6 Results for Model B in G-2 (mm)

	M#1	M#2	M#3	V#1	V#2	V#3
RMSD	228.1	140.5	88.8	164.2	167.2	80.0
RMSD(U1)	166.5	102.0	62.5	105.7	115.7	59.3
RMSD(U2)	155.9	96.6	63.1	125.6	120.7	53.8
U1max	4.0	6.7	6.2	9.1	7.6	3.5
U2max	2.9	5.7	4.9	5.5	5.0	3.4

Table 3.7 Results for Model C in G-2 (mm)

	M#1	M#2	M#3	V#1	V#2	V#3
RMSD	272.9	175.7	197.7	375.8	243.3	100.4
RMSD(U1)	222.8	154.8	185.5	354.3	218.5	84.5
RMSD(U2)	157.5	83.2	68.4	125.3	106.9	54.1
U1max	5.9	9.1	18.8	18.5	13.6	8.6
U2max	3.3	4.0	6.9	5.5	3.7	3.2

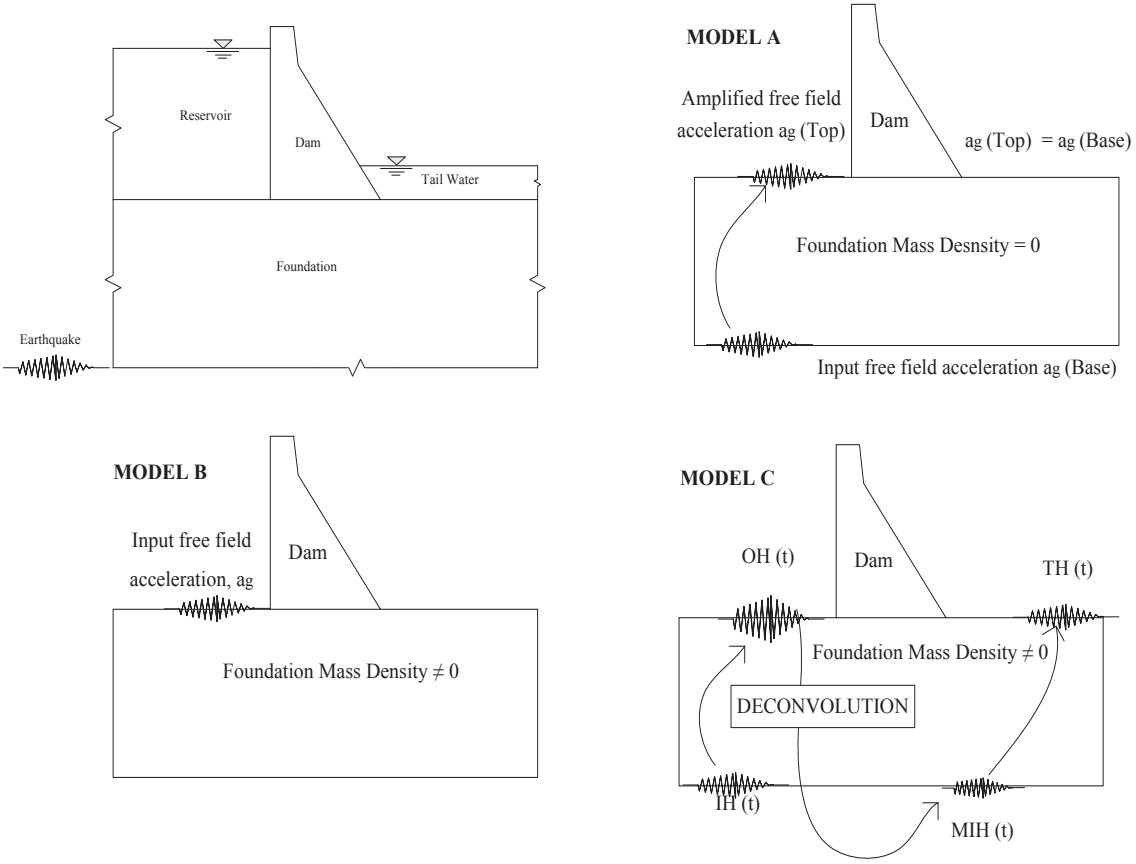

Figure 3.1 Representation of Model A, B and C

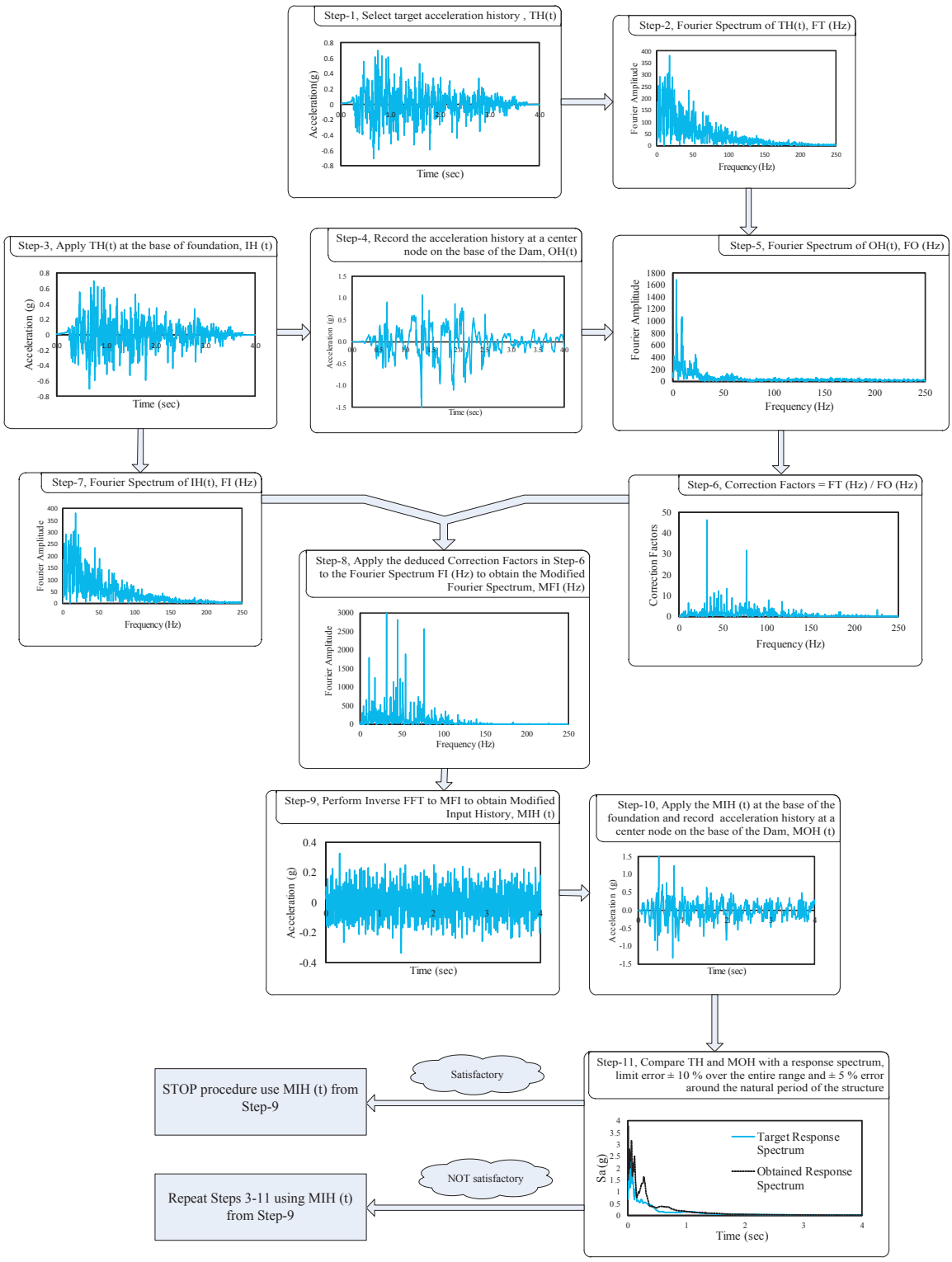

Figure 3.2 Existing deconvolution procedure

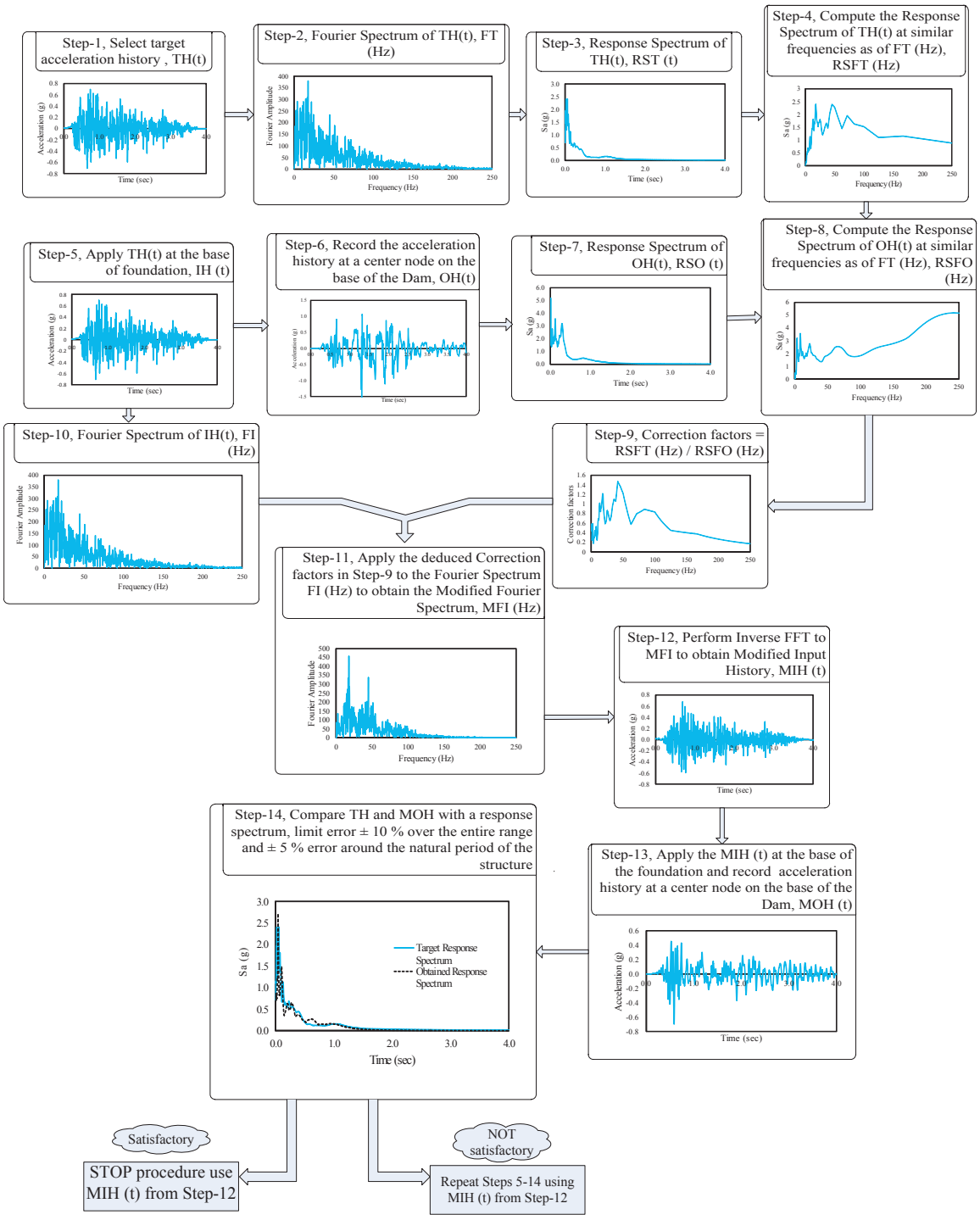

Figure 3.3 Modified deconvolution procedure

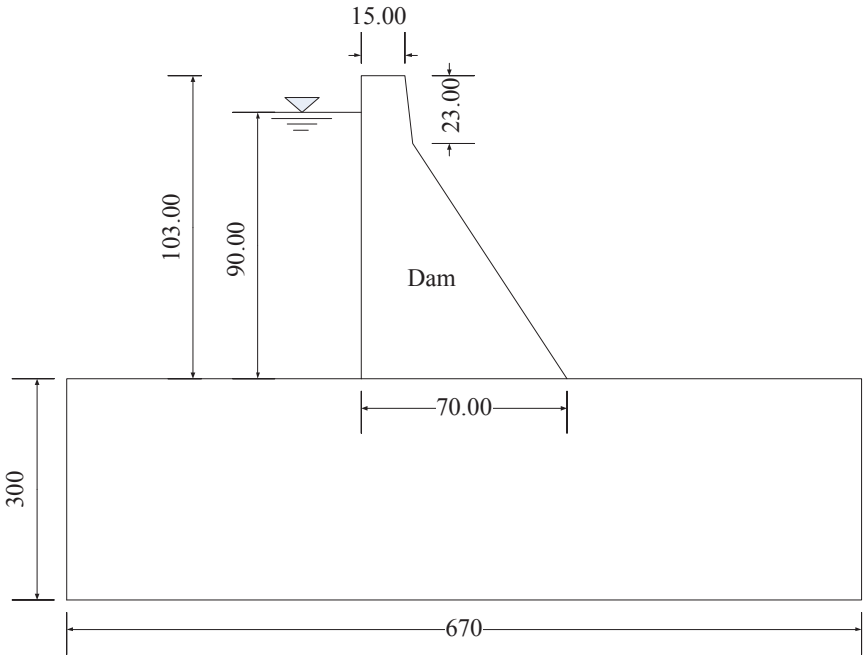

Figure 3.4 Dam foundation system, G-1

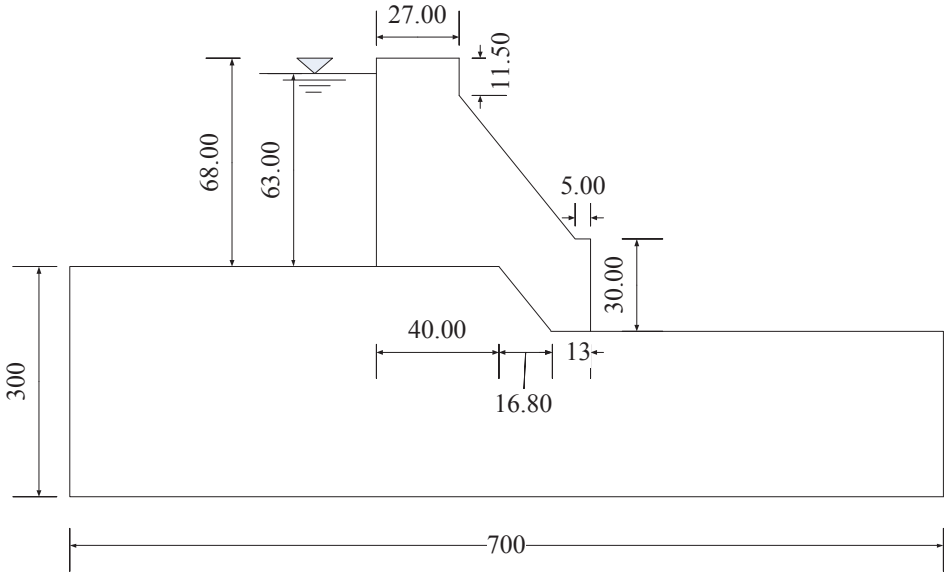

Figure 3.5 Dam foundation system, G-2

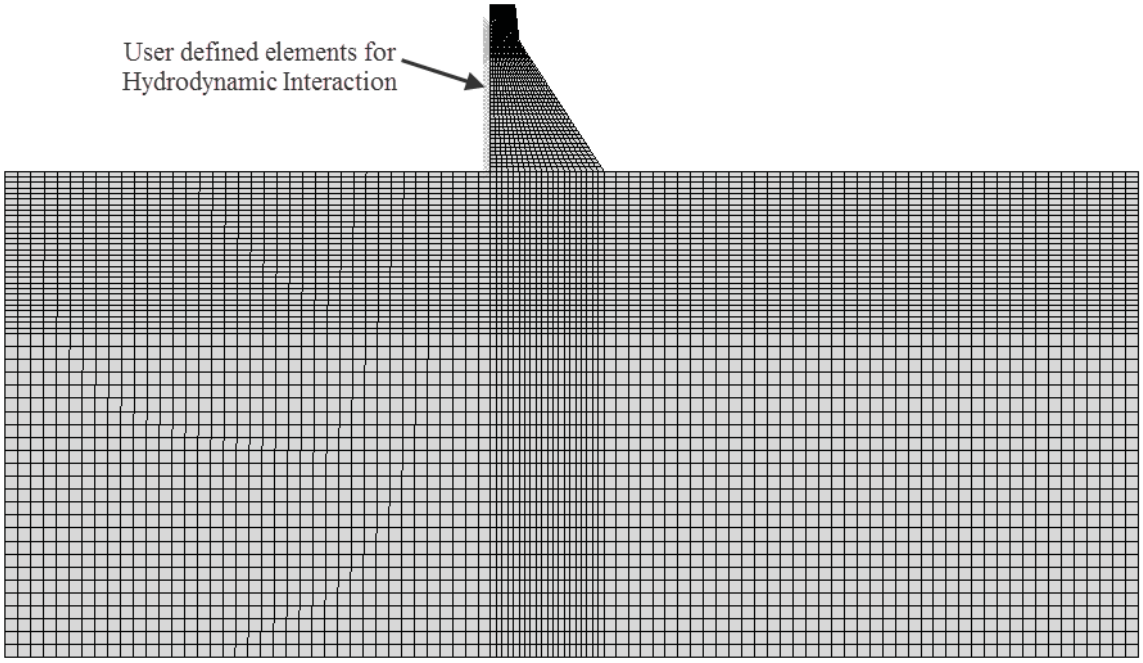

Figure 3.6 Finite element mesh of Dam-Foundation system, G-1 (Model A & C)

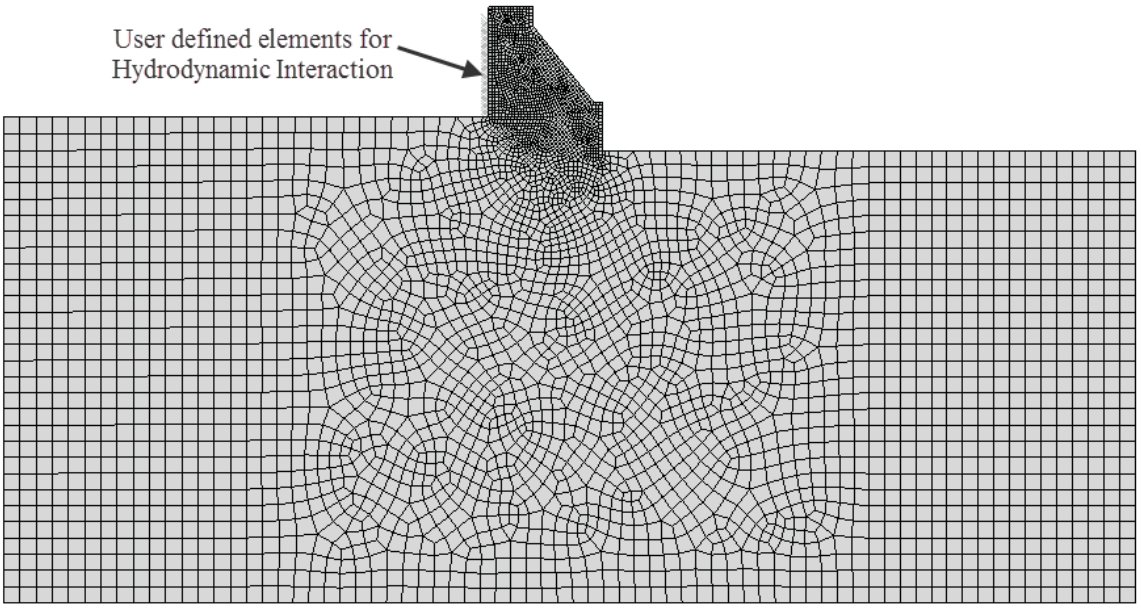

Figure 3.7 Finite element mesh of Dam-Foundation system, G-2 (Model A &C)

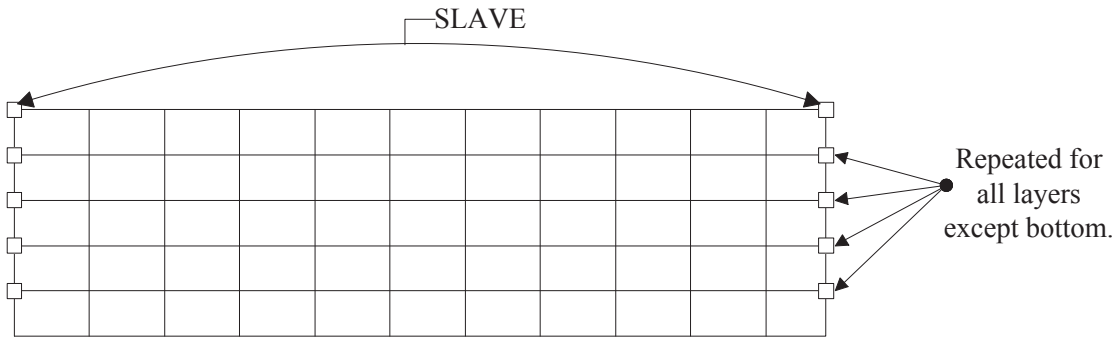

Figure 3.8 Representation of constraints for G-1 for Model C

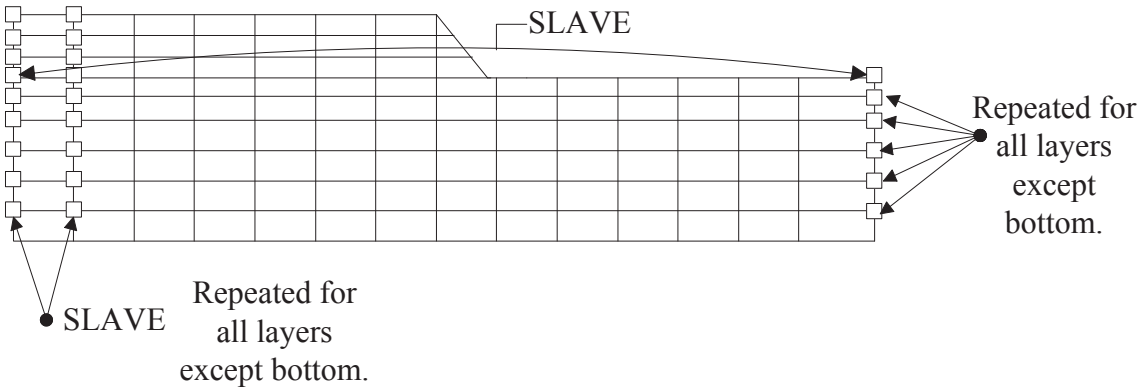

Figure 3.9 Representation of constraints for G-2 for Model C

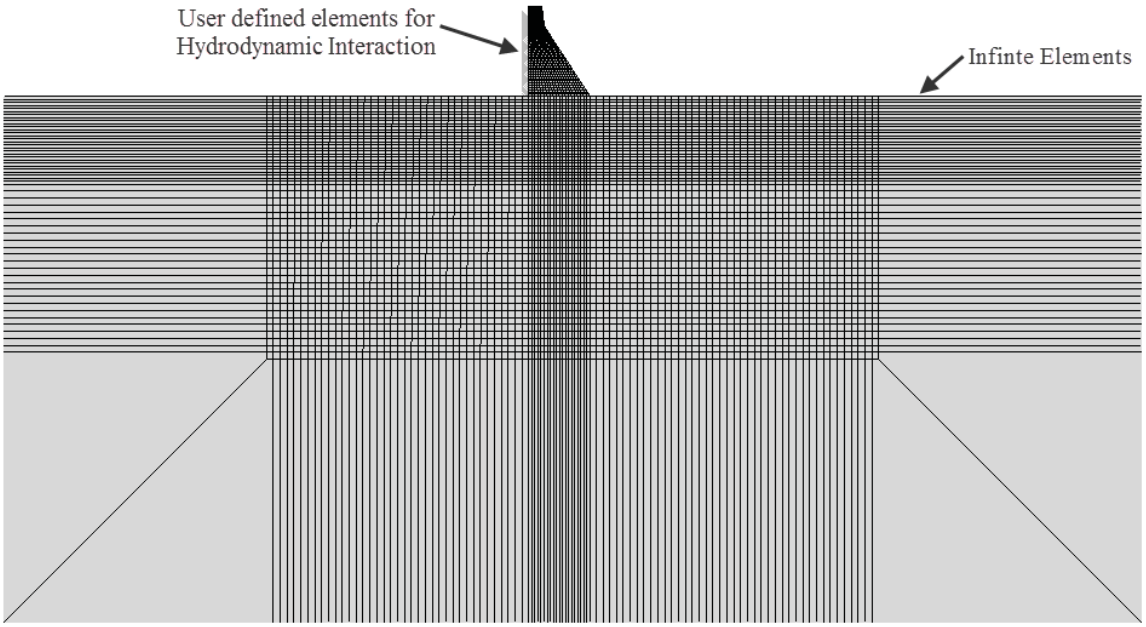

Figure 3.10 Finite element mesh for G-1, Model B

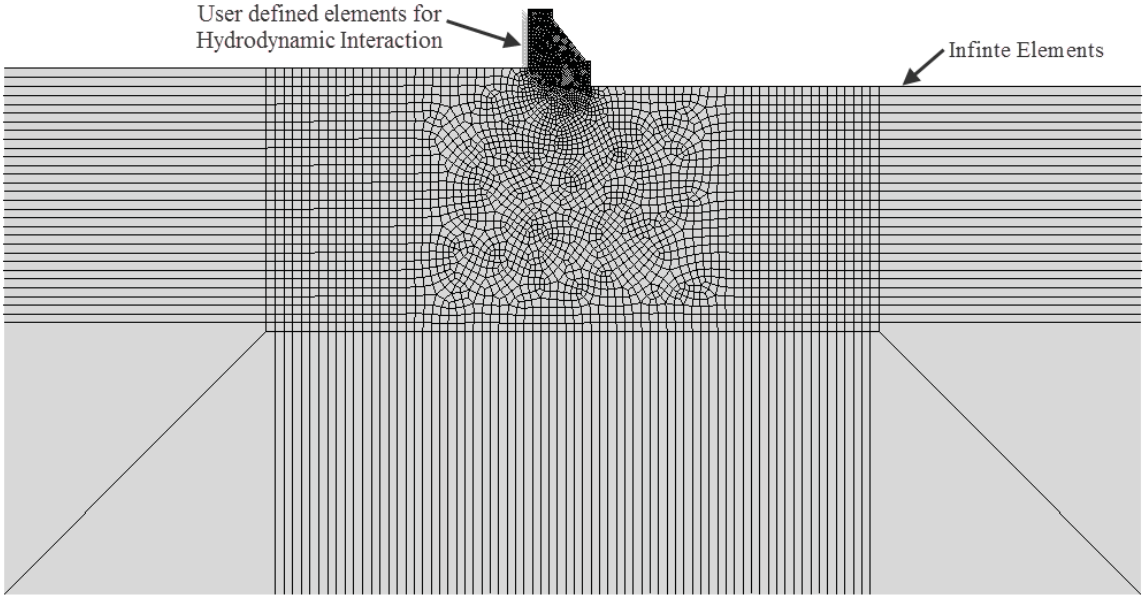

Figure 3.11 Finite element mesh for G-2, Model B

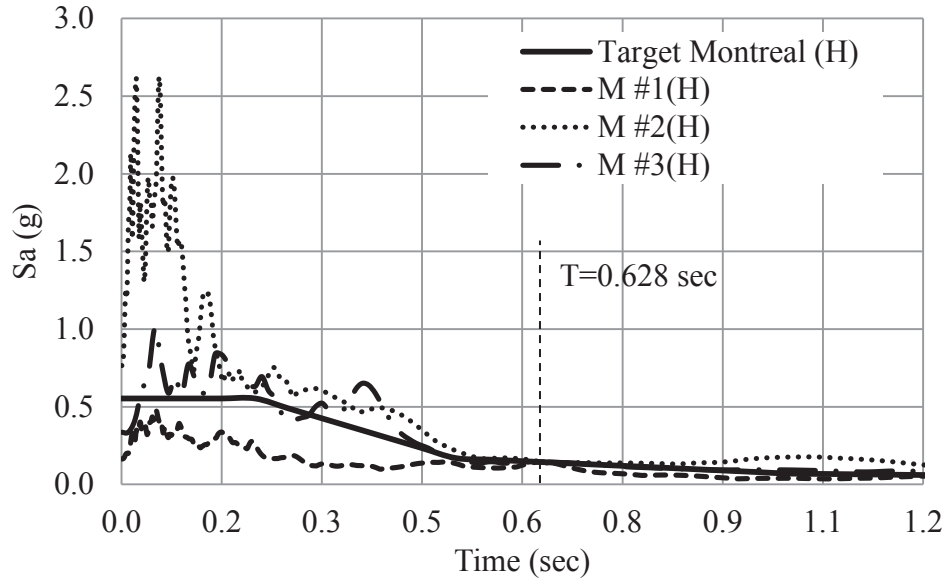

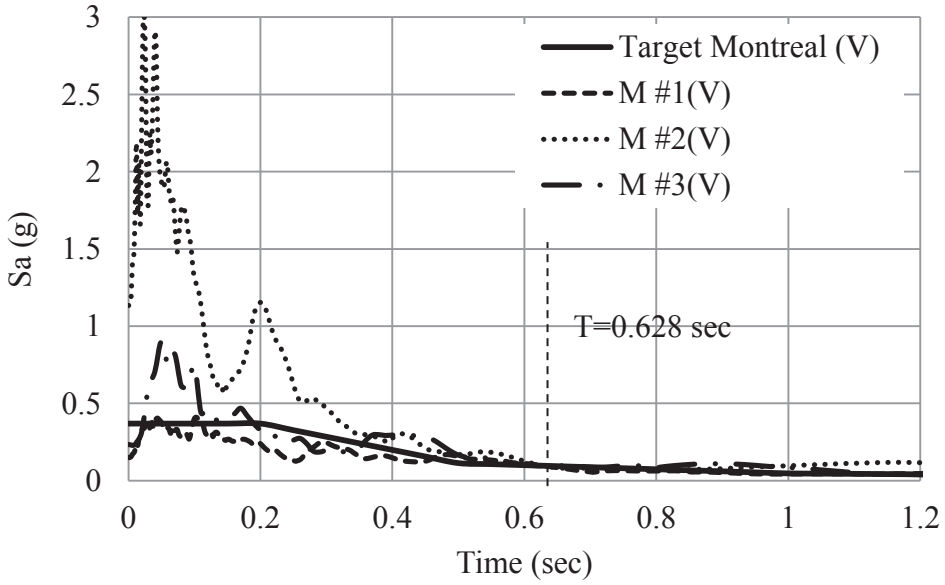

Figure 3.12 Response Spectra for high frequency ground motions conforming to Montréal seismic hazard.

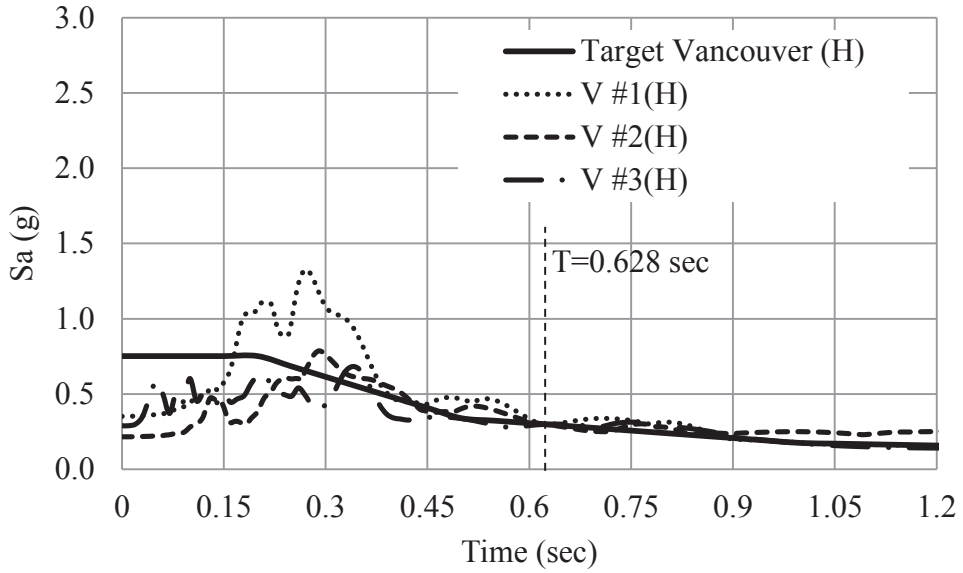

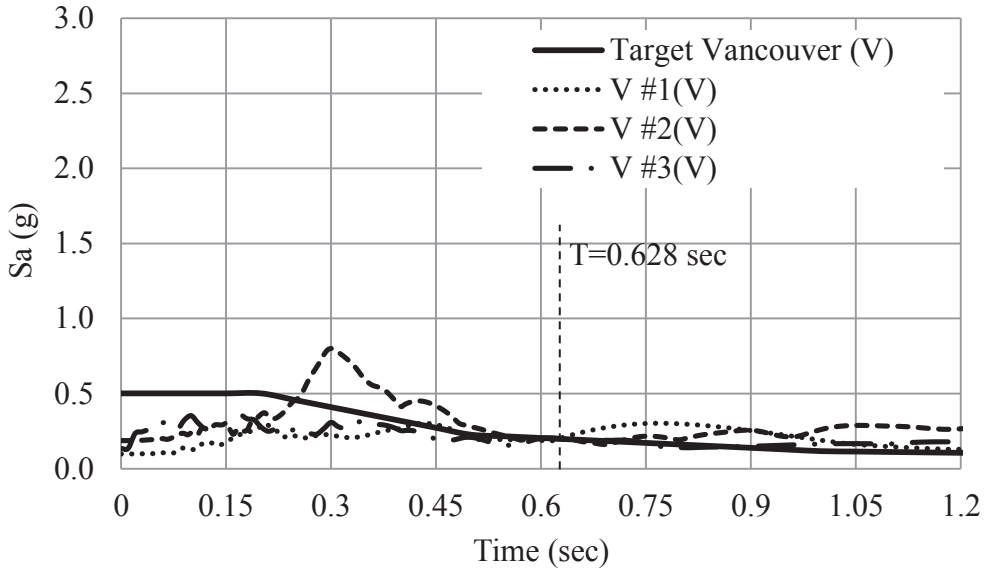

Figure 3.13 Response Spectra for low frequency ground motions conforming to Vancouver seismic hazard.

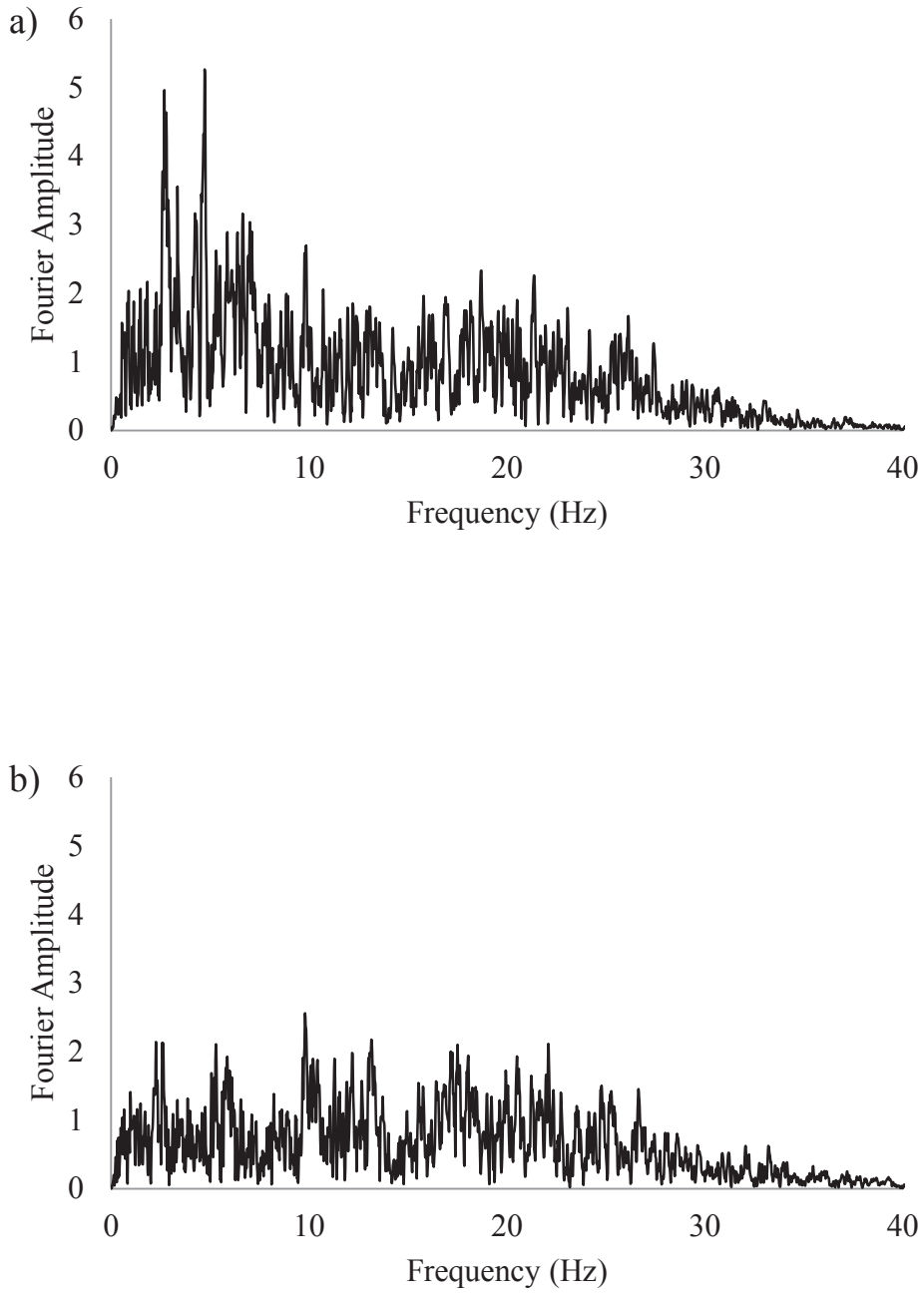

Figure 3.14 Fourier amplitude spectra: a) M #3(H); b) M #3(V)

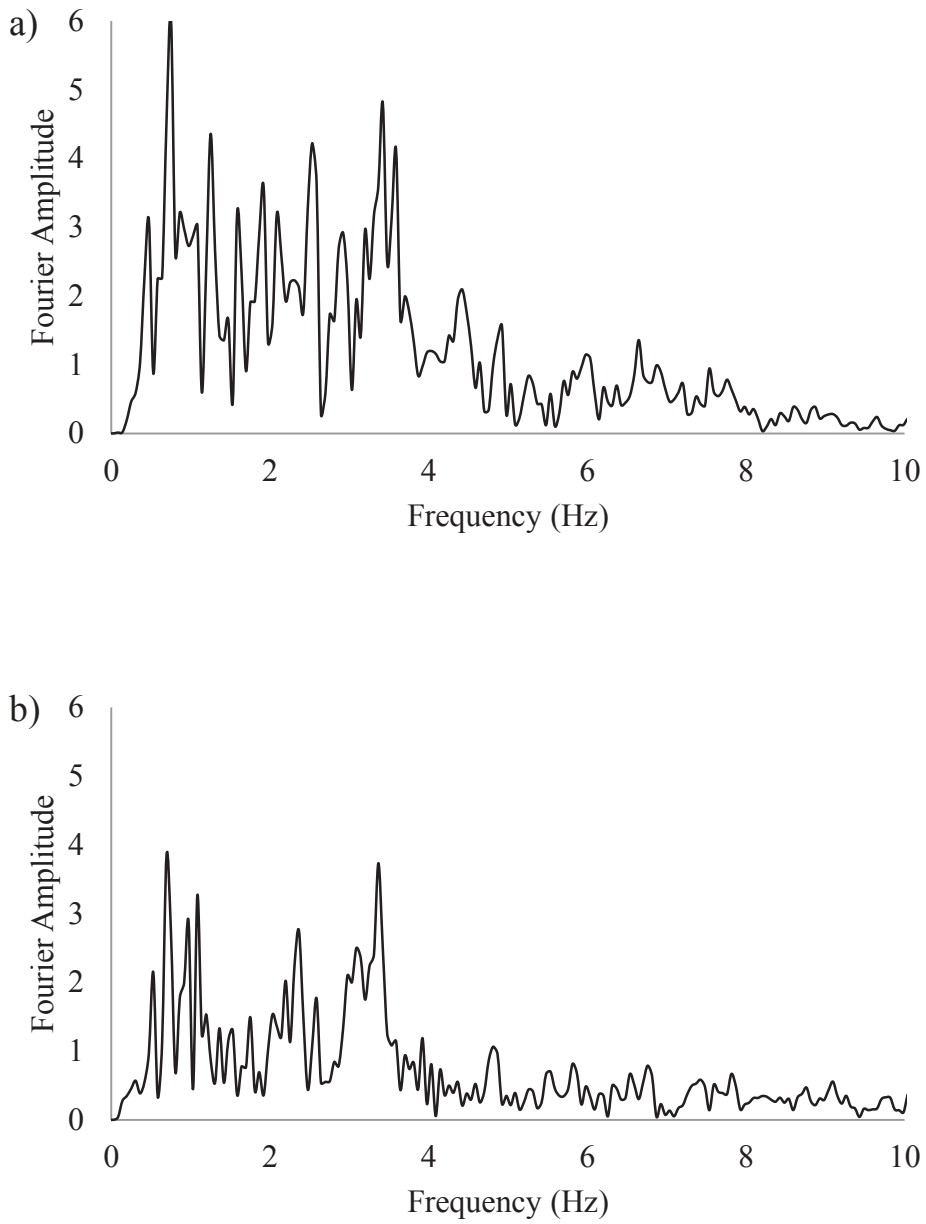

Figure 3.15 Fourier amplitude spectra: a) V #2(H); b) V #2(V)

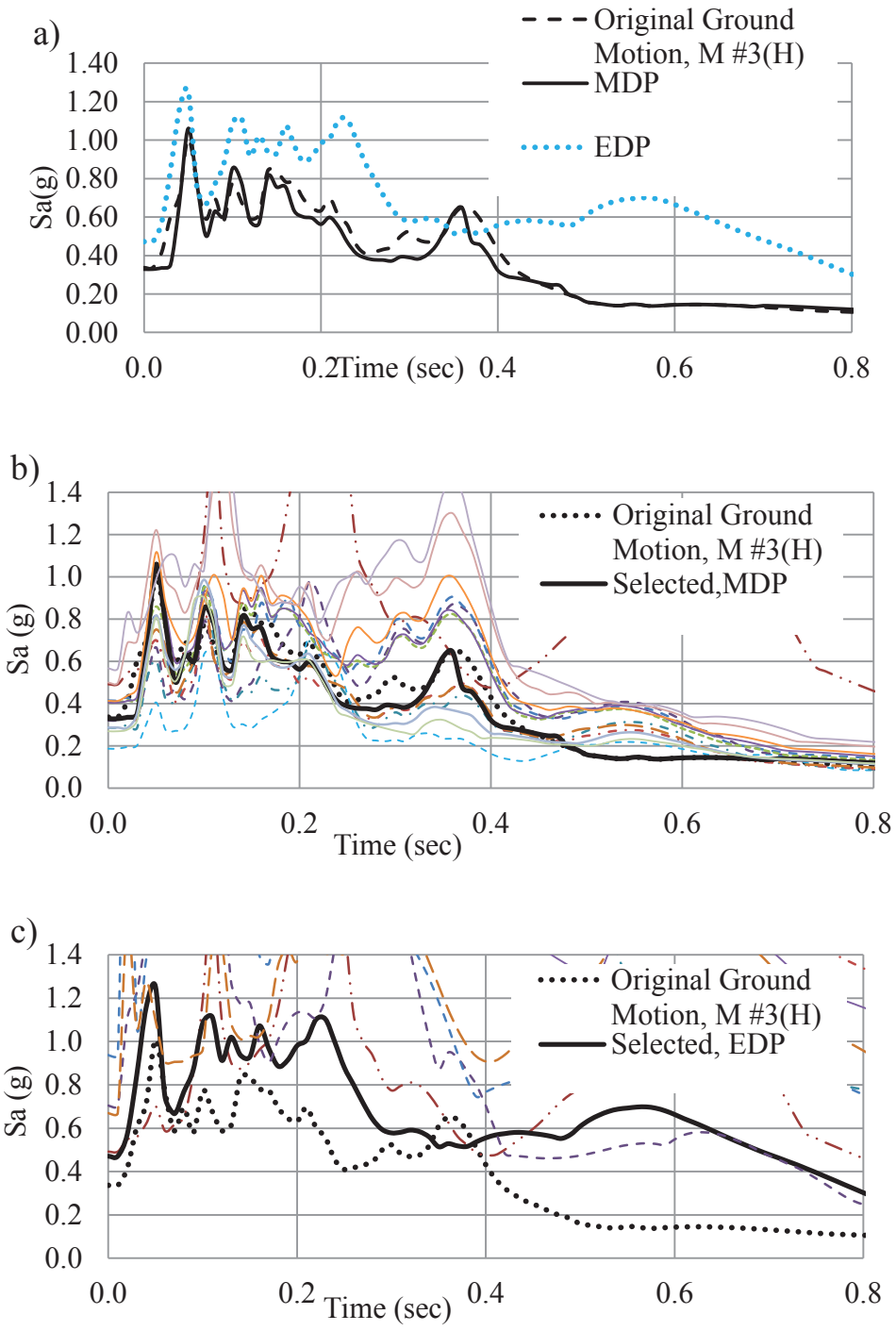

Figure 3.16 Deconvolved ground motions for G1: a) Original Ground Motion, M #3(H) with modified (MDP) and existing deconvolution procedure (EDP); b) M #3(H) with selected MDP and rest of iterations; c) M #3(H) with selected EDP and rest of iterations.

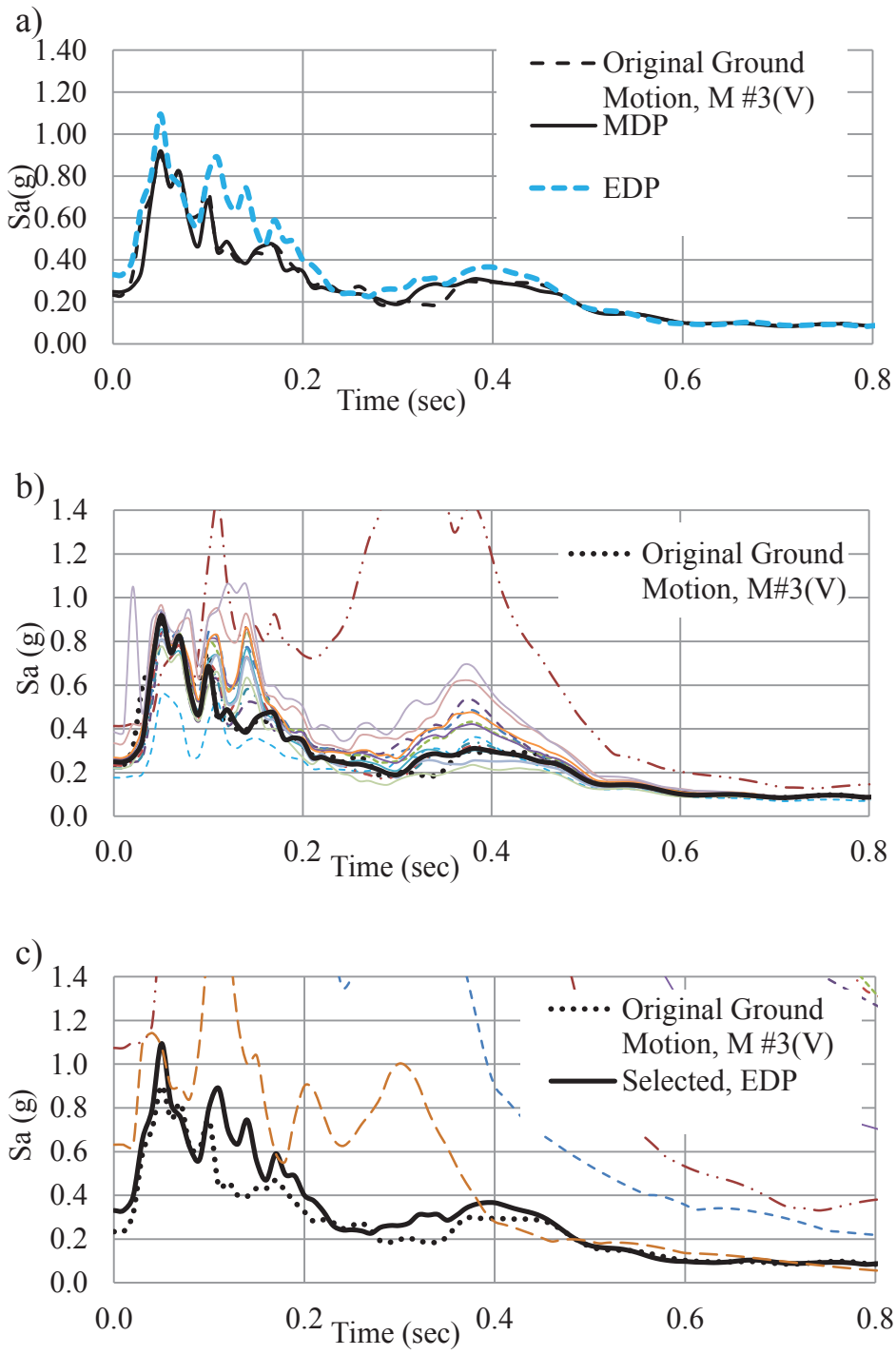

Figure 3.17 Deconvolved ground motions for G1: a) Original Ground Motion, M #3(V) with modified (MDP) and existing deconvolution procedure (EDP); b) M #3(V) with selected MDP and rest of iterations; c) M #3(V) with selected EDP and rest of iterations.

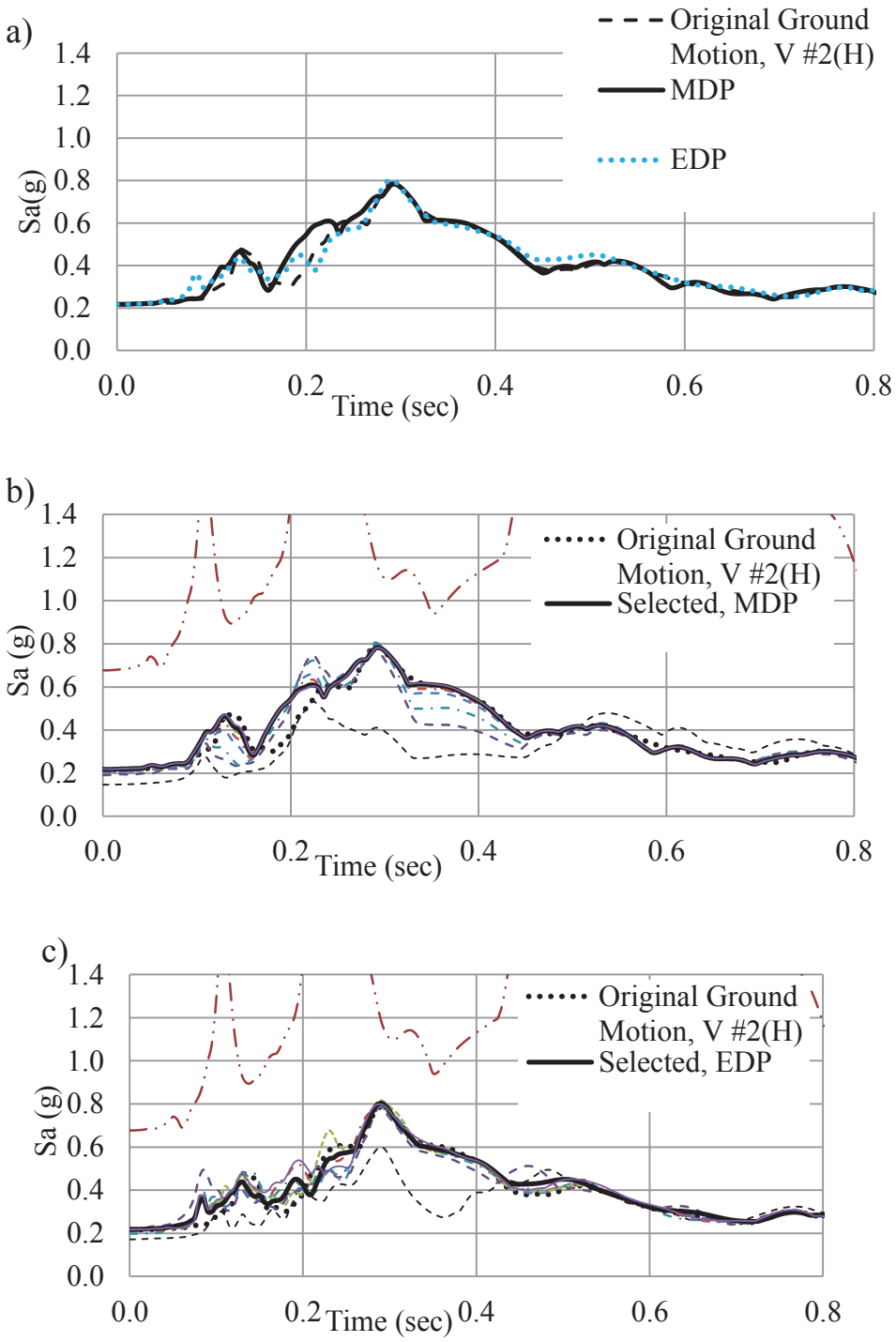

Figure 3.18 Deconvolved ground motions for G1: a) Original Ground Motion, V #2(H) with modified (MDP) and existing deconvolution procedure (EDP); b) V #2(H) with selected MDP and rest of iterations; c) V #2(H) with selected EDP and rest of iterations.

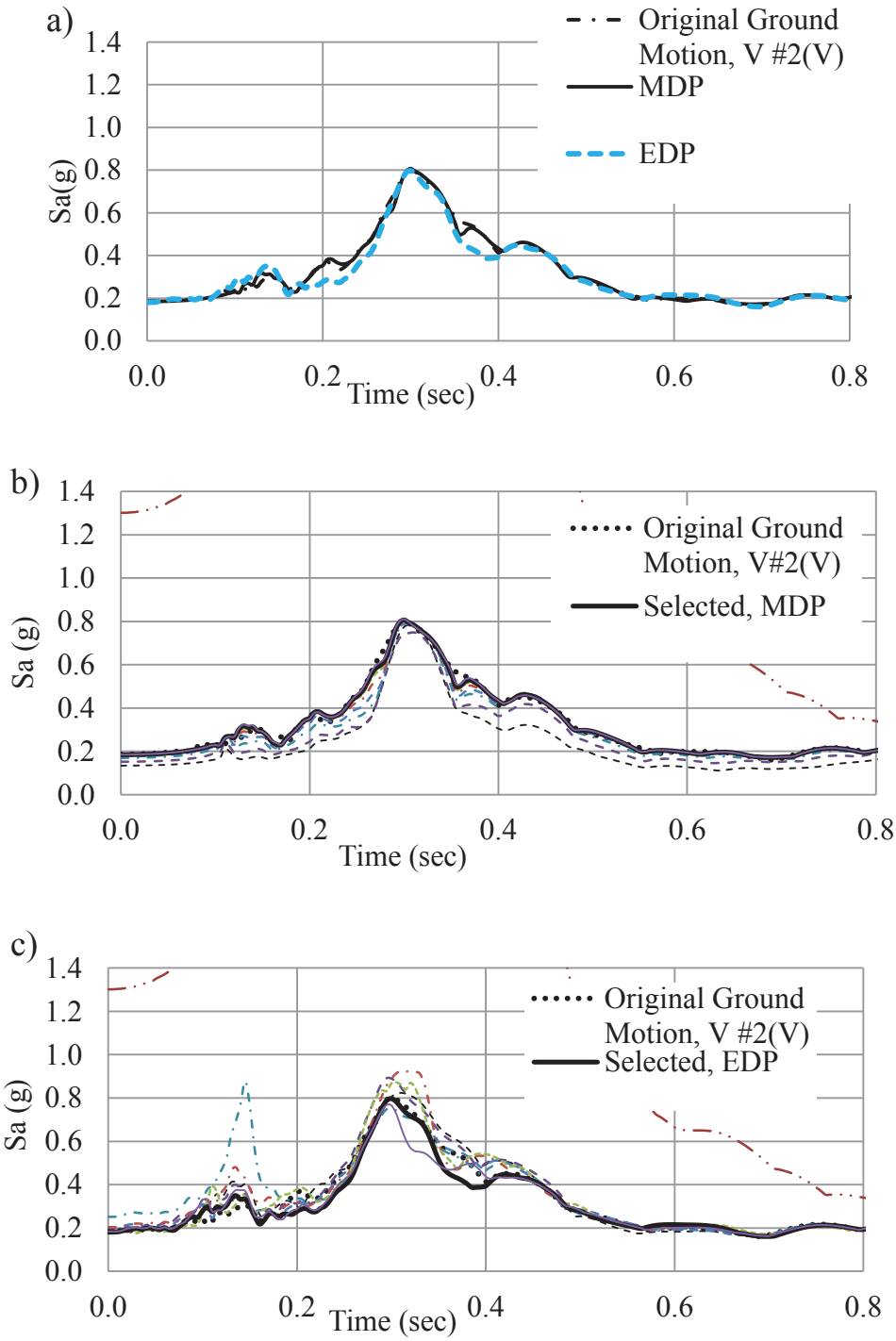

Figure 3.19 Deconvolved ground motions for G1: a) Original Ground Motion, V #2(V) with modified (MDP) and existing deconvolution procedure (EDP); b) V #2(V) with selected MDP and rest of iterations; c) V #2(V) with selected EDP and rest of iterations.

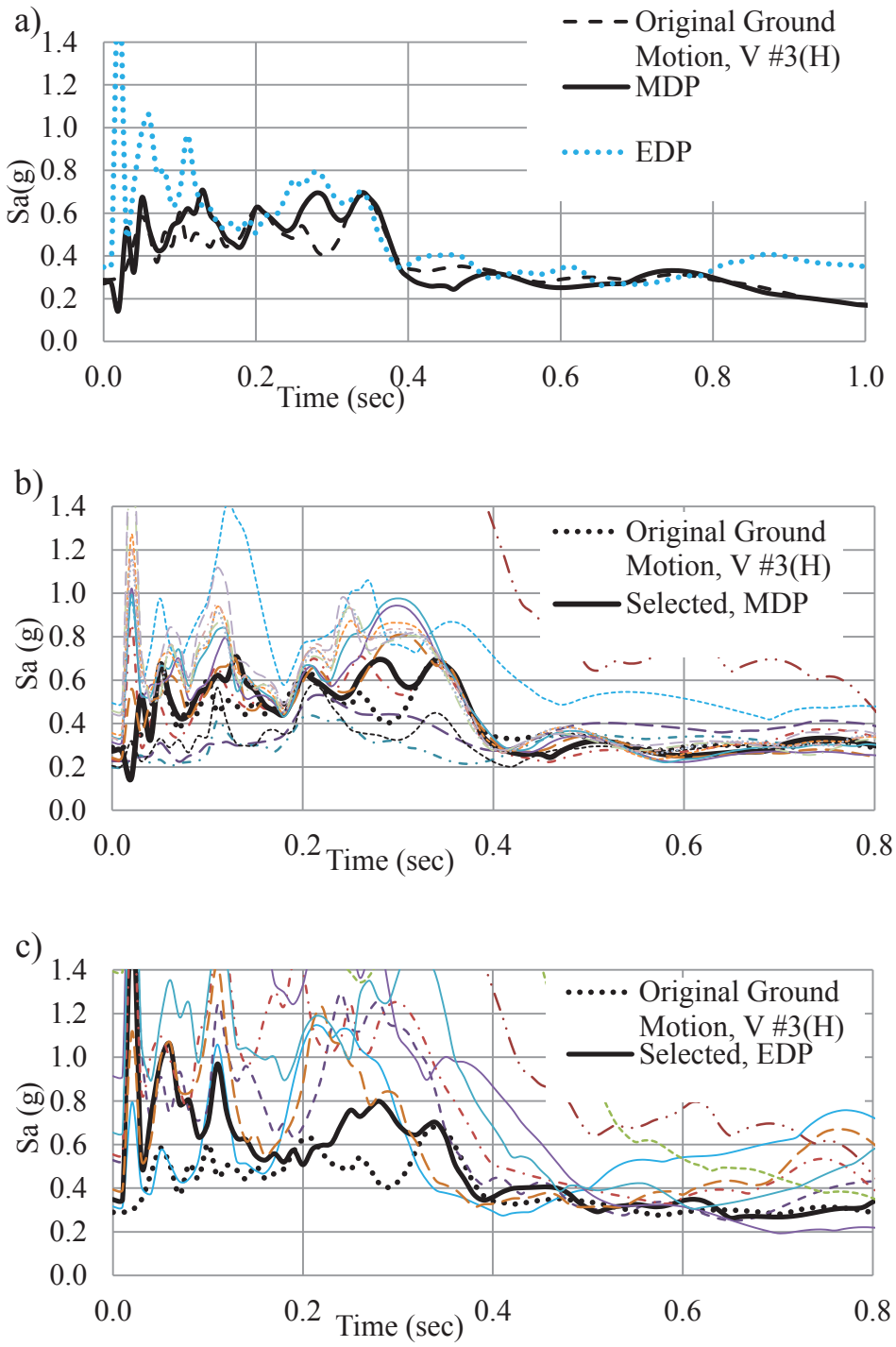

Figure 3.20 Deconvolved ground motions for G1: a) Original Ground Motion, V #3(H) with modified (MDP) and existing deconvolution procedure (EDP); b) V #3(H) with selected MDP and rest of iterations; c) V #3(H) with selected EDP and rest of iterations.

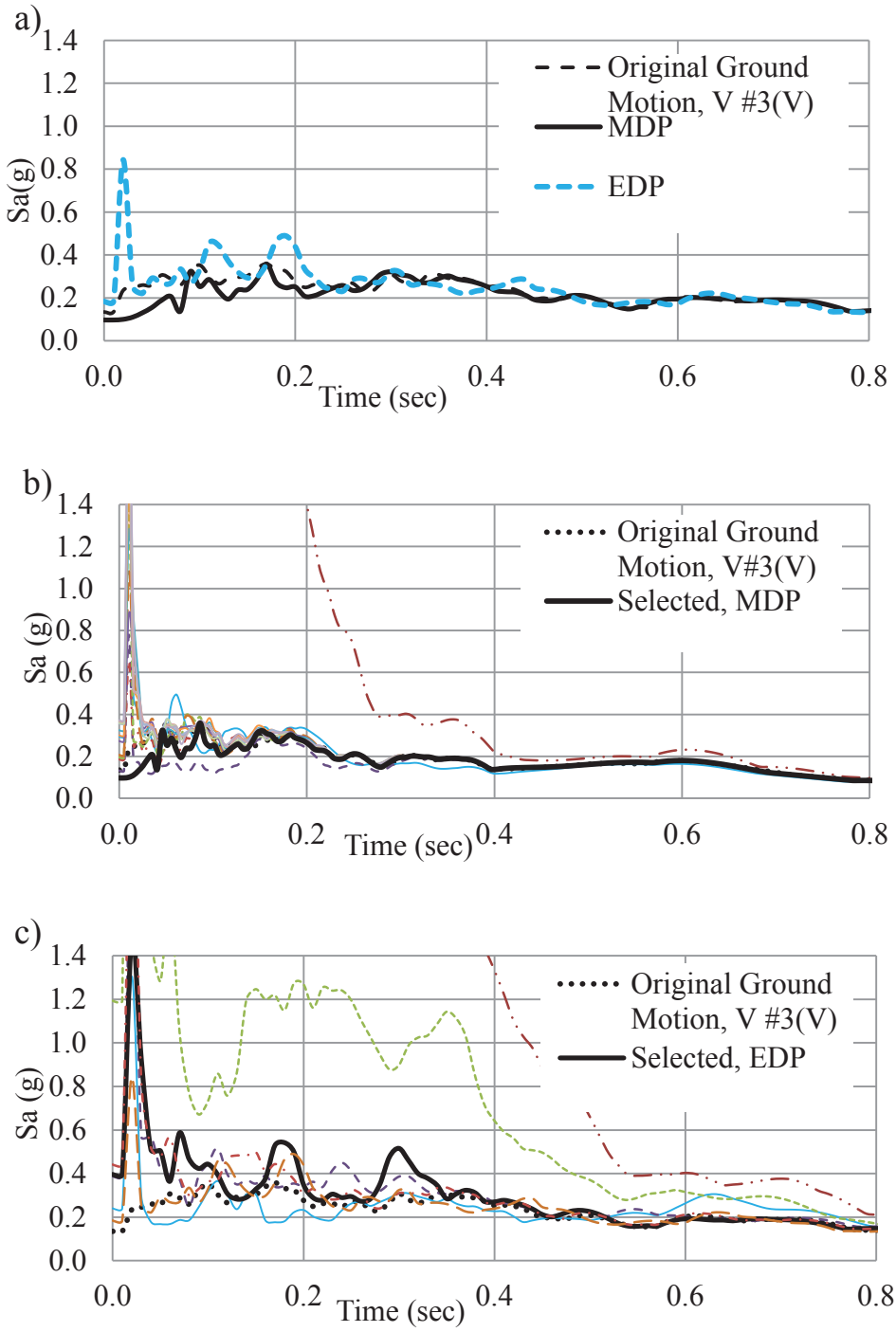

Figure 3.21 Deconvolved ground motions for G1: a) Original Ground Motion, V #3(V) with modified (MDP) and existing deconvolution procedure (EDP); b) V #3(V) with selected MDP and rest of iterations; c) V #3(V) with selected EDP and rest of iterations.

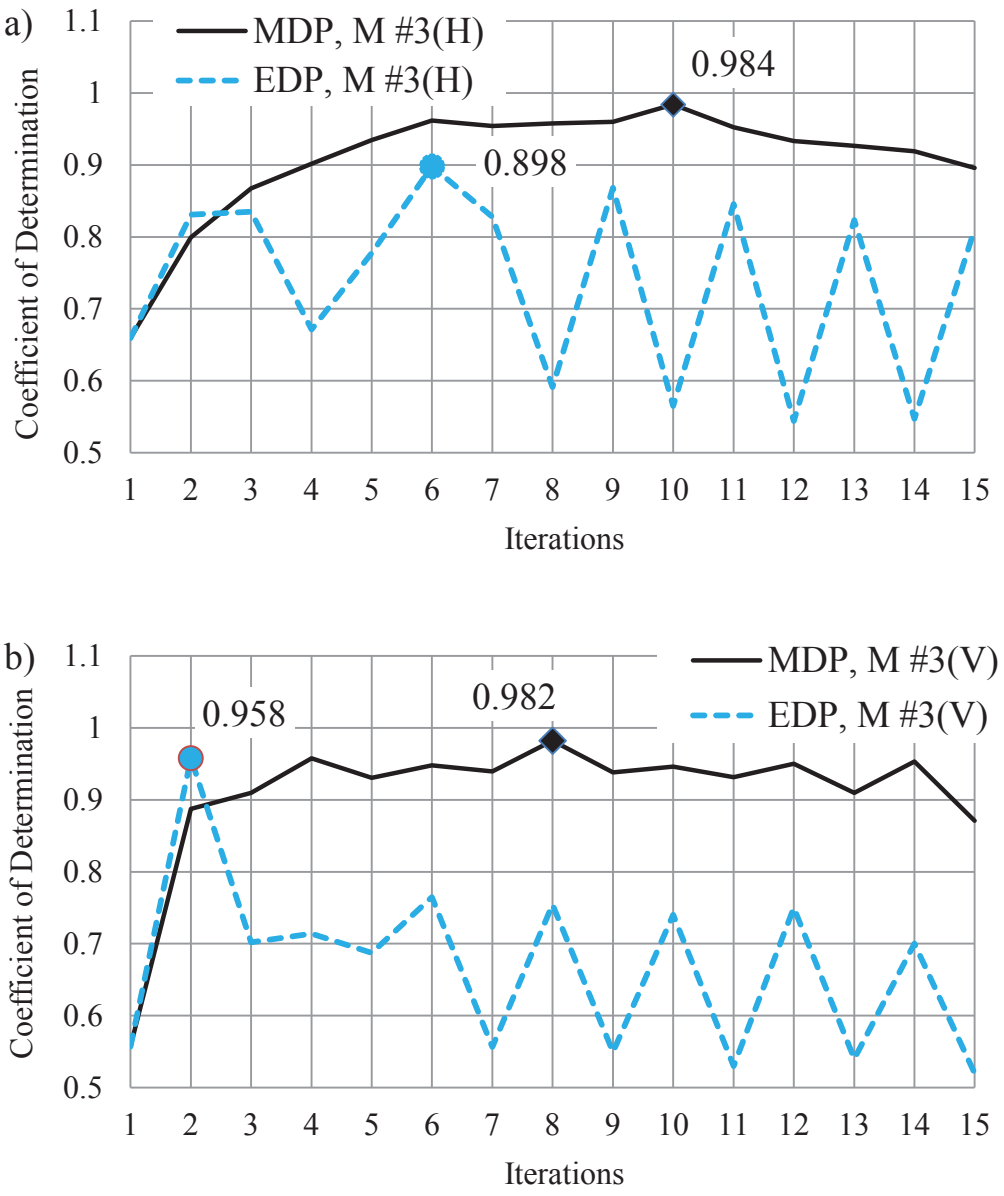

Figure 3.22 Coefficient of Determination (R^2) for G1: a) R^2 values for different iterations for ground motion M #3(H) with MDP and EDP; b) R^2 values for different iterations for ground motion M #3(V) with MDP and EDP.

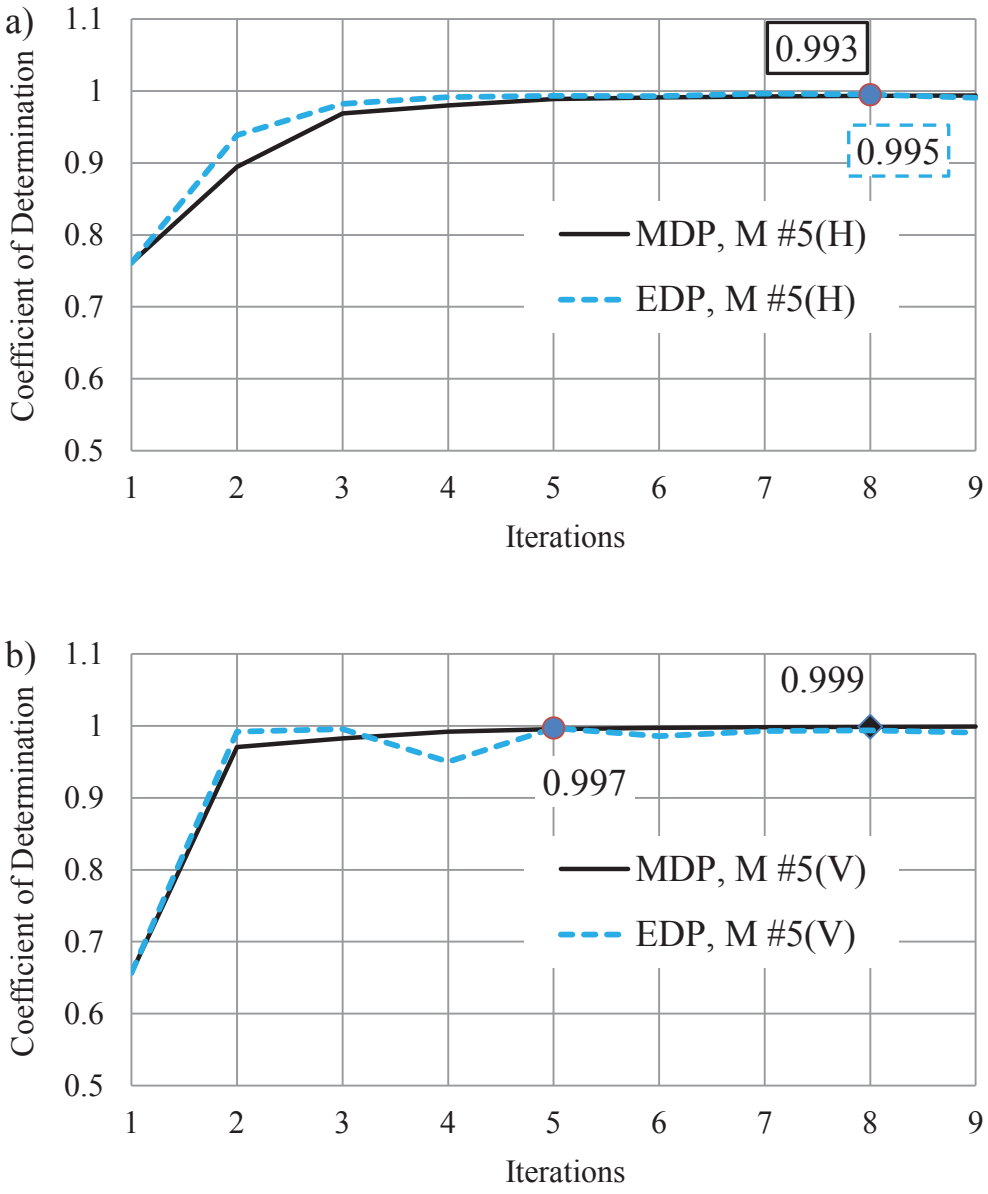

Figure 3.23 Coefficient of Determination (R^2) for G1: a) R^2 values for different iterations for ground motion V #2(H) with MDP and EDP; b) R^2 values for different iterations for ground motion V #2(V) with MDP and EDP.

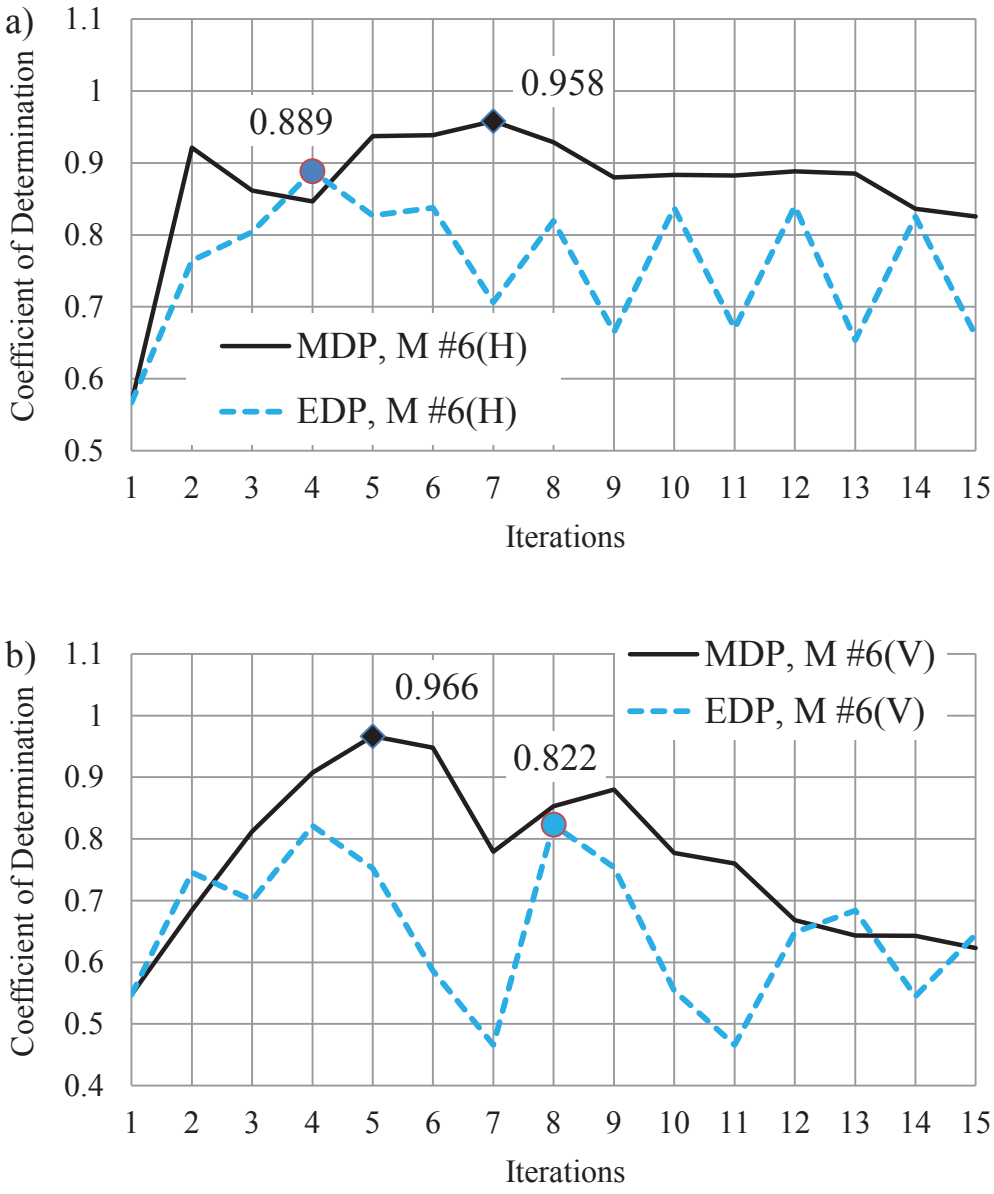

Figure 3.24 Coefficient of Determination (R^2) for G1: a) R^2 values for different iterations for ground motion V #3(H) with MDP and EDP; b) R^2 values for different iterations for ground motion V #3(V) with MDP and EDP.

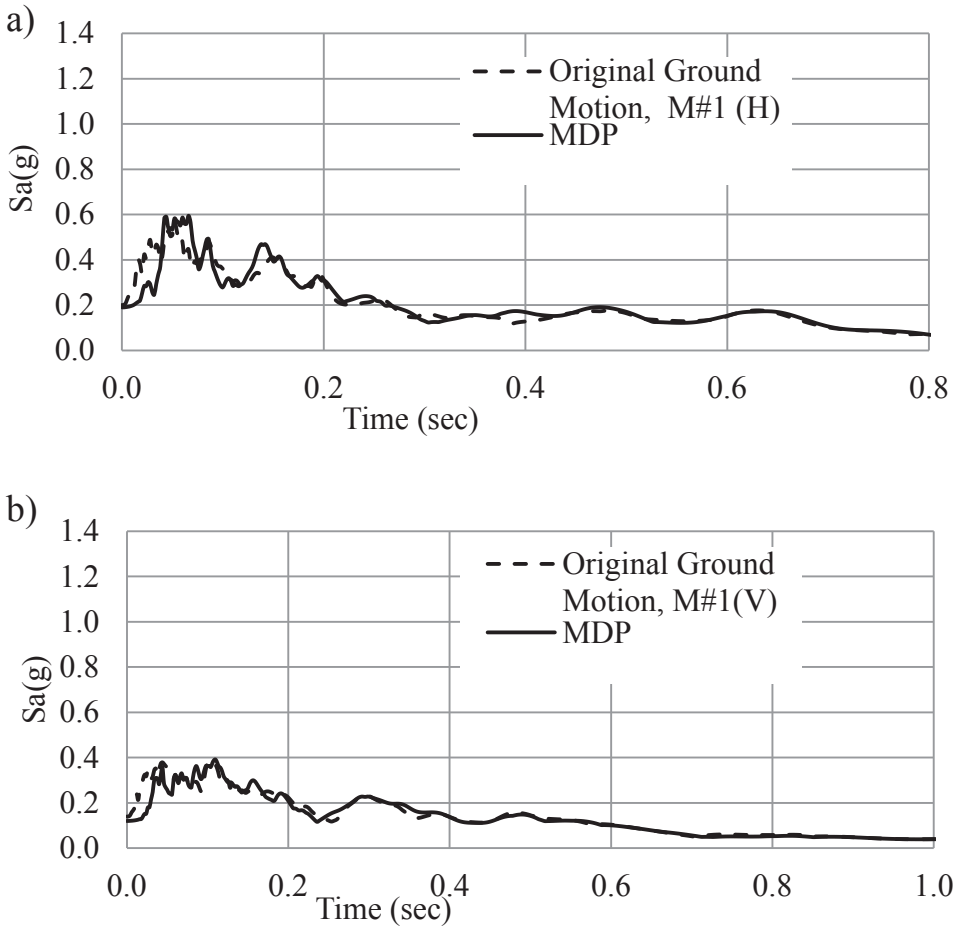

Figure 3.25 Deconvolved ground motions for dam-foundation system, G2: a) Original Ground Motion, M #1(H) with modified deconvolution procedure (MDP); b) Original Ground Motion, M #1(V) with modified deconvolution procedure (MDP).

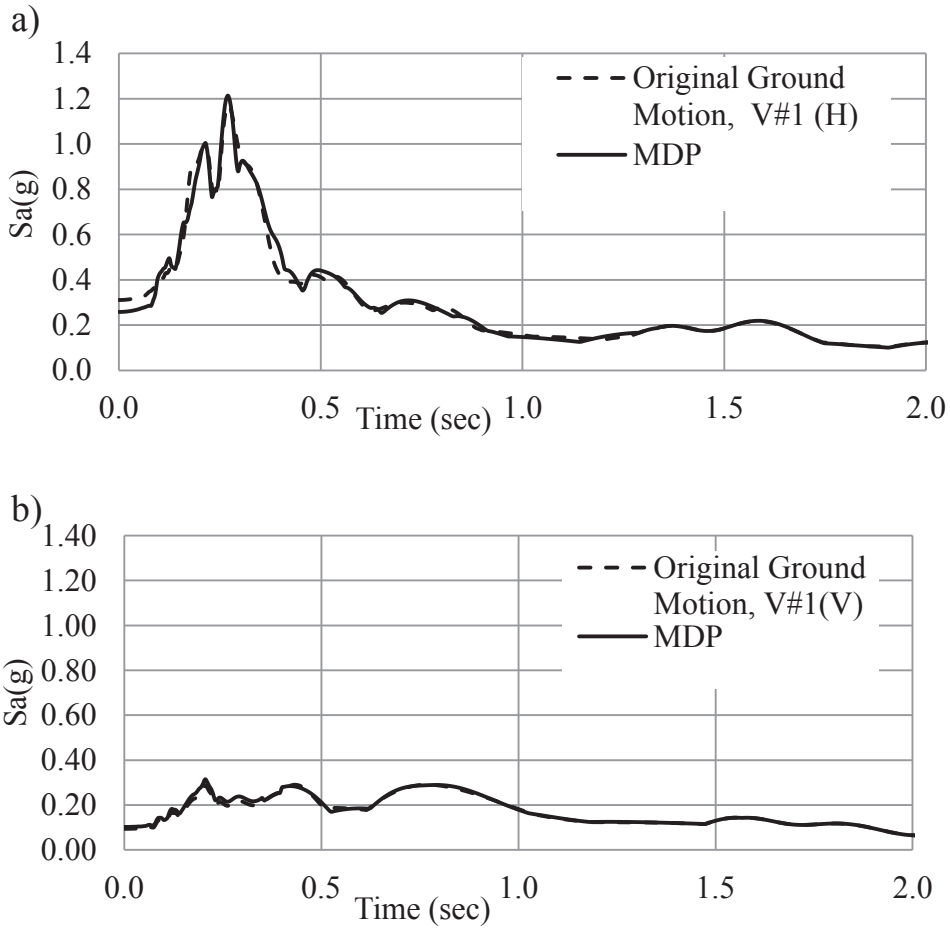

Figure 3.26 Deconvolved ground motions for dam-foundation system, G2: a) Original Ground Motion, V #1(H) with modified deconvolution procedure (MDP); b) Original Ground Motion, V #1(V) with modified deconvolution procedure (MDP).

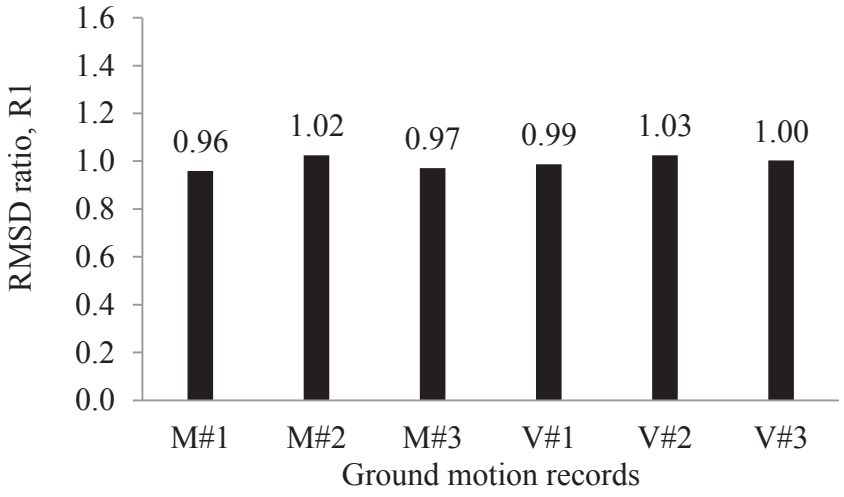

Figure 3.27 RMS displacement, ratio R1 for model B and C in G-1

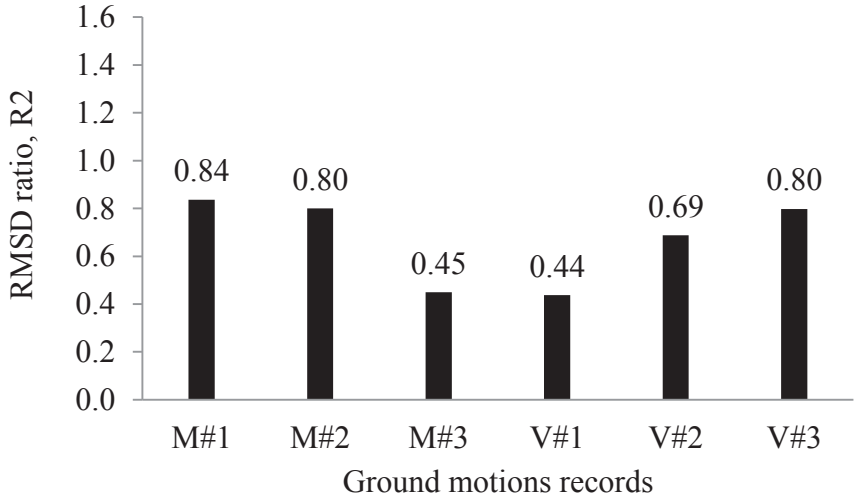

Figure 3.28 RMS displacement, ratio R2 for model B and C in G-2

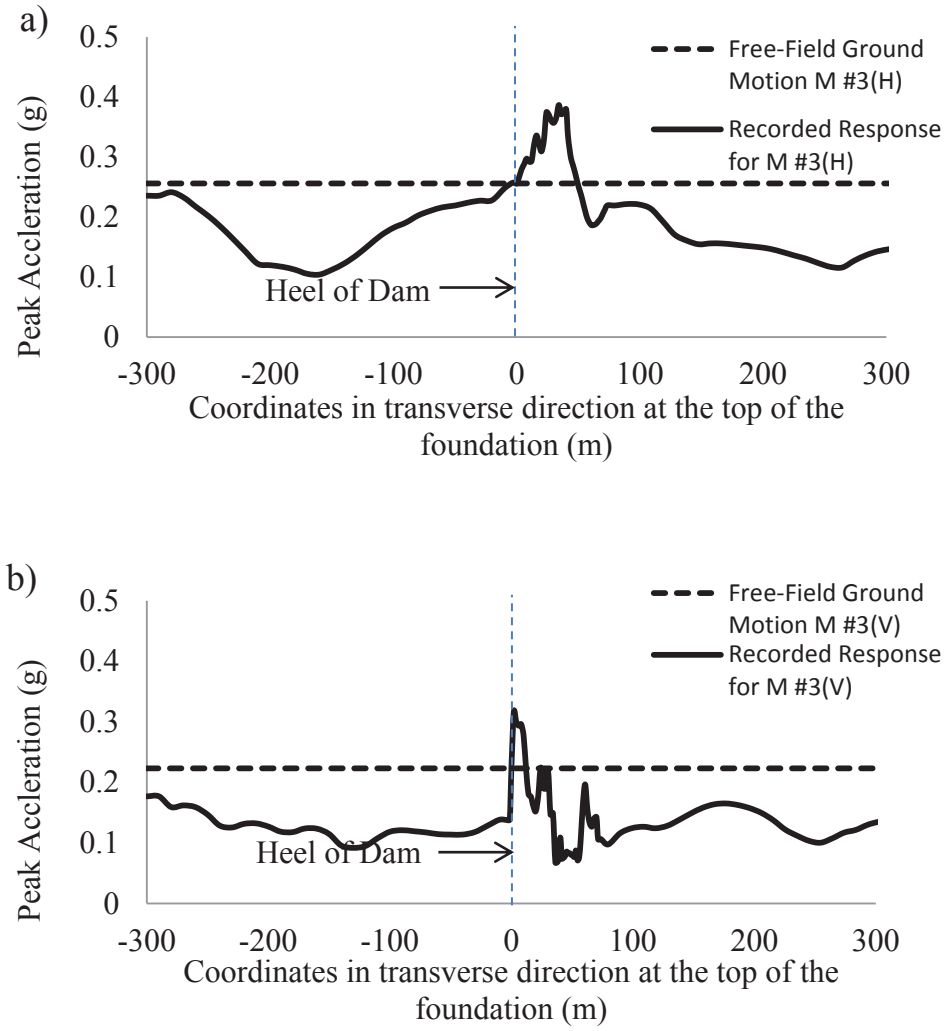

Figure 3.29 Distribution of peak ground acceleration along the top of the foundation in dam-foundation, G-2 for Model B and C: a) M #3(H); b) M #3(V)

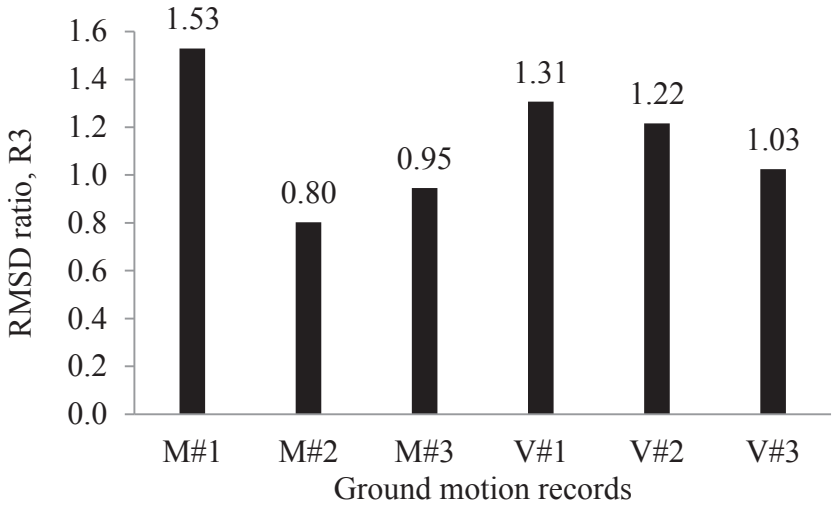

Figure 3.30 RMS displacement, ratio R3 for model A and C in G-1

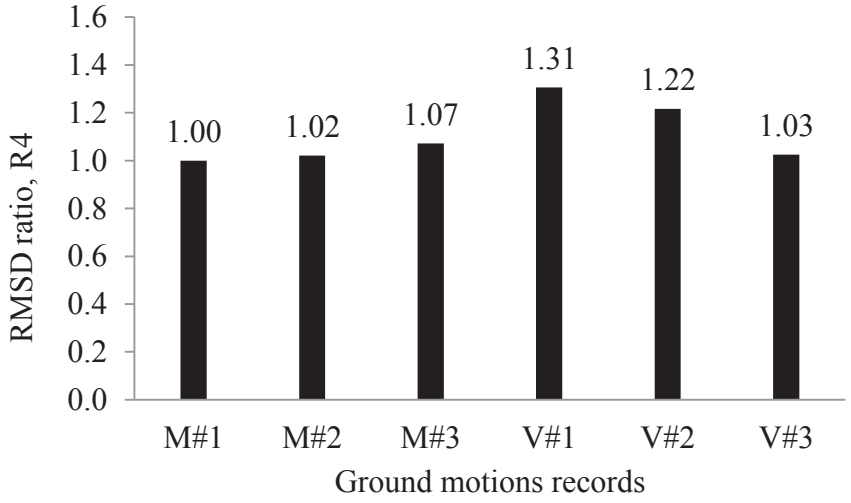

Figure 3.31 RMS displacement, ratio R4 for model A and C in G-2

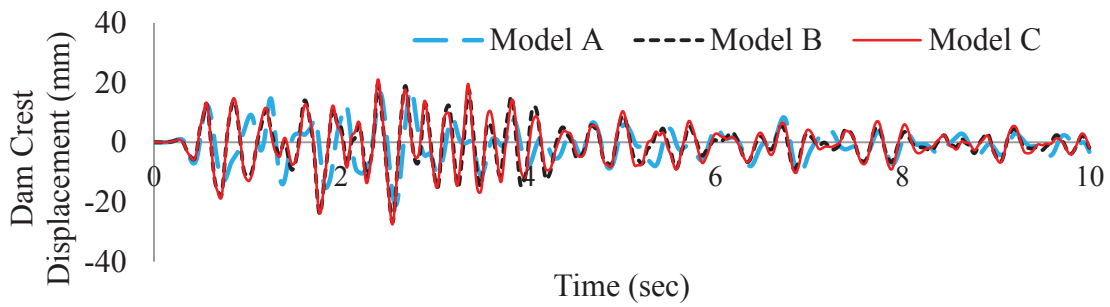

Figure 3.32 Dam crest displacement for San Fernando Earthquake for different models in G-1

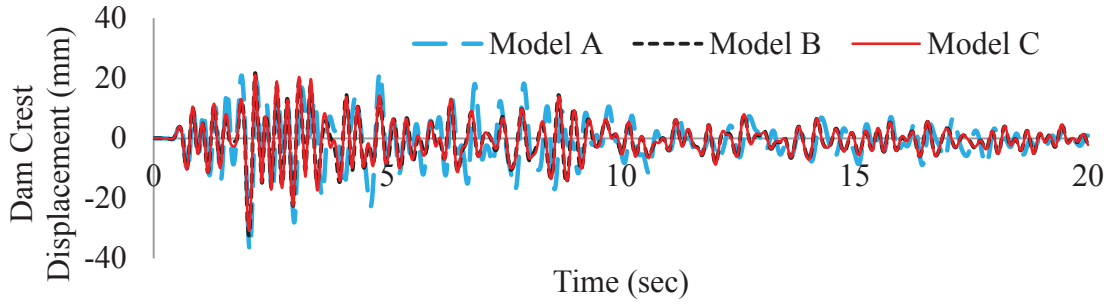

Figure 3.33 Dam crest displacement Friuli 1976 Earthquake for different models in G-1

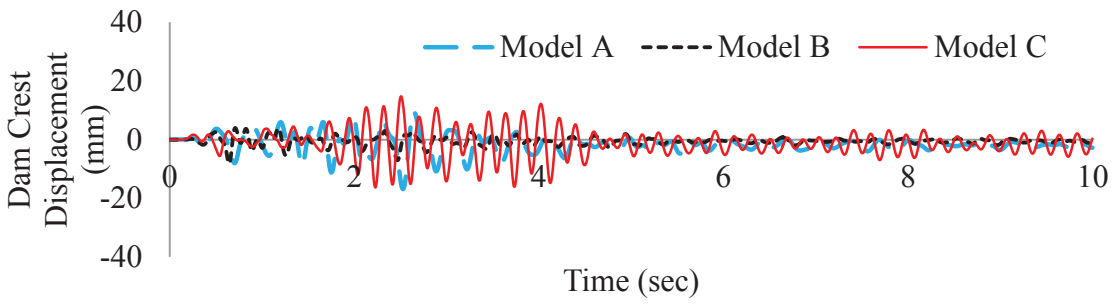

Figure 3.34 Dam crest displacement for San Fernando Earthquake for different models in G-2

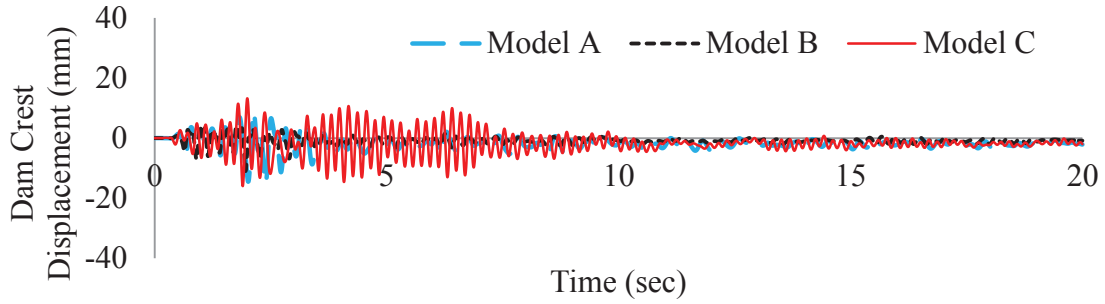

Figure 3.35 Dam crest displacement Friuli 1976 Earthquake for different models in G-2

CHAPTER 4 SEISMIC PERFORMANCE EVALUATION OF CONCRETE GRAVITY DAMS

4.1 Abstract

Elastic and inelastic analysis of dams with different geometries has been performed to study the existing guidelines for the seismic assessment of dams. The performance of the dam models has been assessed using both the high frequency and low frequency earthquake records scaled at 0.35g. Based on the study it can be concluded that the different numerical models induce slight differences in the results relating to the tensile damage in dam foundation system. However, the results are consistent with each other. Also, the results from the linear elastic analysis provided valuable insight about seismic performance of concrete gravity dams but they fail to account for the existing deterioration in the dam.

4.2 Introduction

Satisfactory performance of concrete gravity dams during a seismic event is necessary because the release of the impounded water can cause considerable amount of devastation in the downstream populated areas. The importance of structural reassessment of existing dams has been well recognized. There are existing guidelines developed by several dam managing and owner agencies, dam associations, federal authorities in several countries for seismic evaluation of concrete gravity dams ((CDA, 2007), (FERC, 2002), (FERC, 1999) , (USACE, 2007), (FEMA-65, 2005), (BRE, 1991)). Generally the existing guidelines recommend the linear elastic analysis for the seismic response evaluation of dams under moderate level of seismic hazard and when there is

only a limited extent of damage under the maximum credible earthquake without the release of impounded water. As the inelastic analysis is a time consuming and computationally expensive process, such analysis is recommended only in case of severe damage under a strong earthquake. The performance indicators used for the evaluation in case of linear elastic analysis: (a) the are percentage of area overstressed as compared to the capacity, (b) the cumulative inelastic duration of stresses beyond the capacity of concrete and (c) the sliding safety factor (USACE, 2007).

Ghrib et al. (1995) suggested a progressive analysis methodology for evaluating the seismic safety of concrete gravity dams which involves five analysis levels comprising preliminary screening, pseudo-static, pseudo-dynamic, linear time history and nonlinear history analyses with increasing complexity. In the above methodology, first the possible overstress in a dam using the preliminary screening, pseudo-static and pseudo-dynamic analyses. If the deduced stress distribution is more than the capacity, it is suggested that a linear elastic analysis be followed by a nonlinear dynamic analysis.

Understanding of the behavior of cracked dams during a seismic event is essential for implementation of various rehabilitation schemes. Earlier researchers have used linear elastic analysis (Chakrabarti and Chopra, 1974; Chopra and Gupta, 1982), smeared crack model (Bhattacharjee and Leger, 1993), discrete crack approach based on elastic fracture mechanics (Ayari and Saouma, 1990) and boundary elements model (Pekau et al. , 1995; Batta et al., 1996). In this study the analysis has been performed using a commercial finite element software ABAQUS (Version 6.11). The tensile damage in concrete has been simulated using concrete damage plasticity model proposed by Lubliner et al. (1989) and Lee and Fenves (1998) and extended finite element methods proposed by

Belytschko and Black. (1999). In the extended finite element method, the cohesive damage approach has been used to simulate a discrete crack growth.

The purpose of this paper is to study the behavior of concrete gravity dams during a seismic event and evaluate the sensitivity of the dams behavior to different types of seismic ground motions and analysis models. The results obtained from the elastic analysis are evaluated using the USACE guidelines. The seismic response of the dam of selected geometries has been further evaluated using the nonlinear analysis models such as the extended finite element methods and damaged plasticity model to determine the effectiveness of the linear analysis.

4.3 Numerical Models

4.3.1 *eXtended Finite Element Method (XFEM)*

Belytschko and Black (1999) first introduced the extended finite element method for modeling crack propagation by employing the partition of unity finite element method (Melenk and Babuska, 1996). In this method, additional functions namely enrichment functions are used as tool to a represent discontinuous field variables such as displacement and, stresses. The enrichment functions introduce additional degrees of freedom that are tied to the nodes of the elements intersected by the crack. The crack growth is not associated with the mesh because of the enrichment functions, thus in this method remeshing is not required. The method is considerably efficient in terms of computational power as compared to conventional finite element methods for modeling crack propagation. The approximation for a displacement vector function u is expressed in Equation 4.1.

$$u = \sum_{i=1}^{N} N_1(x)[u_i + H(x)a_i + \sum_{\propto=1}^{4} F_{\propto}(x)b_i^{\propto}] \qquad \text{Equation 4.1}$$

where, N_i (x) are the nodal shape functions, u_i is the nodal displacement associated with the continuous part of the finite element solution, a_i and b_i^{α} are the nodal enriched degrees of freedom vectors associated with discontinuous jump function H(x) (Heaviside function), where H(x) takes on the value of +1 above the crack and -1 below the crack. Figure 4.1 present the node selection for enrichment functions. The crack tip enrichment functions $F_{\propto}$ are obtained from displacement fields as given below.

$$[F_{\propto}(r,\theta), \alpha = 1-4] = \left\{\sqrt{r}\left(\sin\frac{\theta}{2}, \cos\frac{\theta}{2}, \sin\frac{\theta}{2}\ sin\theta, \cos\frac{\theta}{2} sin\theta\right)\right\} \qquad \text{Equation 4.2}$$

where r,θ are local polar co-ordinates defined at the crack tip. Figure 4.2 presents the Normal and Tangential coordinates for a smooth crack. Within the extended finite element framework in ABAQUS the damage modeling has been done using the traction-separation laws based on cohesive damage.

4.3.2 *Concrete damage plasticity model*

The second material model used here is the concrete damage plasticity model which is based on the work of Lubliner et al. (1989) and Lee and Fenves (1998) .The model assumes that the main two failure mechanism are tensile cracking and compressive crushing of the material. The two hardening variables used to characterize the damage states in tension and compression are plastic strains in tension, $\tilde{\varepsilon}_t^{pl}$ and compression, $\tilde{\varepsilon}_c^{pl}$. Figure 4.3 present the response of concrete to uniaxial loading in compression and tension.

$$\sigma_t = \sigma_t(\tilde{\varepsilon}_t^{pl}, \dot{\tilde{\varepsilon}}_t^{pl}, \theta, f_i)$$ Equation 4.3

$$\sigma_c = \sigma_c(\tilde{\varepsilon}_c^{pl}, \dot{\tilde{\varepsilon}}_c^{pl}, \theta, f_i)$$ Equation 4.4

Where, θ is the temperature and $f_i (i = 1,2, \dots)$ are other predefined variables. The degraded response of concrete is characterized by two independent damage variables, d_t and d_c.

$$d_t = d_t\left(\tilde{\varepsilon}_t^{pl}, \dot{\tilde{\varepsilon}}_t^{pl}, \theta, f_i\right), 0 \leq d_t \leq 1$$ Equation 4.5

$$d_c = d_c(\tilde{\varepsilon}_c^{pl}, \dot{\tilde{\varepsilon}}_c^{pl}, \theta, f_i), 0 \leq d_t \leq 1$$ Equation 4.6

4.4 Performance Criteria for concrete gravity dams

Three performance levels considered in (USACE, 2007) are as follows:

a) Minor or no Damage: The response of dam is assumed to be elastic if the Demand Capacity Ratio (DCR) ≤ 1. The dam is considered to behave in elastic range with no possibility of damage.

b) Acceptable Level of Damage: If the DCR ≥ 1 then cracking in dam can be considered with no possibility of failure if the estimated DCR < 2, the overstressed regions are limited to 15 percent of cross sectional area of dam and the cumulative duration of stress excursion also fall below the performance line as shown in Figure 2.3 and Figure 2.4.

c) Severe Damage: If the DCR >2 for a region more than 15 percent of cross section area of dam and the cumulative overstress duration for all values between DCR 1 and 2 fall above the performance curves as shown in Figure

2.3 and Figure 2.4 the damage is considered as severe. It is recommended that the nonlinear time history analysis be performed to further assess the condition of the dam.

4.5 System analyzed

Two different monoliths of concrete gravity dams have been considered in this study. Figure 4.4 and Figure 4.5 present the geometry of the model F-1 and F-2 respectively. The material properties are summarized in Table 4.1. Five percent material damping is considered in the analysis with Rayleigh damping assumptions. However, in case of nonlinear analysis damping was ignored as cracking of concrete provides sufficient damping mechanisms and energy dissipation in the analysis. The hydrodynamic interaction is modeled via added mass model using incompressible water. The dam and foundation system is modeled using four noded bilinear plain strain finite elements. Figure 4.6 and Figure 4.7 present the finite element mesh for dam-foundation system F-1 and F-2 respectively. The time periods for the dam-foundation system F-1 and F-2 are found to be 0.628 s and 0.617 s respectively.

Two different ground motions San Fernando 1971 earthquake and Livermore 1980 earthquake have been considered here. Figure 4.8 and Figure 4.9 present the response spectra of the both ground motions. Both the ground motions have been scaled to the level of 0.35g. The horizontal and vertical components are denoted by H and V respectively. The vertical component of all ground motions were scaled to the two third of the respective horizontal components of the ground motions have been selected based on their different frequency content. San Fernando earthquake and Livermore earthquake

have high and low frequency contents, respectively. The frequency contents of both the ground motions are presented in Figure 4.10 and Figure 4.11 respectively.

The Deconvolution analysis has been performed according to the proposed deconvolution procedure as discussed in the Chapter 3. The results of the deconvolution of dam-foundation system F-1 can be found in Chapter-3 corresponding to G-1. Figure 4.12 through Figure 4.15 present the results of deconvolution of dam-foundation system F-2 for both the ground motions.

4.6 Results

The response of the dam foundation system subjected to an earthquake has been determined in terms of the response parameters such as overstressed areas, cumulated inelastic stress, factor of safety etc. Figure 4.16 and Figure 4.17 present the overstressed area and cumulative inelastic duration stress cycles of dam-foundation system F-1 for San Fernando Earthquake 1971. It is clear from the figures that the dam suffers a considerable damage as the overstressed area is more than 15 %. Figure 4.18 and Figure 4.19 show the overstressed area and cumulative inelastic duration of stress cycles of dam-foundation system F-1 for Livermore Earthquake 1980. Figure 4.18 clearly shows that the overstressed area is under the suggested threshold. However, the cumulative inelastic duration is above the suggested threshold. Therefore, a limited damage around the neck of the dam is expected. Figure 4.20 and Figure 4.21 present the time history of the factor of safety against sliding of dam-foundation system F-1 for different earthquake records. The time history of the factor of safety has been obtained from the ratio of normal gravity forces to the driving shear forces at interface of dam and foundation. The friction of coefficient is assumed to be one unit value. It can be observed that throughout the

analysis the instantaneous factor of safety is above unity; thus, there is no indication of sliding during the earthquake. The tensile damage at the end of the analysis of dam-foundation system F-1 with concrete damage plasticity model for different earthquakes is shown in Figure 4.22 and Figure 4.23 . Figure 4.24 and Figure 4.25 present the tensile damage at the end of the analysis of dam-foundation system F-1 with the extended finite element method with cohesive damage model for different ground motions. It clear from these figures that both the nonlinear numerical models indicate the damage in the dam in appropriate locations. However, there is a slight difference in the extent of the tensile damage estimated by these methods.

The overstressed area and cumulative inelastic duration stress cycles of dam-foundation system F-2 for San Fernando Earthquake 1971 are presented in Figure 4.26 and Figure 4.27. It can be inferred from the figures that the dam suffers significant damage as the overstressed area is around 16% which is more than 15%. Figure 4.28 and Figure 4.29 present the overstressed area and cumulative inelastic duration of stress cycles of dam-foundation system F-2 for Livermore Earthquake 1980. The overstressed area as shown in Figure 4.28 is under the suggested threshold. However, the cumulative inelastic duration is above the threshold. Therefore, a limited damage is expected. Figure 4.30 and Figure 4.31 present the time history of factor of safety against sliding of dam-foundation system F-2 for different earthquake records. As presented in the figures that instantaneous factor of safety against sliding is always more than unity, thus no sliding is expected. The tensile damage at the end of the analysis of dam-foundation system F-2 with concrete damaged plasticity model for different earthquake is present by Figure 4.32 and Figure 4.33 . Figure 4.34 and Figure 4.35 show the tensile damage at the end of the

analysis of dam-foundation system F-2 with extended finite element methods with cohesive damage model for different ground motions.

The failure of the dam cannot be merely attributed to the seismic activity; perhaps it is a sequence of events that lead to the failure of structure. In short as in case of San Fernando earthquake the seismic event causes excessive cracks in the dam that may lead to independent block failure, if the seismic event remains for a sufficient period of time. In case of Livermore earthquake less cracks are predicted by the numerical models for both the geometries. However it may still lead to failure of the dams as the small cracks can propagate along the lift lines and ultimately lead to the failure of dam. The effects of the load may also be enhanced as due to the deterioration of the structures over the years due to the freeze-thaw cycles and alkali aggregate reaction. The present guidelines recommend the acceptance limits in the forms of overstresses, cumulative time periods etc. However, the elastic analysis fails to account for the already deteriorated condition of the structure. Non-linear analysis can be employed to consider all these parameters such as the already existing deterioration, nonlinearity in the materials etc. However, in case of nonlinear analysis there is also addition of uncertainty in the model because of the complexity in input parameters in these models. Therefore, even after performing a complex nonlinear analysis the decision is made based on engineering judgment because of the lack of confidence in the numerical model due to added uncertainty in the results.

4.7 Conclusion

Elastic and inelastic analyses of dams with different geometries have been performed here to study the existing guidelines for the seismic assessment of dams. The elastic and inelastic analyses provide generally consistent results with respects to the existing

guidelines. It has been observed that under San Fernando earthquake the considered dam models are expected to suffer more damage as compared to Livermore earthquake. It has been observed that different numerical models induce slight differences in the results relating to the tensile damage in dam foundation system. However, the results are consistent with each other. Thus, the influence of the nonlinear models and input parameters needs be studied in depth to ensure the reliability of the nonlinear analysis and techniques.

Table 4.1 Material properties for models F-1 and F-2

Material	Concrete	Rock
Elastic Modulus (MPa)	3.45×10^4	2.76×10^4
Poisson's ratio	0.2	0.33
Unit weight (kN/m3)	23.5	25.9
Compressive strength, kPa	15×10^3	-
Static tensile strength, kPa	1.5×10^3	-
Static fracture energy, N/m	150	-

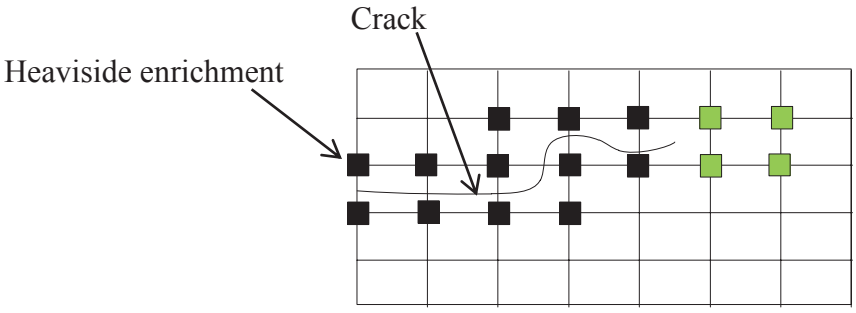

Figure 4.1 Node selection for enrichment functions

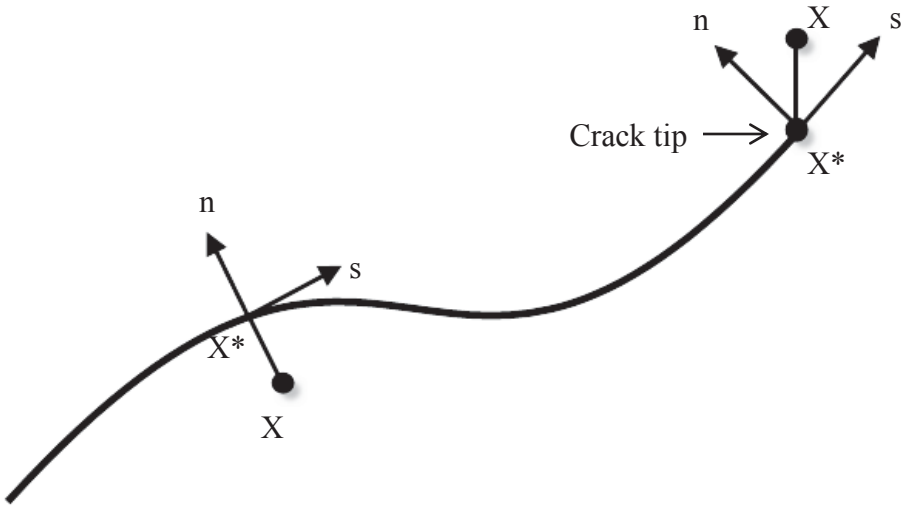

Figure 4.2 Normal and tangential coordinates for a smooth crack

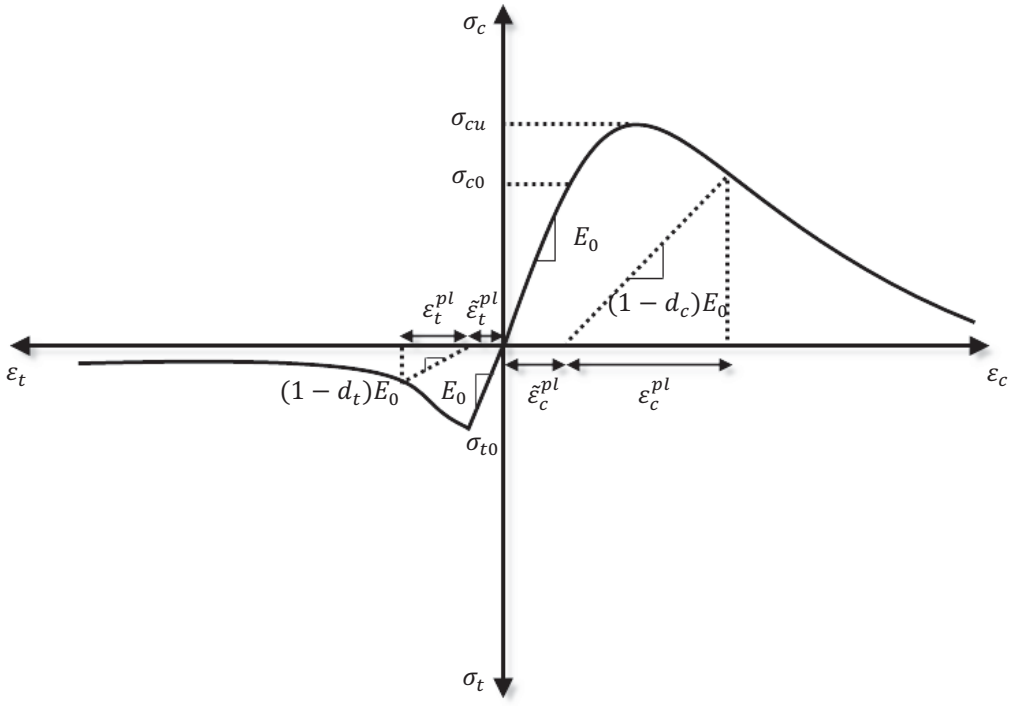

Figure 4.3 Response of concrete to uniaxial loading in tension and compression

Figure 4.4 Dam foundation system, F-1

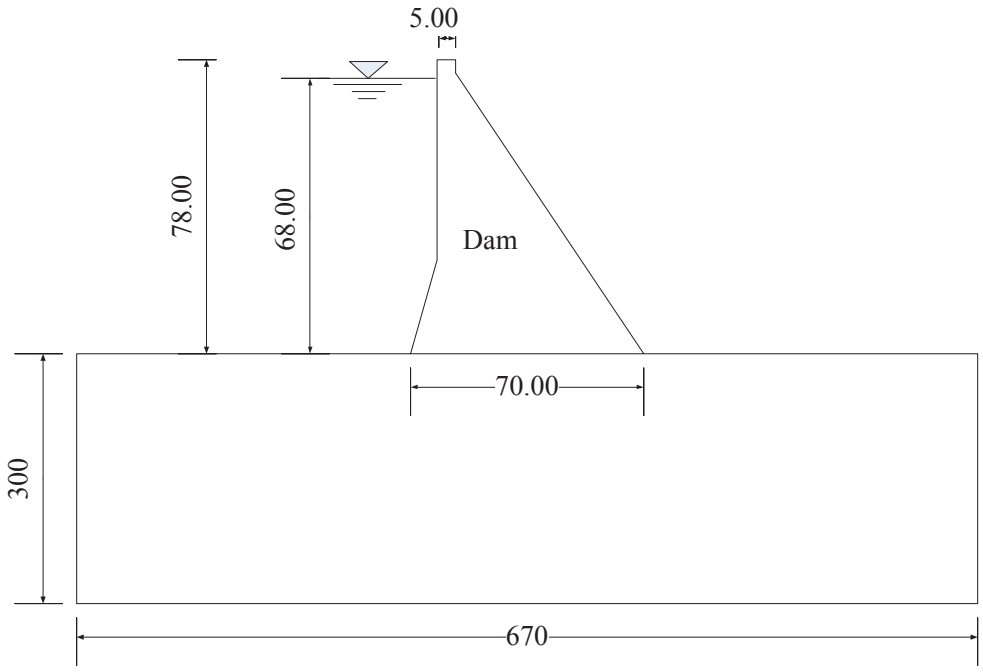

Figure 4.5 Dam foundation system, F-2

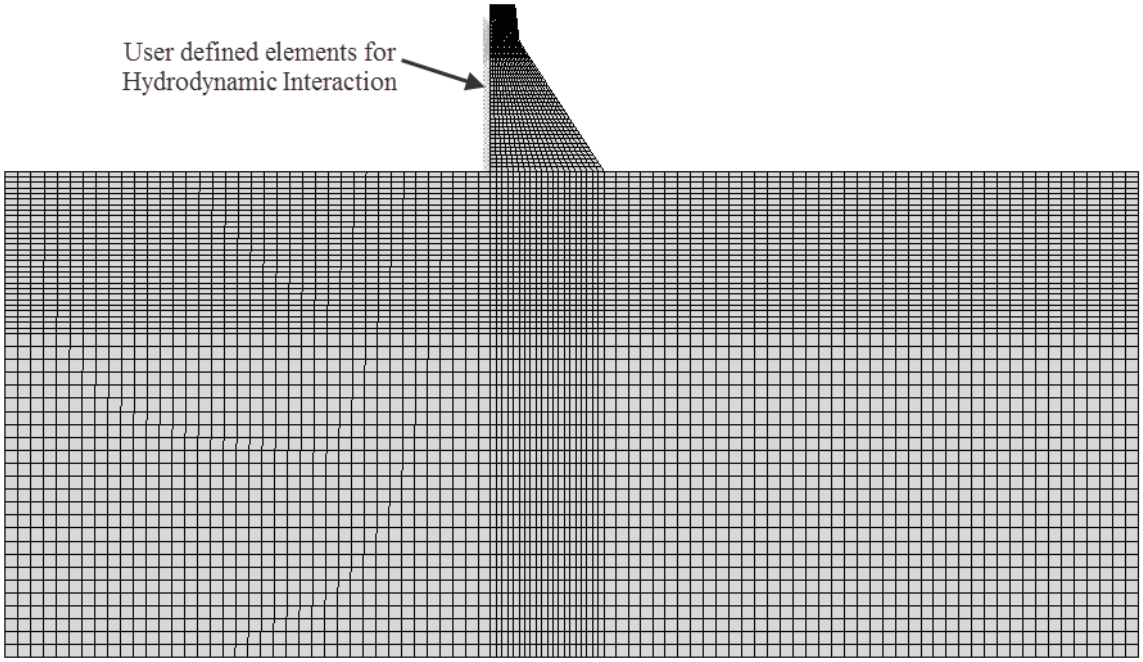

Figure 4.6 Finite element mesh of Dam-Foundation system, F-1

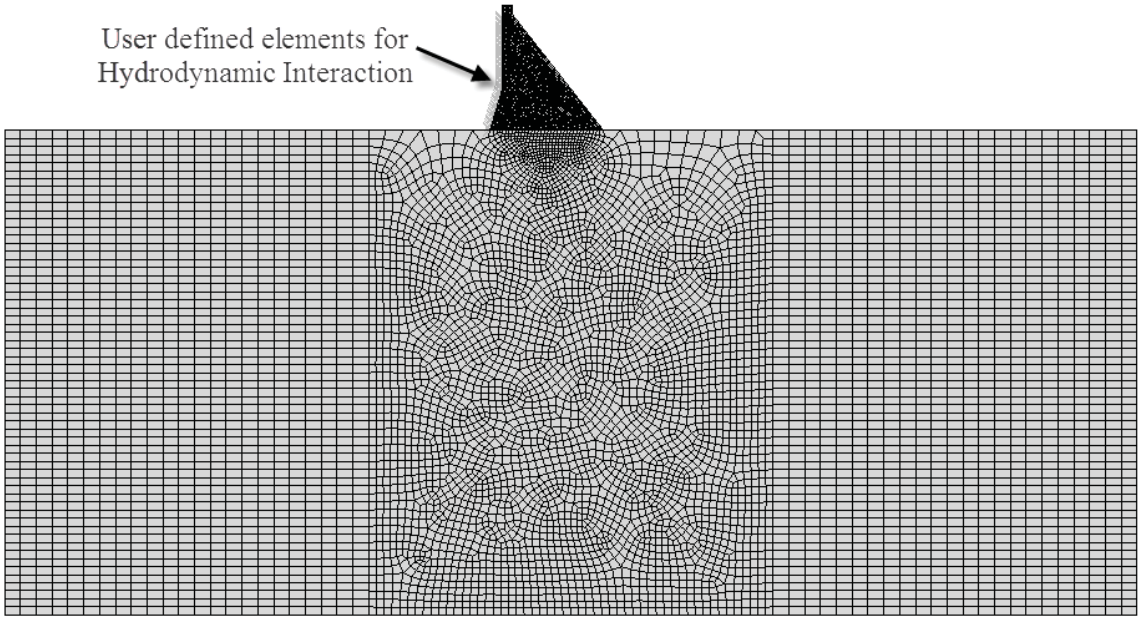

Figure 4.7 Finite element mesh of Dam-Foundation system, F-2

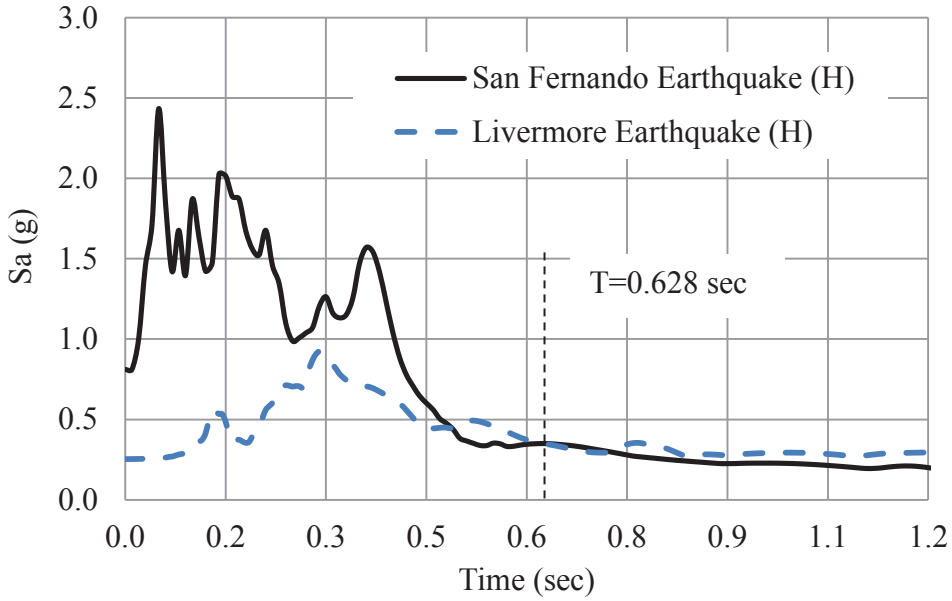

Figure 4.8 Response spectra for San Fernando (H) and Livermore (H) earthquake scaled to 0.35g at 0.628 sec

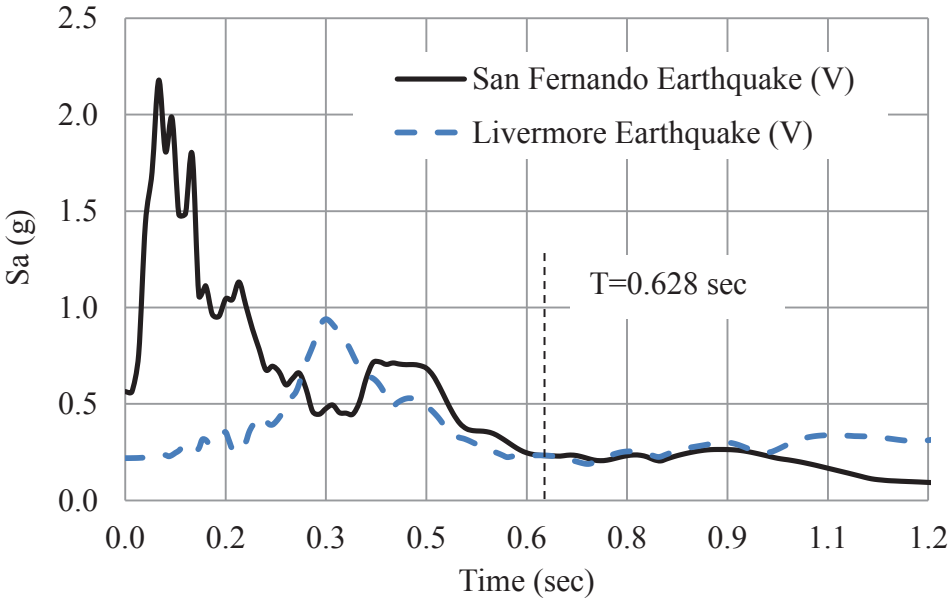

Figure 4.9 Response spectra for San Fernando (V) and Livermore (V) earthquake scaled to 0.35g at 0.628 sec

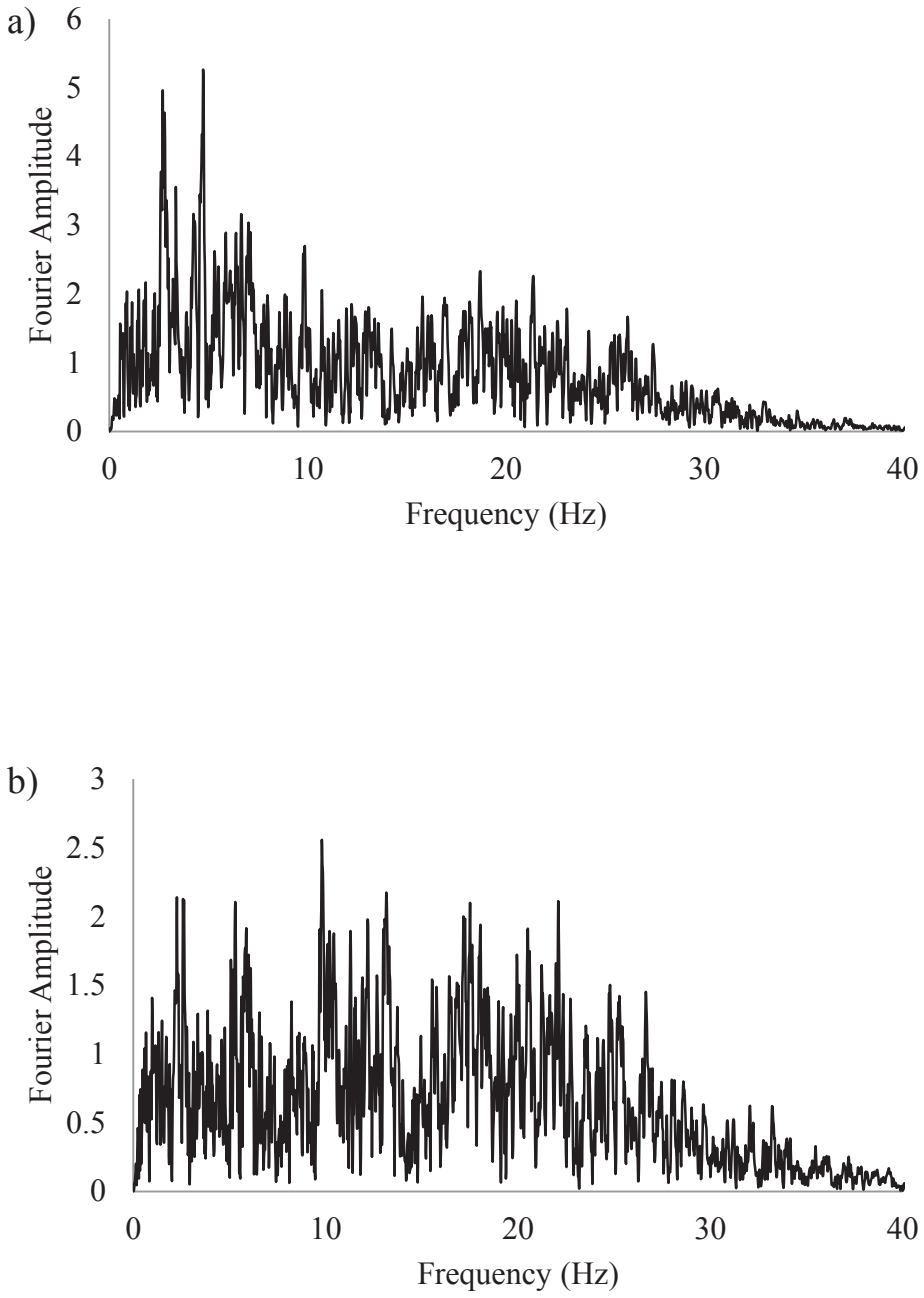

Figure 4.10 Fourier amplitude spectra for San Fernando earthquake: a) Horizontal component; b) Vertical component

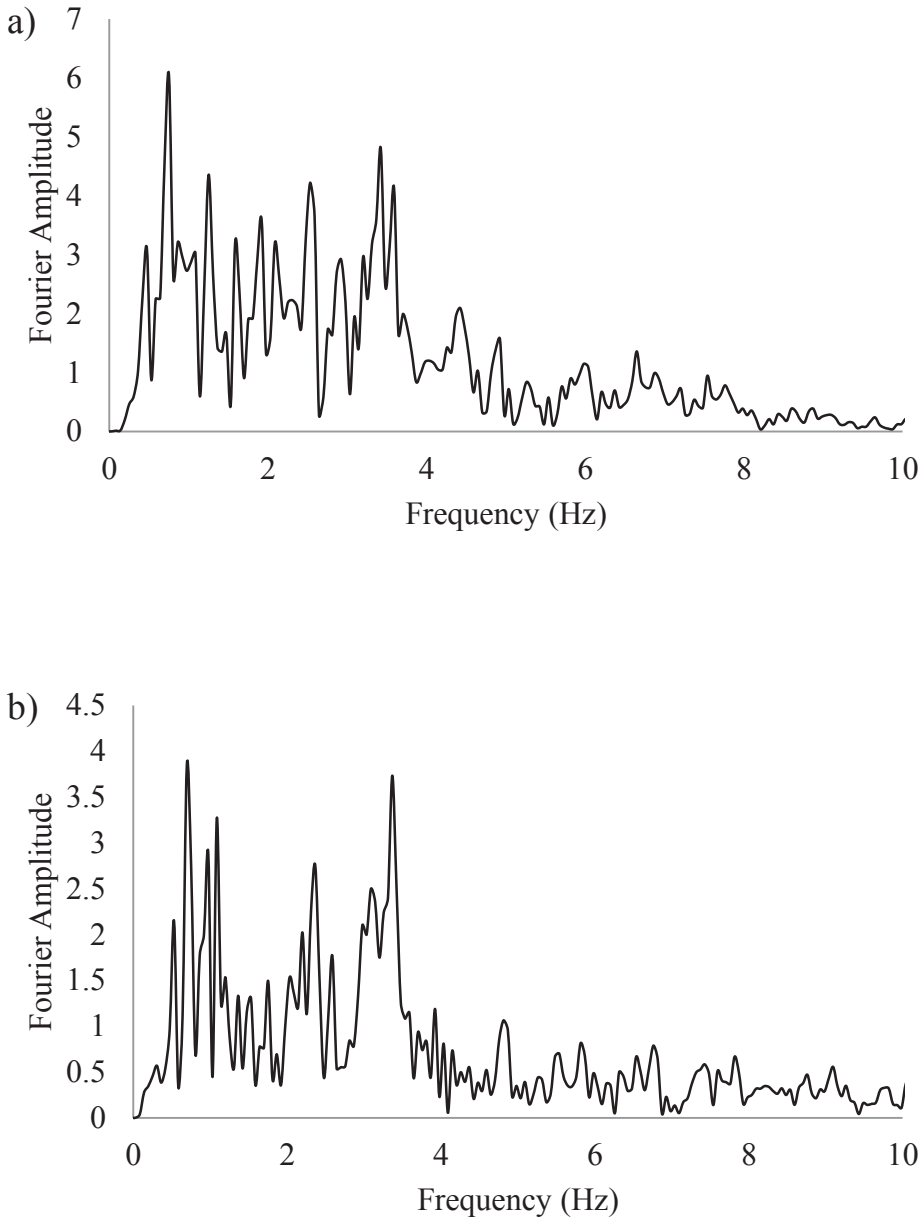

Figure 4.11 Fourier amplitude spectra for Livermore earthquake: a) Horizontal component; b) Vertical component

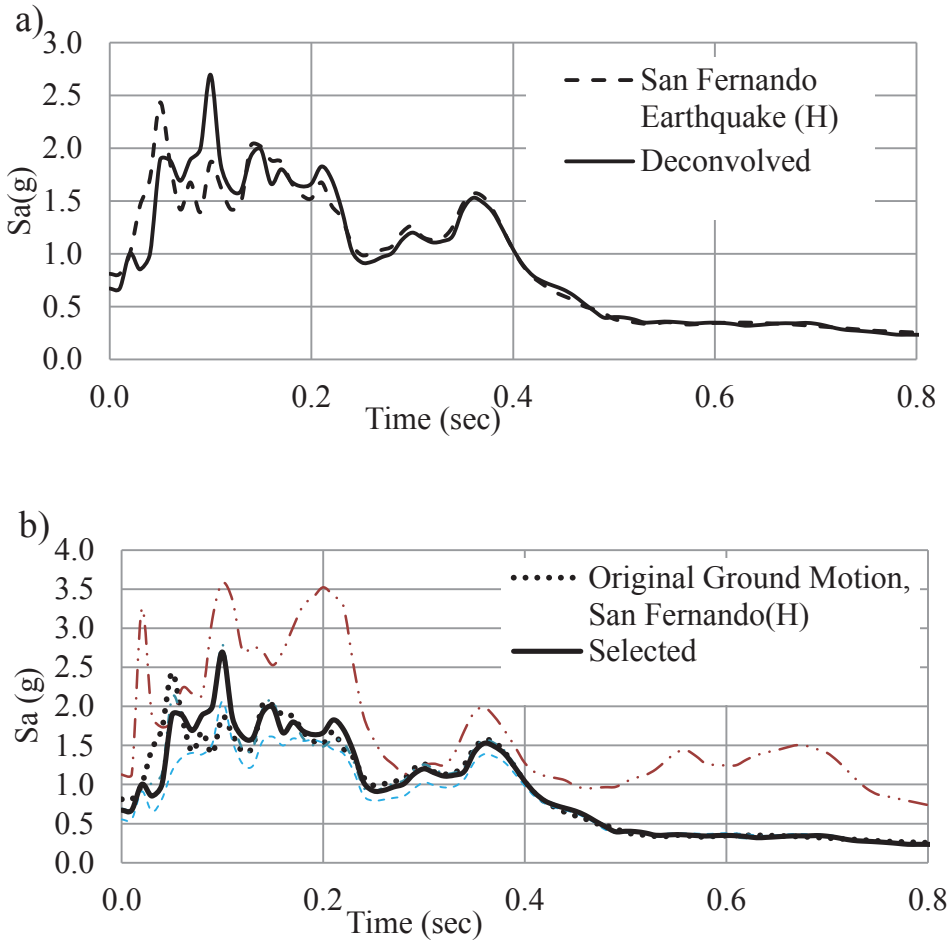

Figure 4.12 Deconvolved ground motions for dam-foundation system F-2: a) San Fernando Earthquake (H) with selected deconvolved ground motion; b) San Fernando Earthquake (H) with selected deconvolved ground motion and rest of iterations.

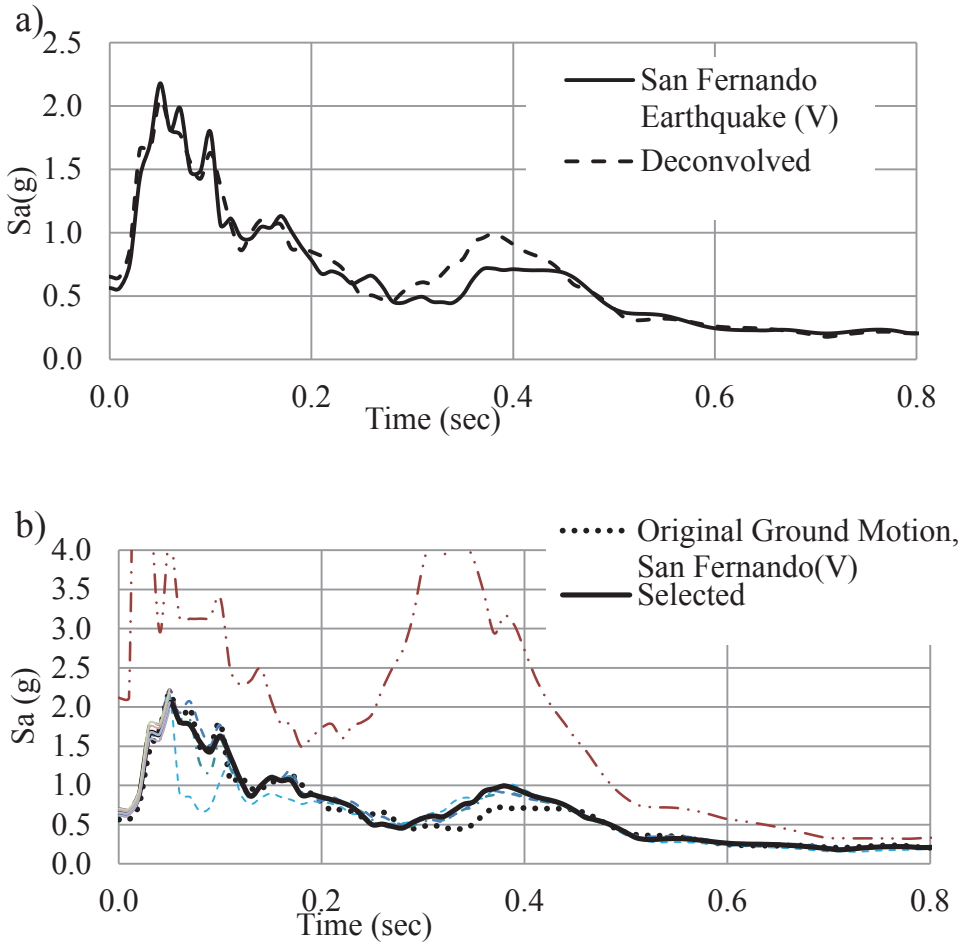

Figure 4.13 Deconvolved ground motions for dam-foundation system F-2: a) San Fernando Earthquake (V) with selected deconvolved ground motion; b) San Fernando Earthquake (V) with selected deconvolved ground motion and rest of iterations.

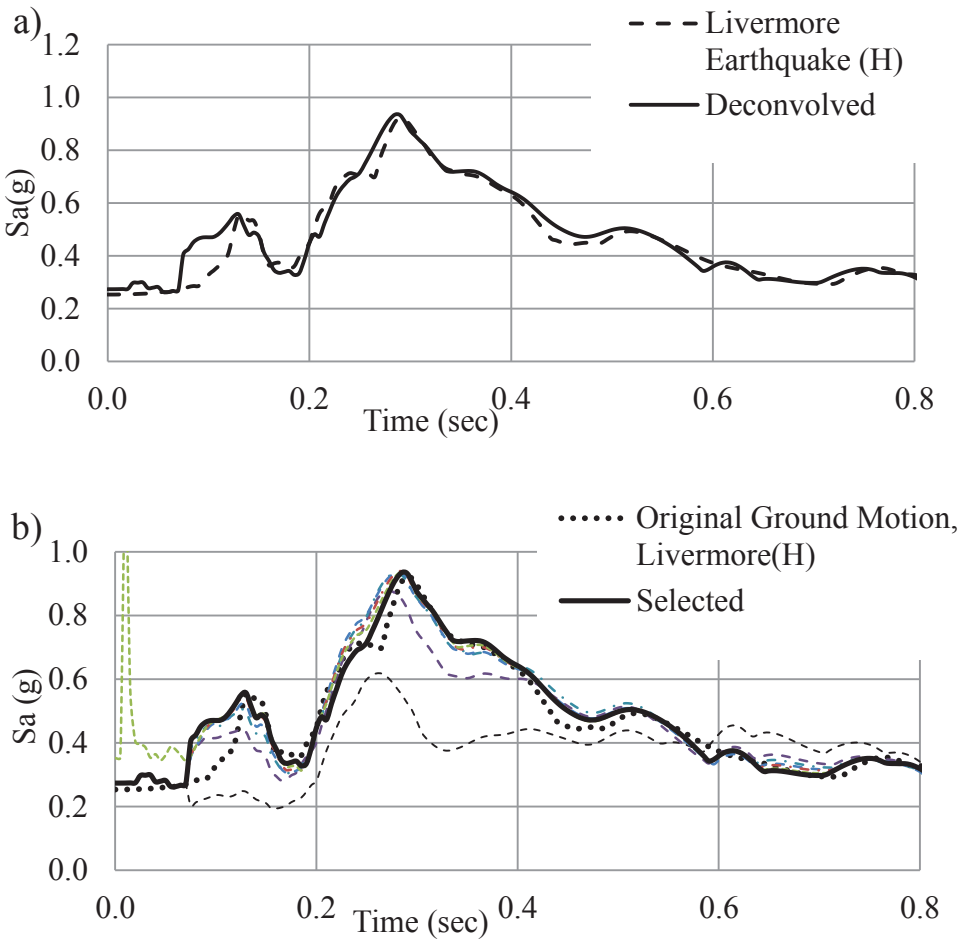

Figure 4.14 Deconvolved ground motions for dam-foundation system F-2: a) Livermore Earthquake (H) with selected deconvolved ground motion; b) Livermore Earthquake (H) with selected deconvolved ground motion and rest of iterations.

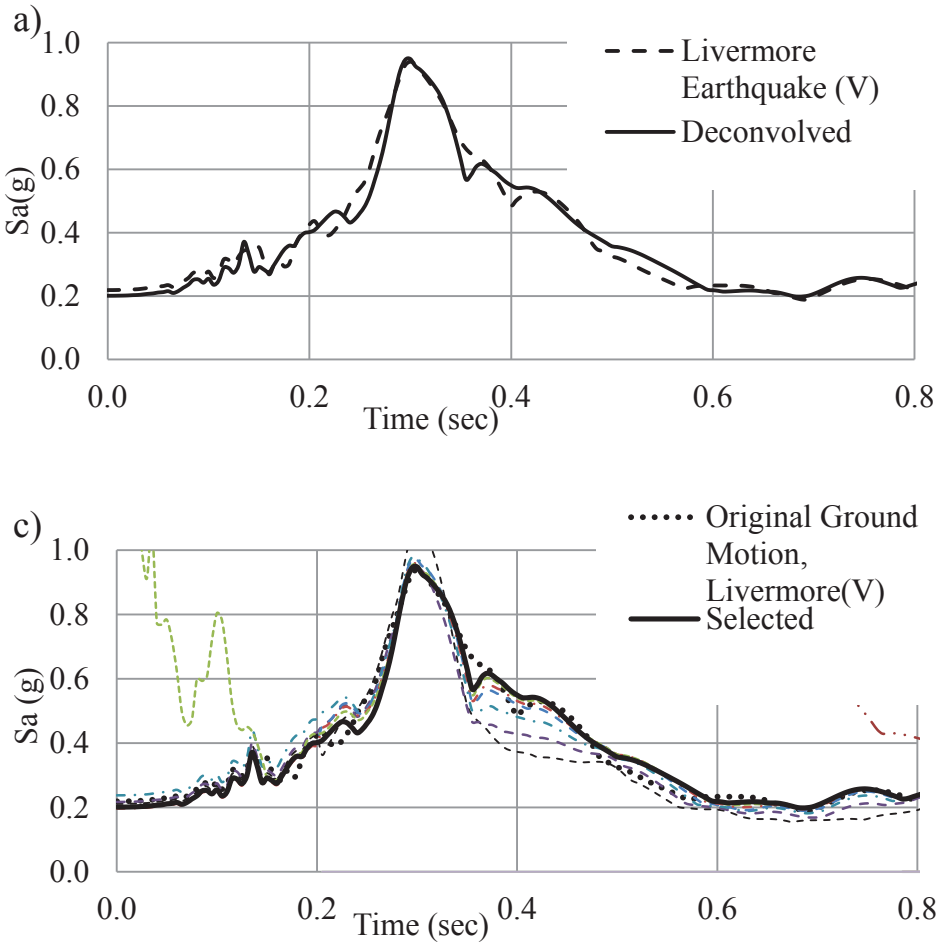

Figure 4.15 Deconvolved ground motions for dam-foundation system F-2: a) Livermore Earthquake (V) with selected deconvolved ground motion; b) Livermore Earthquake (V) with selected deconvolved ground motion and rest of iterations.

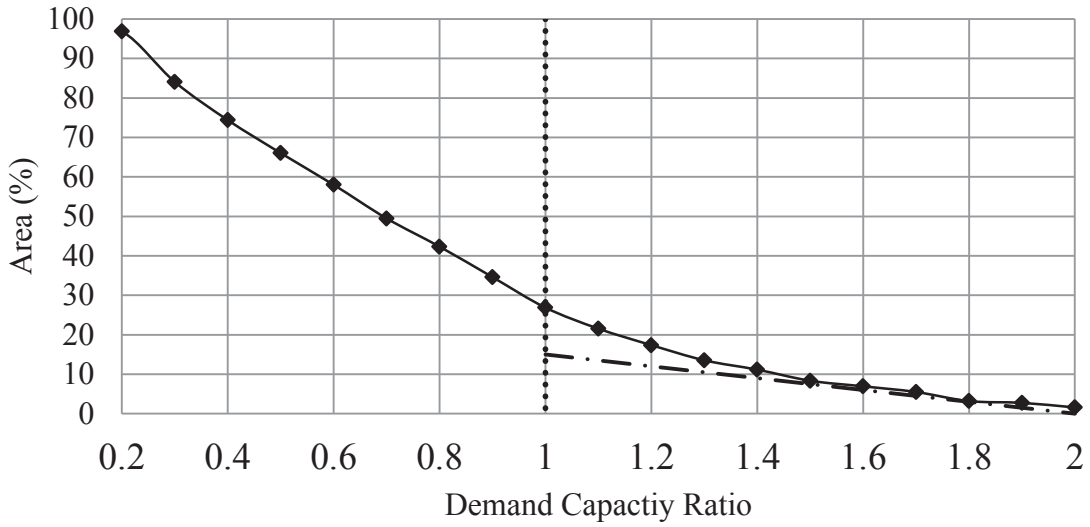

Figure 4.16 Percentage of Overstressed area with acceptance limit of dam-foundation system F-1 for San Fernando Earthquake, 1971

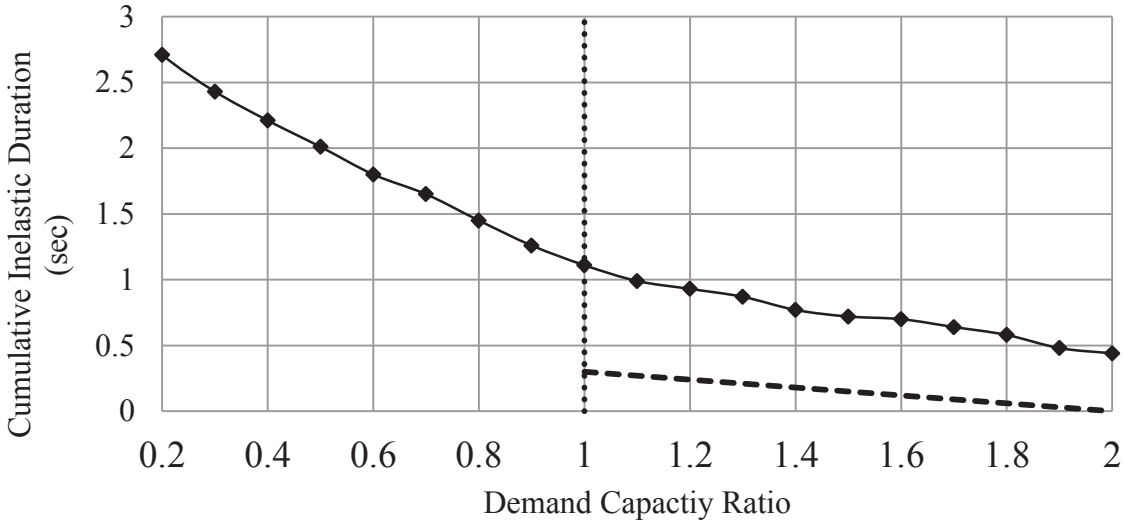

Figure 4.17 Cumulative duration of stress cycles of dam-foundation system F-1 with acceptance limits for the stresses at the change of slope on downstream face for San Fernando Earthquake, 1971

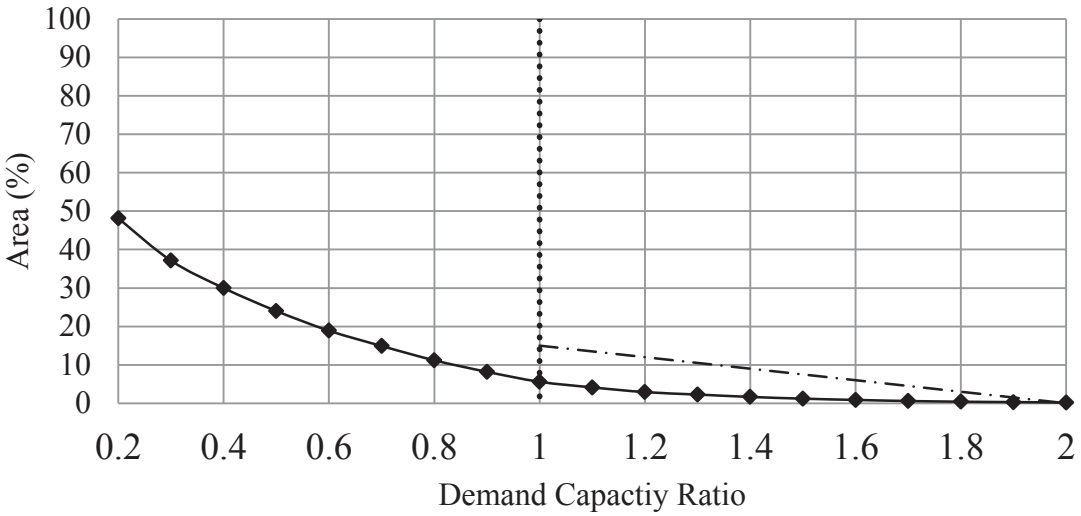

Figure 4.18 Percentage of Overstressed area of dam-foundation system F-1 with acceptance limit for Livermore Earthquake, 1980

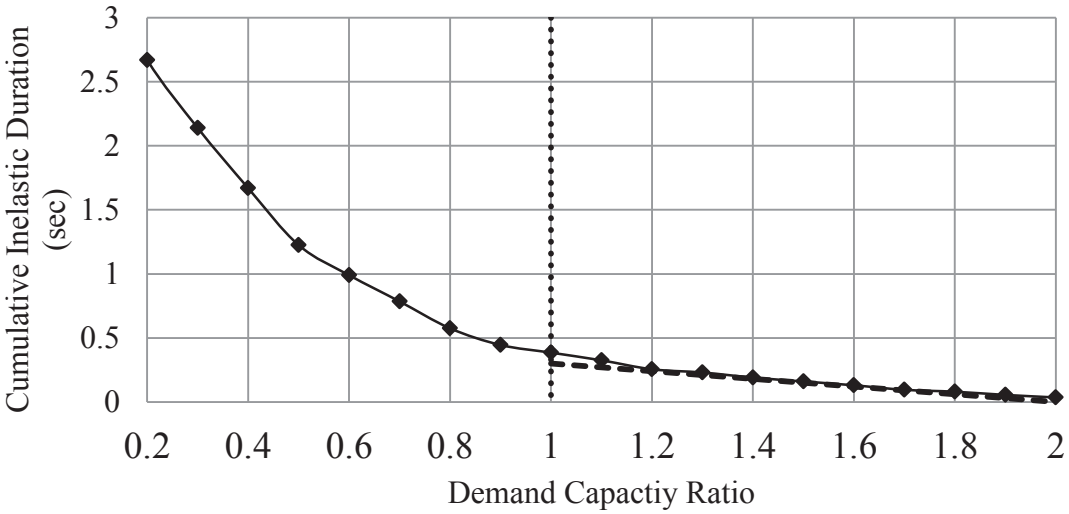

Figure 4.19 Cumulative duration of stress cycles of dam-foundation system F-1 with acceptance limits for the stresses at the change of slope on downstream face for Livermore Earthquake, 1980

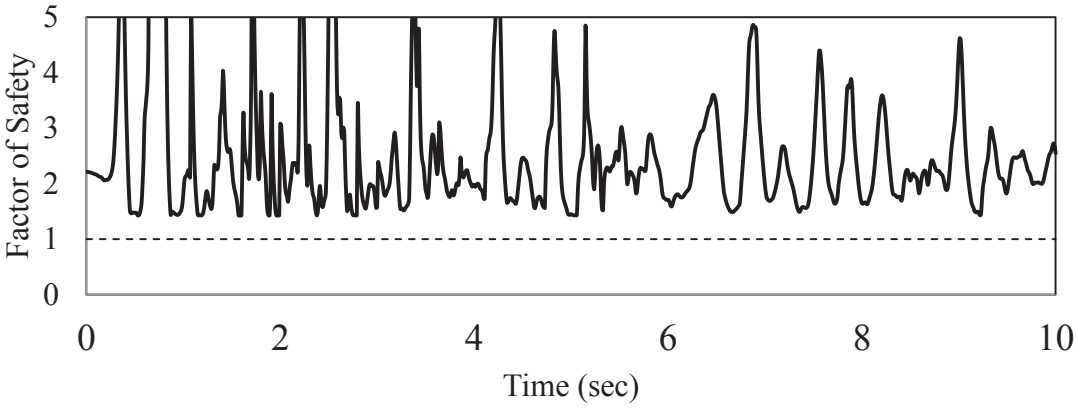

Figure 4.20 Factor of Safety against sliding of dam-foundation system F-1 for San Fernando Earthquake, 1971

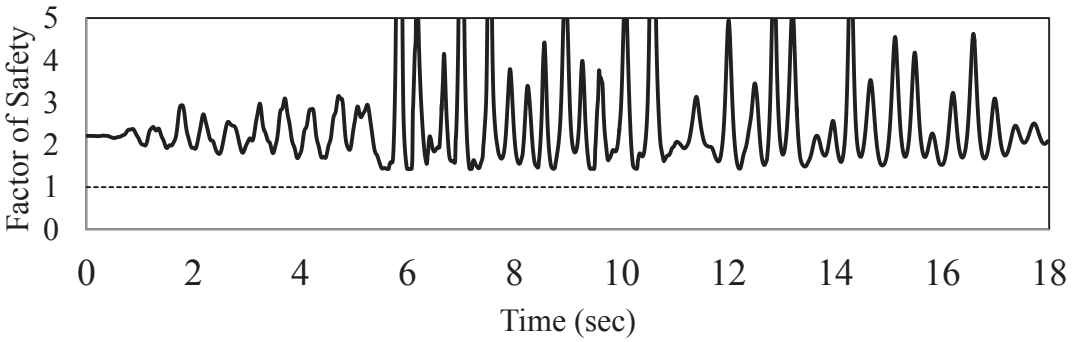

Figure 4.21 Factor of Safety against sliding of dam-foundation system F-1 for Livermore Earthquake, 1980

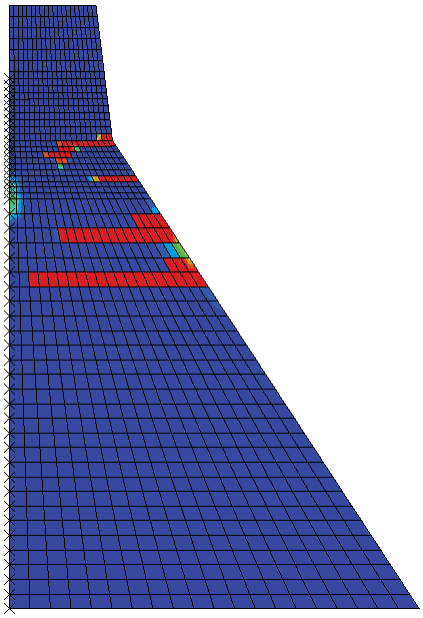

Figure 4.22 Tensile damage of dam-foundation system F-1 at the end of the analysis with Concrete Damaged Plasticity Model for San Fernando Earthquake, 1971

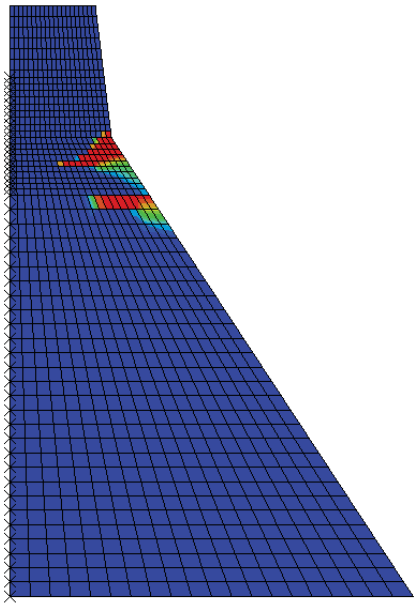

Figure 4.23 Tensile damage of dam-foundation system F-1 at the end of the analysis with Concrete Damaged Plasticity Material Model for Livermore Earthquake, 1980

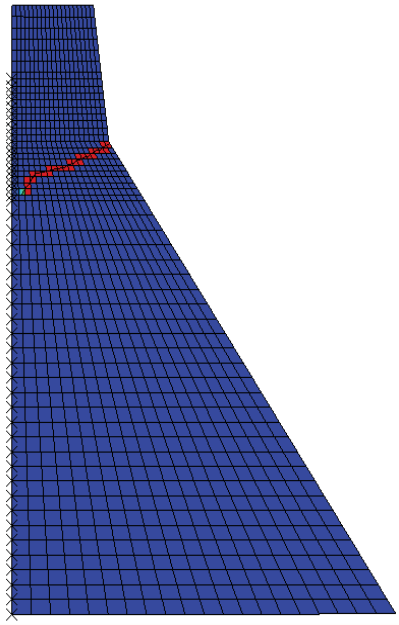

Figure 4.24 Tensile damage of dam-foundation system F-1 at the end of the analysis with Extended Finite Element Methods for San Fernando Earthquake, 1971

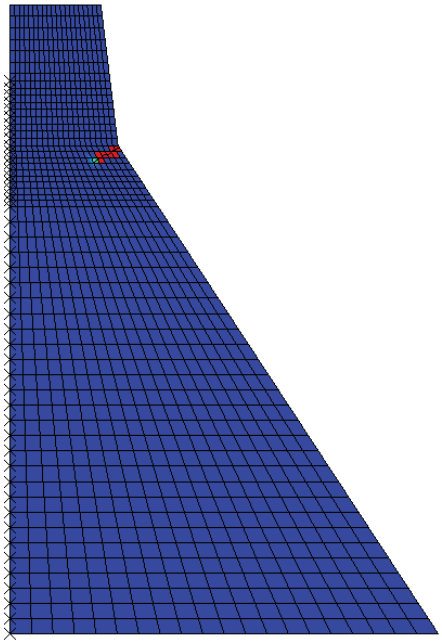

Figure 4.25 Tensile damage of dam-foundation system F-1 at the end of the analysis with Extended Finite Element Methods for Livermore Earthquake, 1980

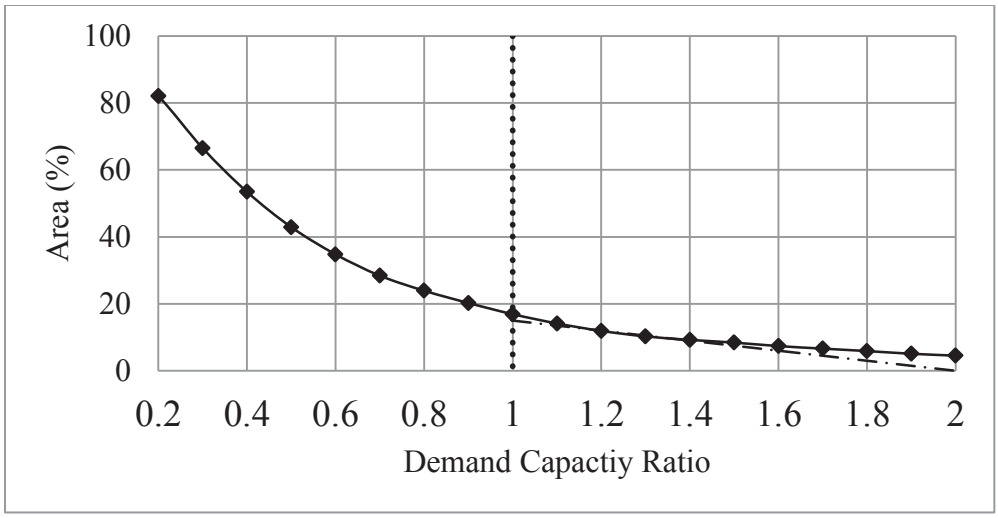

Figure 4.26 Percentage of Overstressed area of dam foundation system F-2 with acceptance limit for San Fernando Earthquake, 1971

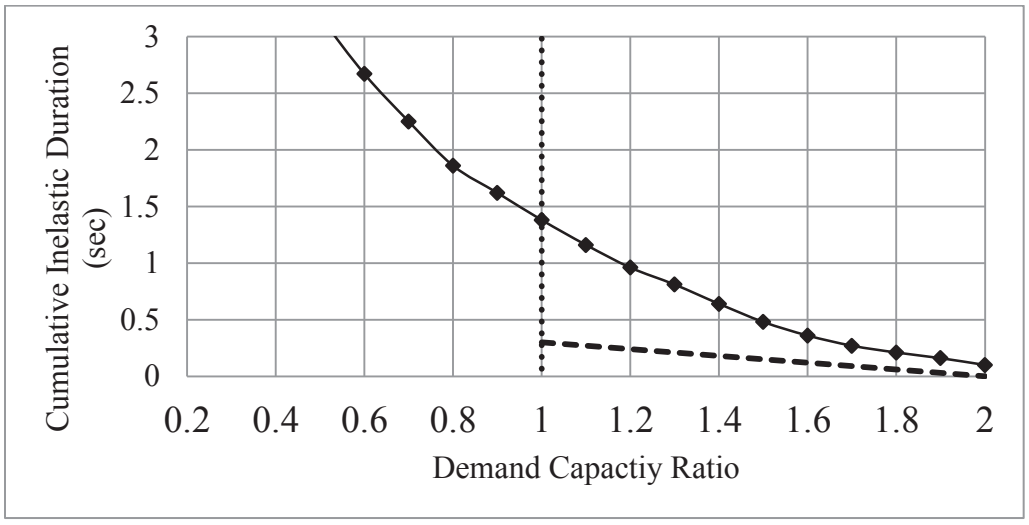

Figure 4.27 Cumulative duration of stress cycles of dam foundation system F-2 with acceptance limits for the stresses at the change of slope on upstream face for San Fernando Earthquake, 1971

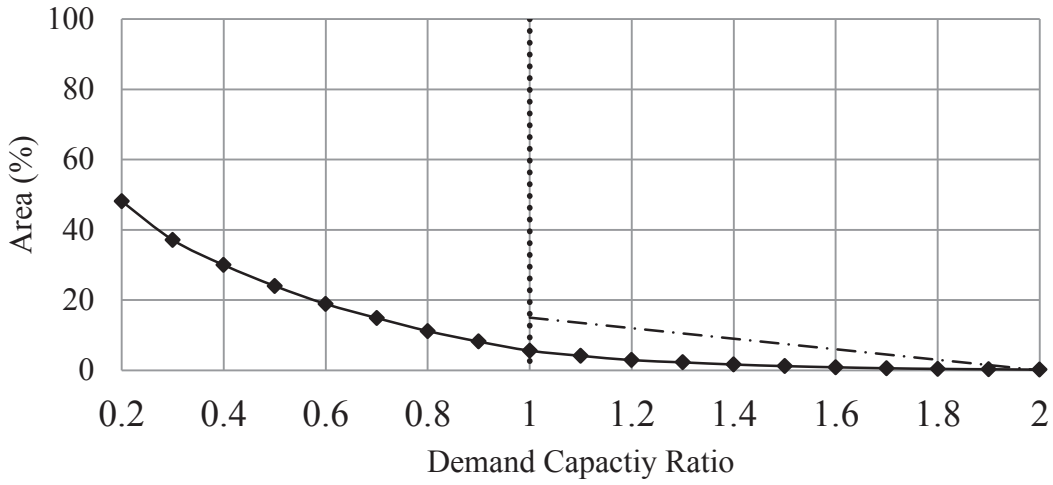

Figure 4.28 Percentage of Overstressed area of dam-foundation system F-2 with acceptance limit for Livermore Earthquake, 1980

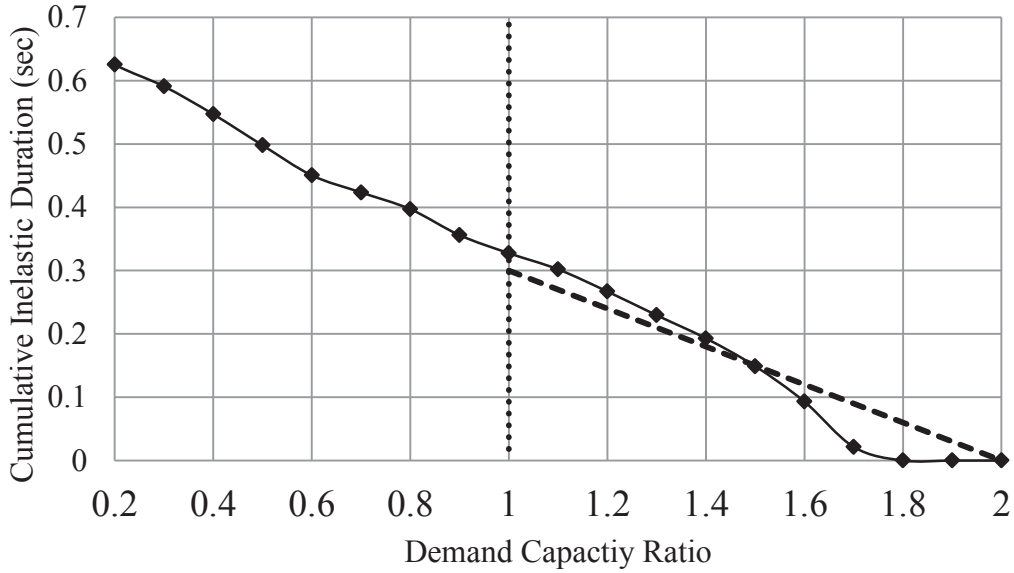

Figure 4.29 Cumulative duration of stress cycles of dam-foundation system F-2 with acceptance limits for the stresses at the change of slope on upstream face for Livermore Earthquake, 1980

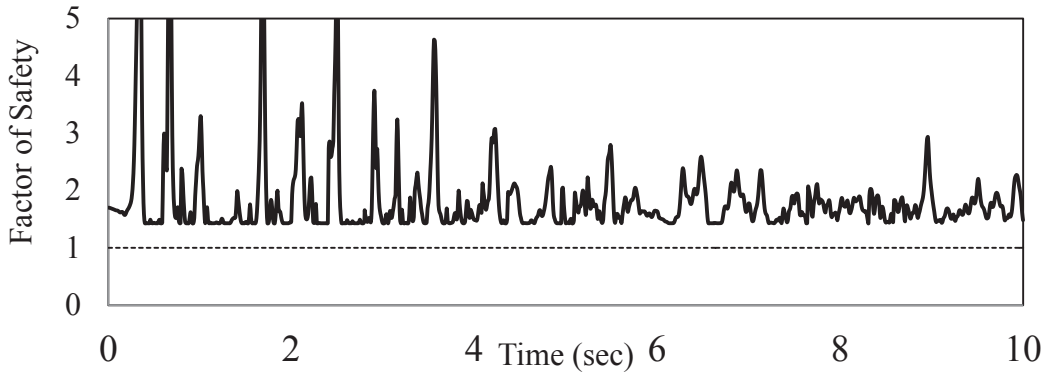

Figure 4.30 Safety of factor against sliding of dam foundation system F-2 for San Fernando Earthquake, 1971

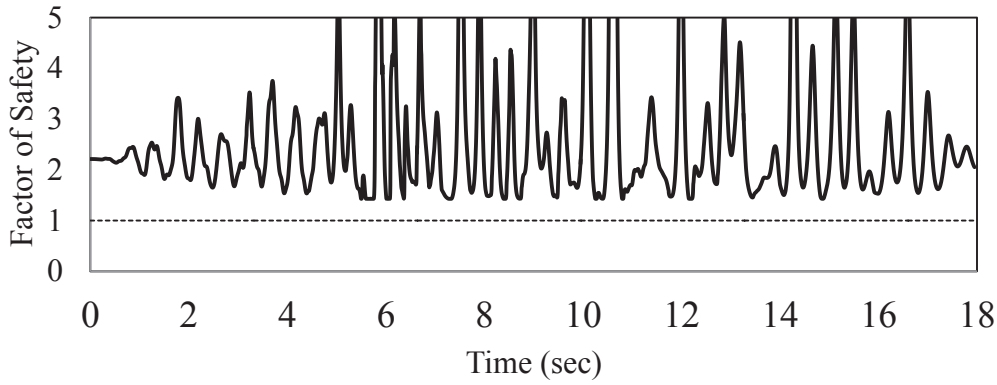

Figure 4.31 Factor of Safety against sliding of dam-foundation system F-2 for Livermore Earthquake, 1980

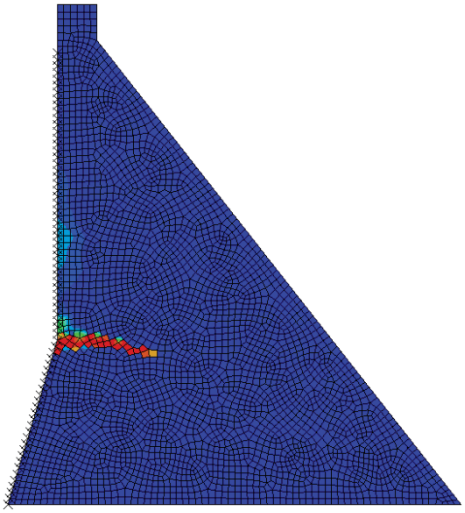

Figure 4.32 Tensile damage of dam-foundation system F-2 at the end of the analysis with Concrete Damaged Plasticity Model for San Fernando Earthquake, 1971

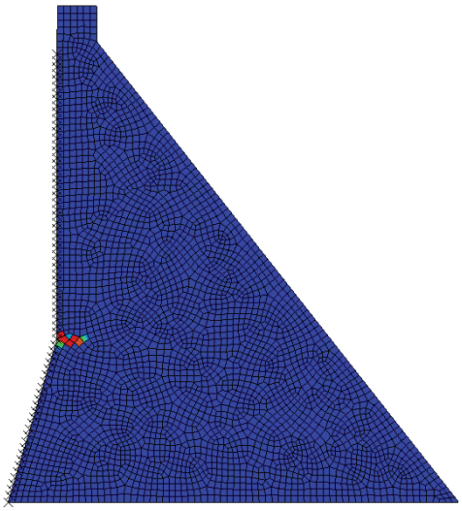

Figure 4.33 Tensile damage of dam-foundation system F-2 at the end of the analysis with Concrete Damaged Plasticity Material Model for Livermore Earthquake, 1980

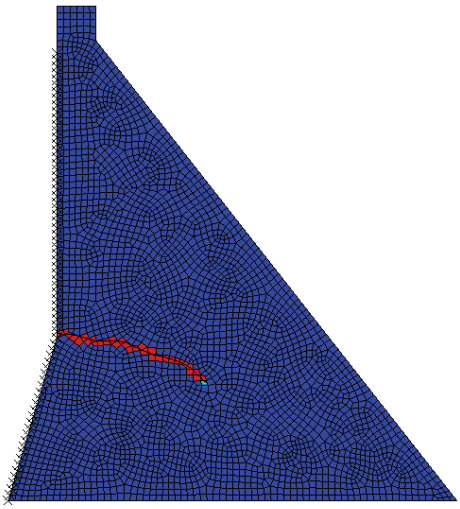

Figure 4.34 Tensile damage of dam-foundation system F-2 at the end of the analysis with Extended Finite Element Methods for San Fernando Earthquake, 1971

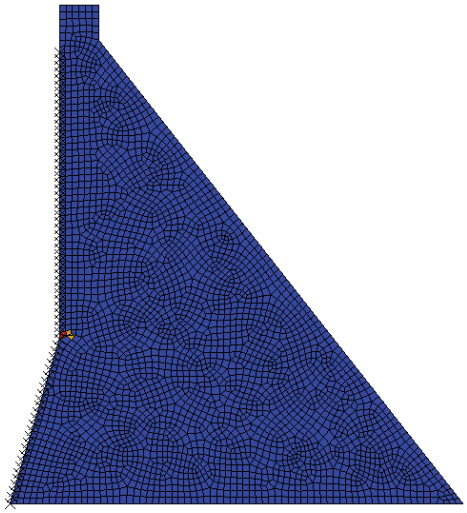

Figure 4.35 Tensile damage of dam-foundation system F-2 at the end of the analysis with Extended Finite Element Methods for Livermore Earthquake, 1980

CHAPTER 5 SUMMARY AND CONCLUSIONS

5.1 Summary

The consequences of the failure of the concrete gravity dam have been long recognized. Therefore, it is important that the interaction among dam, foundation and reservoir is considered for the seismic evaluation of concrete gravity dams. The sub-structuring approach employed in previous studies (Chakrabarti and Chopra, 1974; Fenves and Chopra, 1985) cannot be used in solving nonlinear problems. Therefore, seismic response analysis must be carried out in time domain as it allows the inclusion of nonlinear behavior in a system. In the present study, the following different earthquake input mechanisms have been considered: A) massless foundation input model, B) free-field earthquake input at dam foundation interface model, C) deconvolved earthquake input model. Also, in this study a modified deconvolution procedure has been proposed for the efficient deconvolution of both high and low frequency earthquake records. Two different geometrical models have been selected to represent a dam-foundation system, and they are used here to evaluate the performance of different earthquake input mechanism. It is concluded that Model C is the most accurate one as compared to the other models. Model B does not yield appropriate results for irregular geometries. The performance of Model A is also questionable as it neglects dam-foundation interaction effects.

In the second part of this study, elastic and inelastic analyses have been performed to study the existing guidelines for the seismic assessment of dams. Concrete damage plasticity model and extended finite element method haven been utilized here for the nonlinear analysis of dam-foundation systems. It has been observed that different

numerical models yield slightly different results. Thus, the influence of the nonlinear models and input parameters should be studied in depth to ensure the reliability of the nonlinear analysis and techniques.

5.2 Conclusions

Based on the study on the seismic input mechanism as presented in Chapter 3, the following conclusions are made.

- The modified deconvolution procedure reproduces the free-field ground motion more accurately than the existing procedure. The exiting procedure does not converge on many occasions, especially, for high frequency ground motions. On the other hand, the proposed modified procedure for deconvolution provides better convergence.
- The modified deconvolution procedure can efficiently perform deconvolution for both high and low frequency ground motions.
- Quality of the deconvolution procedure affects the performance of seismic evaluation.
- Among various models of dam-foundation systems, the one with foundation mass and deconvolved seismic input motions (i.e., Model C) provides the most rational and accurate model where spatial variation in ground motion can be easily accounted for.
- Model B, where the free-field ground motion is applied directly at the dam-foundation interface, does not yield appropriate response for irregular geometries as the spatial variation of ground motion cannot be accounted for in this model.

- Model A, where the foundation mass is ignored may not produce realistic response unless special care is taken to artificially adjust other parameters like foundation damping.

Based on the study on the evaluation of the guidelines for seismic evaluation as presented in Chapter 4, the following conclusions are made.

- The elastic and inelastic analyses provide generally consistent results with respect to existing guidelines.
- Based on the two inelastic models (damage plasticity, and extended FEM using fracture mechanics), different numerical models induce slight differences in the results relating to the tensile damage in dam foundation system. However, the results are consistent with each other.
- The present study on the influence of the different numerical models and input parameters on the response of dam-foundation systems is still limited in scope, and they should be studied in further detail.

5.3 Future research and developments

Following are few points regarding to the future research and development

- Development of non-uniform ground motions for dams derived through mathematical modeling and experimental testing and their performance in 3D representation in case of free-field input model.
- More detailed analysis including the material nonlinearities and dynamic uplift is required.

REFERENCES

Alves, S. (2004). *Nonlinear analysis of Pacoima Dam with spatially-uniform ground motion, Report No. EERL 2004-11.* Calif. Inst. of Tech., Pasadena, California.

Ayari, M. and Saouma, V. (1990). A fracture mechanics based seismic analysis of concrete gravity dams using discrete cracks. *Engineering Fracture Mechanics*, , Volume 35, Issues 1-3, 1990, Pages 587-598, ISSN 0013-7944, 10.1016/0013-7944(90)90233-7.

Batta, V. and Pekau, O.A. (1996). Application of boundary element analysis for multiple seismic cracking in concrete gravity dams. *Earthquake Engineering & Structural Dynamics, 25*(1), 15-30.

Bayraktar, A., Türker, T., Akköse, M., and Ateş, S. (2009). The effect of reservoir length on seismic performance of gravity dams to near- and far-fault ground motions. *Natural Hazards*,Volume 52, Number 2, 257-275, DOI: 10.1007/s11069-009-9368-1

Belytschko, T. and Black, T. (1999). Elastic crack growth in finite elements with minimal remeshing. *International Journal for Numerical Methods in Engineering, 45*(5), 601-620.

Bhattacharjee, S. and Leger, P. (1993). Seismic cracking and energy dissipation in concrete gravity dams. *Earthquake Engineering & Structural Dynamics, 22*(11), 991-1007.

Bolt, B.A. and Cloud, W.K. (1974). Recorded Strong Motion on Hsinfengkiang Dam,China. *Bullentin of the Seismological Society of America*, 64,4.

Booth, E. D. (2006). *Earthquake design practice for buildings.* Thomas Telford Publishing, London.

Boughoufalah, M. (1988). *Earthquake Input Mechanisms for Dam-Foundation Interaction.* Montreal, Canada: Department of Civil Engineering and Applied Mechanics, McGill University.

BRE. (1991). *An Engineering Guide to Seismic Risk to Dam in the United Kingdom.* Building Regulation Establishment, BRE Report CI/SfB 187 (H16).

CDA. (2003). Dams in Canada (CD-Rom). *Canadian Dam Association.* Montréal, Québec.

CDA. (2007). *Dam safety guidelines.* Canadian Dam Association.

Chakrabarti, P. and Chopra, A. K. (1974). Hydrodynamic Effects in Earthquake Response of Gravity Dams. *Journal of the Structural Division, 100*(6), 1211-1224.

Chopra, A.K., and Chakrabarti, P. (1971). *The Koyna Earthquake of December 11, 1967 and the performance of Koyna Dam.* California: Earthquake Engineering Reserach Center, University of California, Berkely, EERC 71-1.

Chopra, A. K. and Gupta S. (1982). Hydrodynamic and foundation interaction effects in frequency response functions for concrete gravity dams. *Earthquake Engineering & Structural Dynamics, 10*(1), 89-106.

Chopra, A. K. (2008). Earthquake Analysis of Arch Dams: Factors to be considered. *The Fourteenth World Conference on Earthquake Engineering.* Beijing,China.

Chopra, A. K., and Wang, J.-T. (2010). Earthquake response of arch dams to spatially varying ground motion. *Earthquake Engineering & Structural Dynamics, 39*(8), 887-906.

Chuhan, Z., Feng, J. and Pekau, O.A. (1995). Time domain procedure of FE-BE-IBE coupling for seismic interaction of arch dams and canyons. *Earthquake Engineering & Structural Dynamics, 24*(12), 1651-1666.

Chuhan, Z., Jianwen, P., and Jinting, W. (2009). Influence of seismic input mechanisms and radiation damping on arch dam response. *Soil Dynamics and Earthquake Engineering, 29*(9), 1282-1293.

Clough, R.W. and Chopra, A.K. (1977). Earthquake response analysis of concrete dams. *Structural and geotechnical mechanics*, Prentice-Hall.

Clough, R. W. (1980). Nonlinear mechanisms in the seismic response of arch dams. (pp. 669-684).*Proc., Int. Research Conf. on Earthquake Engineering, Skopje, Yugoslavia.*

Clough, R., Chang, K., Chen, H. Q. and Ghanaat, Y. (1985). *Dynamic Interaction effects in arch dams.* Earthquake Engineering Reserach Center, UCB/EERC-85-11.

Cohen, M. (1980). *Silent boundary methods for transient wave analysis.* PhD, 1981: PB-82-201831,California Institute of Technology.

Cooley, J. W., and Tukey, J. W. (1965). An Algorithm for the Machine Computation of the Complex Fourier Series. *Mathematics of Computation, 19*, 297-301.

Cooley, J., Lewis, P., and Welch, P. (1967). Application of the fast Fourier transform to computation of Fourier integrals. *IEEE Trans. Audio and Electroacoustics*, 79-84.

FEMA-65 (2005). *Federal Guidelines for Dam Safety: Earthquake Analyses and Design of Dams.* Federal Emergency Management Agency.

Fenves, G. and Chopra, A.K. (1985). Effects of reservoir bottom absorption and dam-water-foundation rock interaction on frequency response functions for concrete gravity dams. *13*(1), 13-31.

FERC. (1999). *Engineering Guidelines for the Evaluation of Hydropower Projects, Chapter 11, Arch Dams.* Federal Energy Regulatory Commission, Office of Energy Projects.

FERC. (2002). *Engineering Guidelines for the Evaluation of Hydropower Porjects, Chapter 3, Concrete Gravity Dams.* Federal Engergy Regulatory Commission, Office of Engergy Projects.

Ghanaat, Y. (2004). Failure modes approach to safety evaluation of dams. *Thirteen World Conference on Earthquake Engineering*, (p. 1115). Vancouver, B.C., Canada.

Ghrib, F., Lupien, R., Veineux, M., Léger, P., and Tinawi, R. (1995). A Progressive methodology for seismic safety evaluation of gravity dams. *Canadian Dam Association Conference*, (p. 83). Banff.

Gupta, R. L., Bajpai, O. N., and Alagh, P.K, (2009). Lower Siang H.E. Project -(9x 300 MW), India. *The International Journal on Hydropower & Dams.* Lyon, France.

Hall, J.F. (1996). *Efficient nonlinear seismic analysis of arch dams, user's manual for SCADA (Smeared Crack Arch Dam Anslysis), Report No. EERL 96-01.* Pasadena,CA: Earthquake Engineering Reserach Laboratory, California Institute of Technology.

Hall, J. F. (1988). The Dynamic and Earthquake behaviour of Concrete Dams: review of experimental behaviour and observation evidence. *Soil dynamic and earthquake engineering, 7*.

PoLam, I. , Law,H. and Yang, C.T. (2007). *Modeling of Seismic Wave Scattering on Pile Groups and Caissons, Technical Report MCEER-07-0017.* MCEER, University at Buffalo, The State University of New York.

ICOD. (1974). *Lessons from Dam Incidents.* Paris: International Commission on Large Dams.

ICOLD. (1986). *Earthqukae analysis for dams, Bulletin 52, Paris.* International Commission on Large Dams.

Idriss, I. M., & Sun, J. I. (1992). *User's manual for SHAKE91: a computer program for conducting equivalent linear seismic response analyses of horizontally layered soil deposits.* Davis, CA: Program modified based on the original SHAKE program published in December 1972 by Schnabel, Lysmer and Seed. University of California, Davis.

Abaqus Inc. (2011). *Abaqus Theory Manual, Version 6.11.* Abaqus Inc.

JSCE. (1999). *The 1999 Chi Chi Earthquake, Taiwan Investigation into the damage to civil engineering structures.* Japan Society of Civil Engineers.

Lee, J., and Fenves, G. (1998). Plastic-Damage Model for Cyclic Loading of Concrete Structures. *Journal of Engineering Mechanics, 124*, 892-900.

Léger, P. and Boughoufalah, M. (1989). Earthquake input mechanisms for time-domain analysis of dam—foundation systems. *Engineering Structures, 11*(1), 37-46.

Lubliner, J., Oliver, J., Oller, S., and Onate, E. (1989). A Plastic-Damage Model for Concrete. *International Journal of Solids and Structures, 25*, 229-326.

Liang, H., Bailey, C., and Dreese, T. (2011). Stability evaluation of leftmost power-unit monoliths of the Three Gorges Dam. *31st Annual USSD Conference.* San Diego, California: U.S. Society of Dams.

Luk, V., Spencer, B., Lann, I., and Dameron, R. (2005). *Parametric evaluation of seismic behavior of freestanding spent fuel dry cask storage systems,NUREG/CR-6865,SAND2004-5794P.* Washington, DC: Sandia National laboratories,Office of Nuclear Regulatory Reserach, U.S. Nuclear Regulatory Commission.

Lysmer J. and Kuhlemeyer. R. L. (1969). Finite dynamic model for infinite media. *Journal of the Engineering Mechanics Division(ASCE)*, 759-877.

Melenk, J. and Babuska, I. (1996). The Partition of Unity Finite Element Method: Basic Theory and Applications. *Computer Methods in Applied Mechanics and Engineering, 39*, 289-314.

Mojtahedi,S. and Fenves, G.L. (2000). *Effect of Conctraction Joint Opening on Pacoima Dam in the 1994 Northridge Earthquake.* California Department of Conservation.

Noble, C. R. and Nuss, L.K. (2004). *Nonlinear Seismic Analysis of Morrow Point Dam, UCRL-TR-202545.* Structural and Applied Mechanics Group, Lwarence Livermore National Laboratory.

Pekau, O. A., Lingmin, F. and Chuhan, Z. (1995). Seismic fracture of koyna dam: Case study. *Earthquake Engineering & Structural Dynamics, 24*(1), 15-33.

Reimer, R. B. (1973). *Deconvolution of seismic response for linear systems.* UCB/EERC-73/10, Earthquake Engineering Research Center, University of California, Berkeley.

Schnabel, P. B., Lysmer, J., and Seed, H. B. (1972). *SHAKE: a computer program for earthquake response analysis of horizontally layered sites.* UCB/EERC-72/12,Earthquake Engineering Research Center, University of California, Berkeley.

Tan, H. and Chopra A.K. (1995). Earthquake analysis of arch dams including dam-water-foundation rock interaction. *Earthquake Engineering & Structural Dynamics, 24*(11), 1453-1474.

USACE. (1995). *Engineering and design, gravity dams. Em 1110-2-2200.* US Army Corp of Engineers.

USACE. (2003). *Time-History Dynamic Analysis of Concrete Hydraulic Structures,EM 1110-2-6051.* US Army Corps of Engineers.

USACE. (2007). *Earthquake Design and Evaluation of Concrete Hydraulic Structures, EM 1110-2-6053.* US Army Corps of Engineers.

USBR. (1987). *Deisgn of Small Dams, Third Edition.* United States Bureau of Reclamation, United States Department of the Interior.

USSD. (2000). *Observed Performance of Dams During Earthquakes,* Volume II. United States Society on Dams.

Wolf, J.P. (1986). A comparison of time-domain transmitting boundaries. *14*(4), 655-673.

APPENDIX A : DECONVOLVED GROUND MOTIONS FOR DAM FOUNDATION SYSTEM, G-1

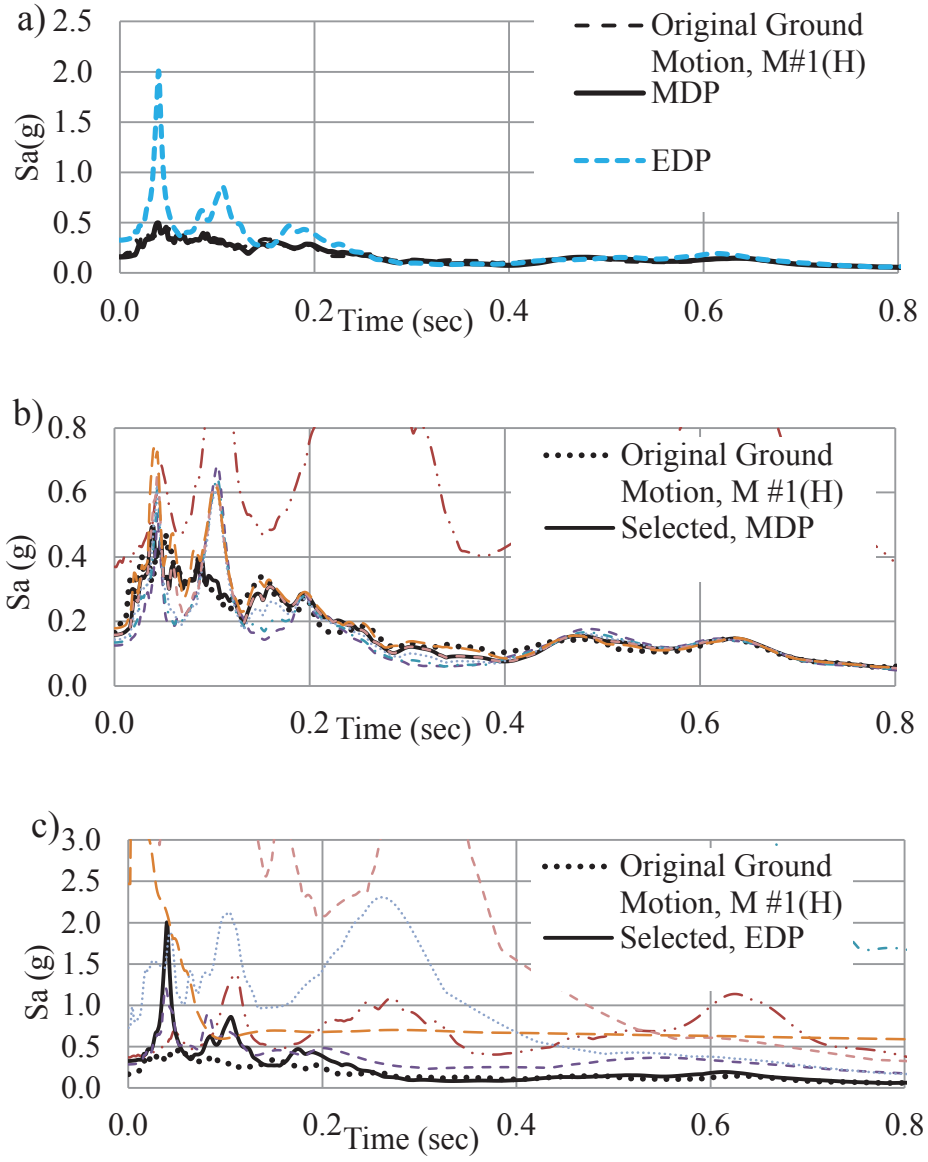

Figure A.1 Deconvolved ground motions: a) Original Ground Motion, M #1(H) with modified (MDP) and existing deconvolution procedure (EDP); b) M #1(H) with selected MDP and rest of iterations; c) M #1(H) with selected EDP and rest of iterations

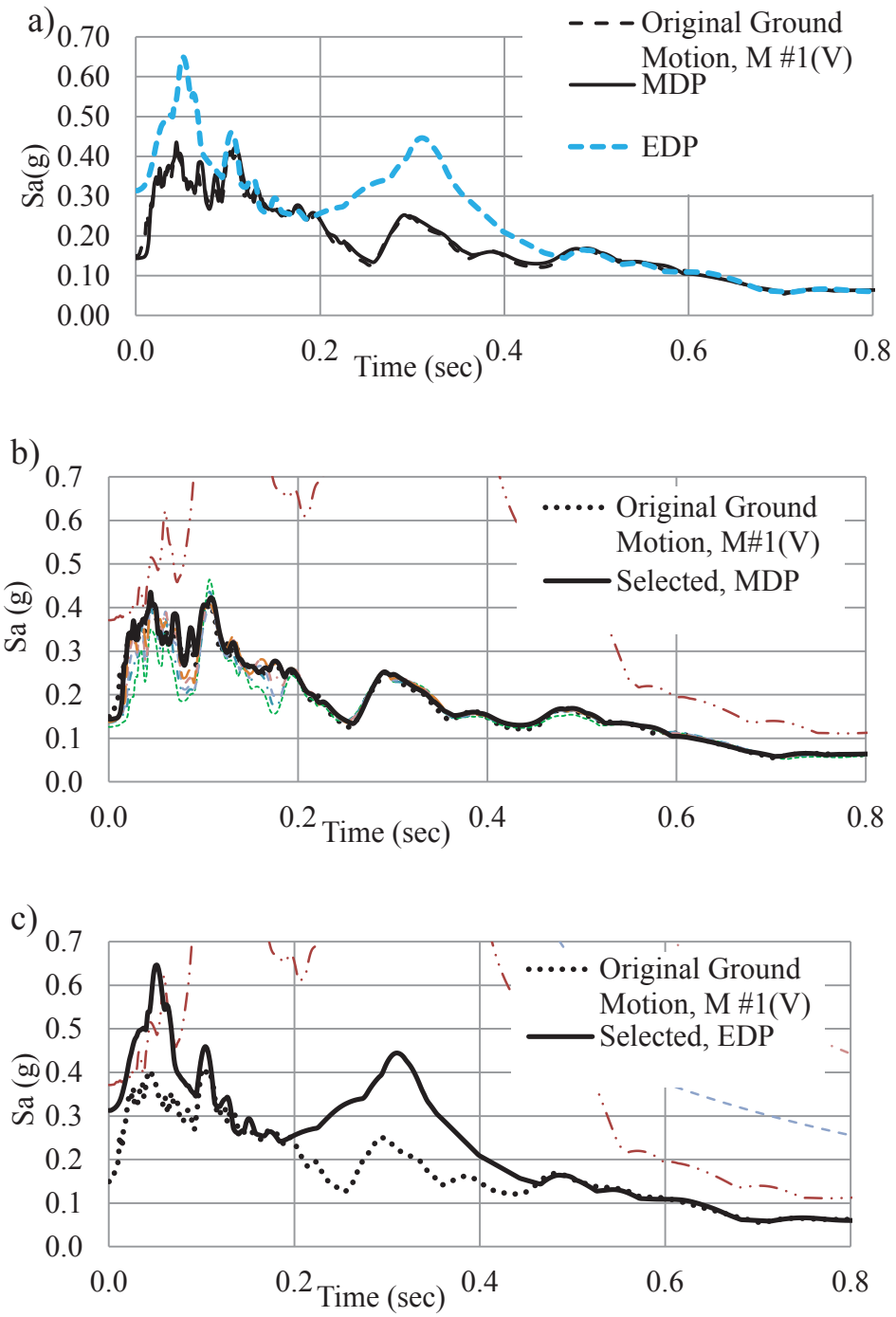

Figure A.2 Deconvolved ground motions: a) Original Ground Motion, M #1(V) with modified (MDP) and existing deconvolution procedure (EDP); b) M #1(V) with selected MDP and rest of iterations; c) M #1(V) with selected EDP and rest of iterations.

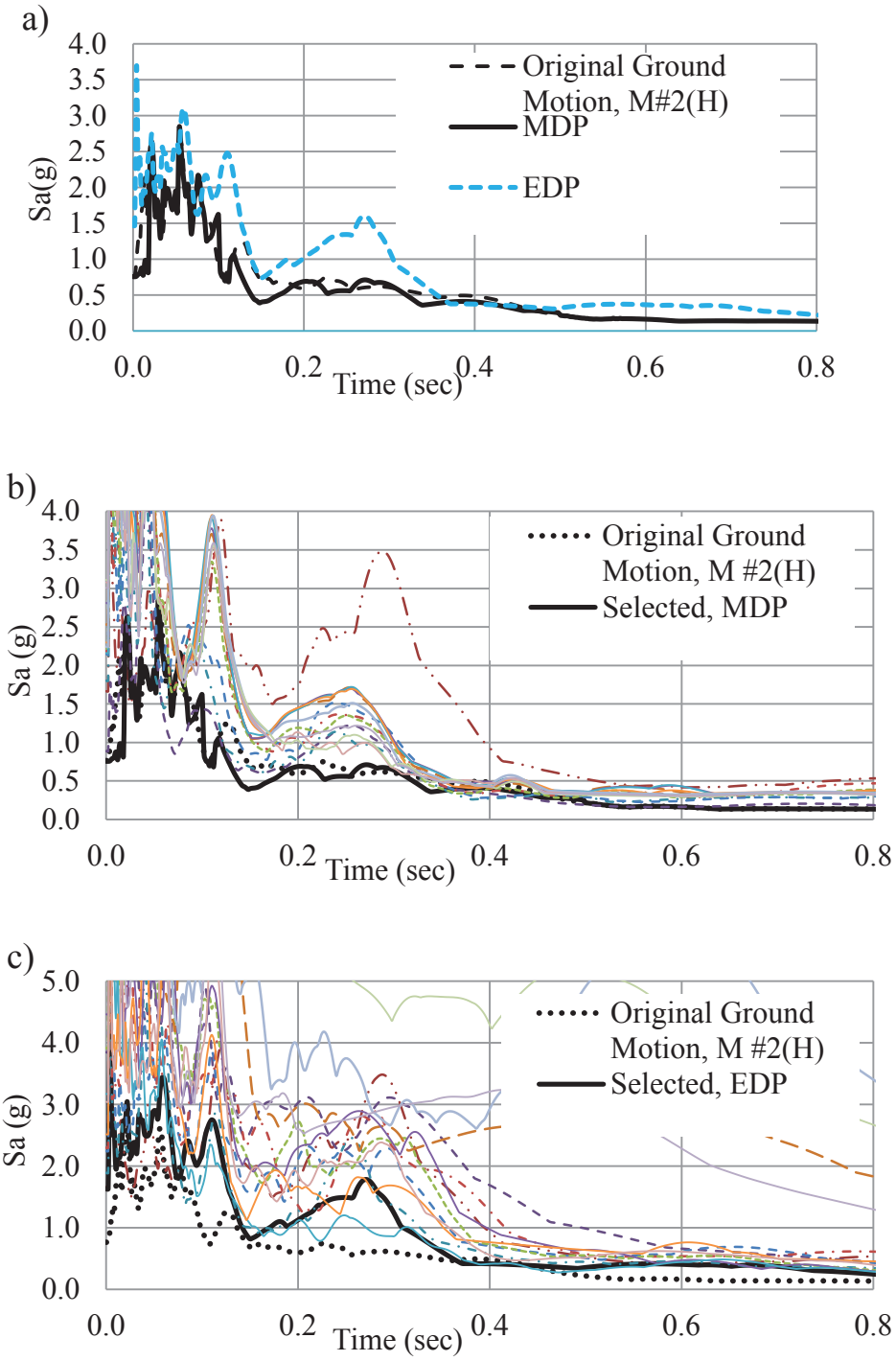

Figure A.3 Deconvolved ground motions: a) Original Ground Motion, M #2(H) with modified (MDP) and existing deconvolution procedure (EDP); b) M #2(H) with selected MDP and rest of iterations; c) M #2(H) with selected EDP and rest of iterations.

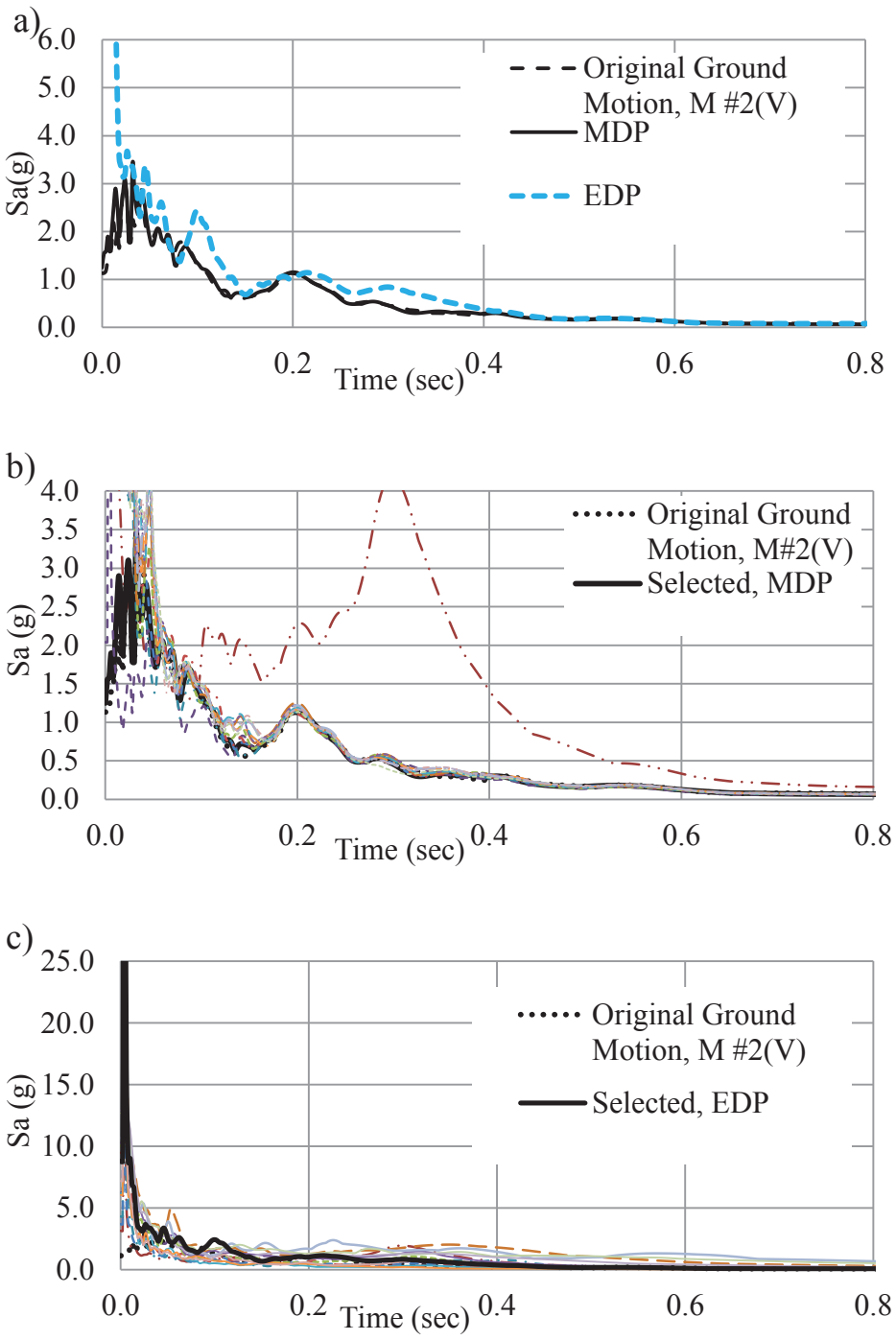

Figure A.4 Deconvolved ground motions: a) Original Ground Motion, M #2(V) with modified (MDP) and existing deconvolution procedure (EDP); b) M #2(V) with selected MDP and rest of iterations; c) M #2(V) with selected EDP and rest of iterations.

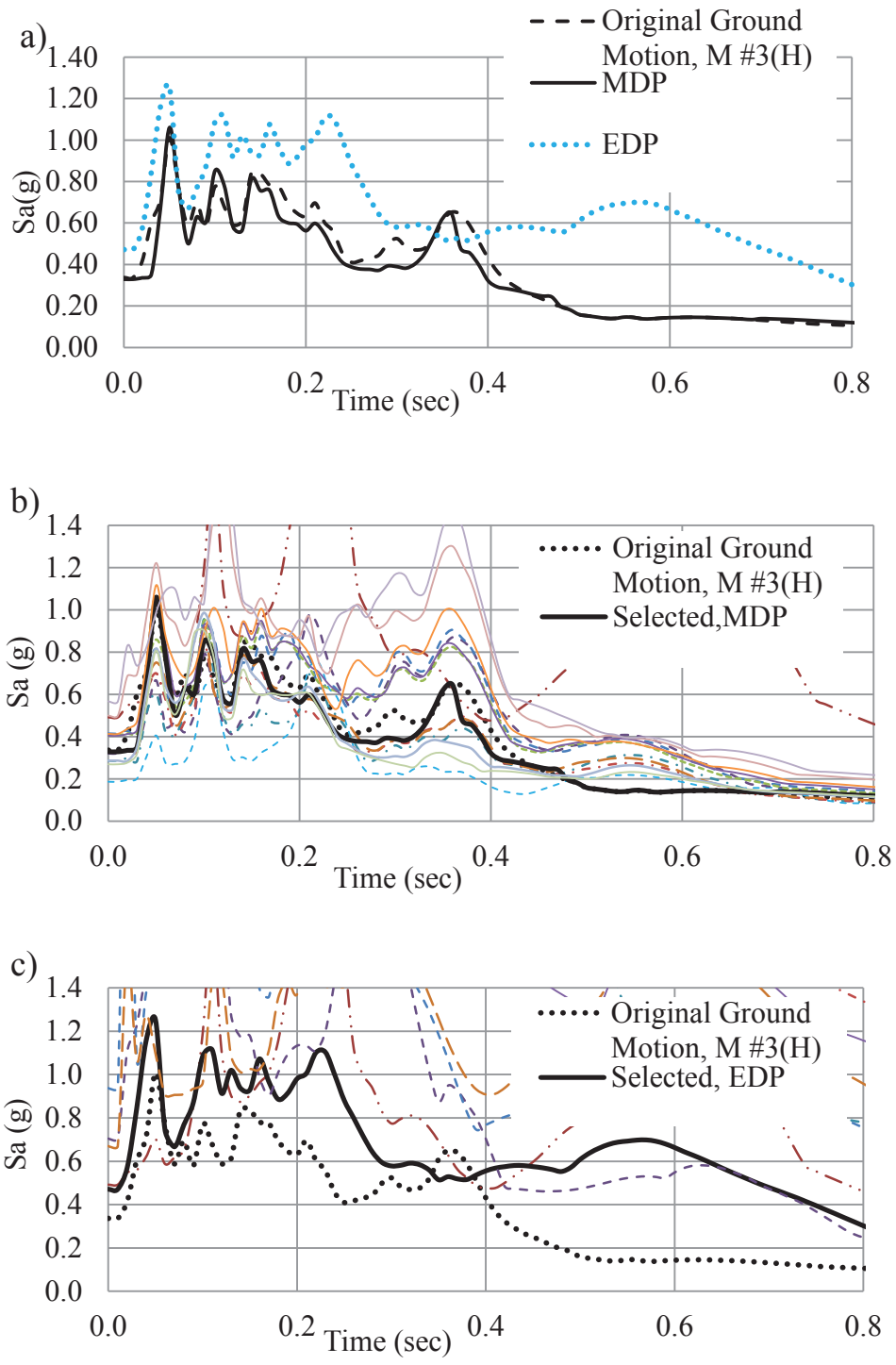

Figure A.5 Deconvolved ground motions: a) Original Ground Motion, M #3(H) with modified (MDP) and existing deconvolution procedure (EDP); b) M #3(H) with selected MDP and rest of iterations; c) M #3(H) with selected EDP and rest of iterations.

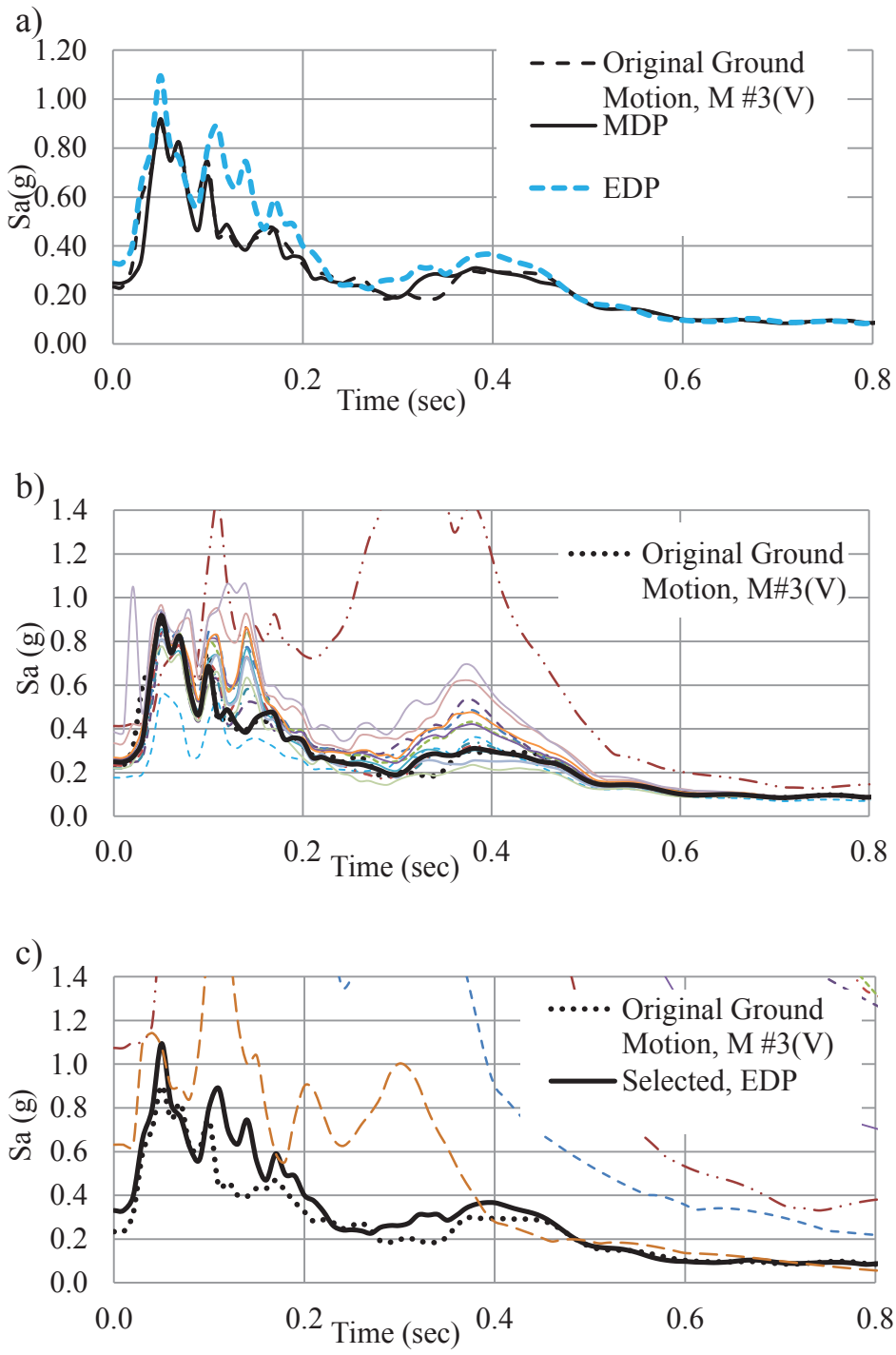

Figure A.6 Deconvolved ground motions: a) Original Ground Motion, M #3(V) with modified (MDP) and existing deconvolution procedure (EDP); b) M #3(V) with selected MDP and rest of iterations; c) M #3(V) with selected EDP and rest of iterations.

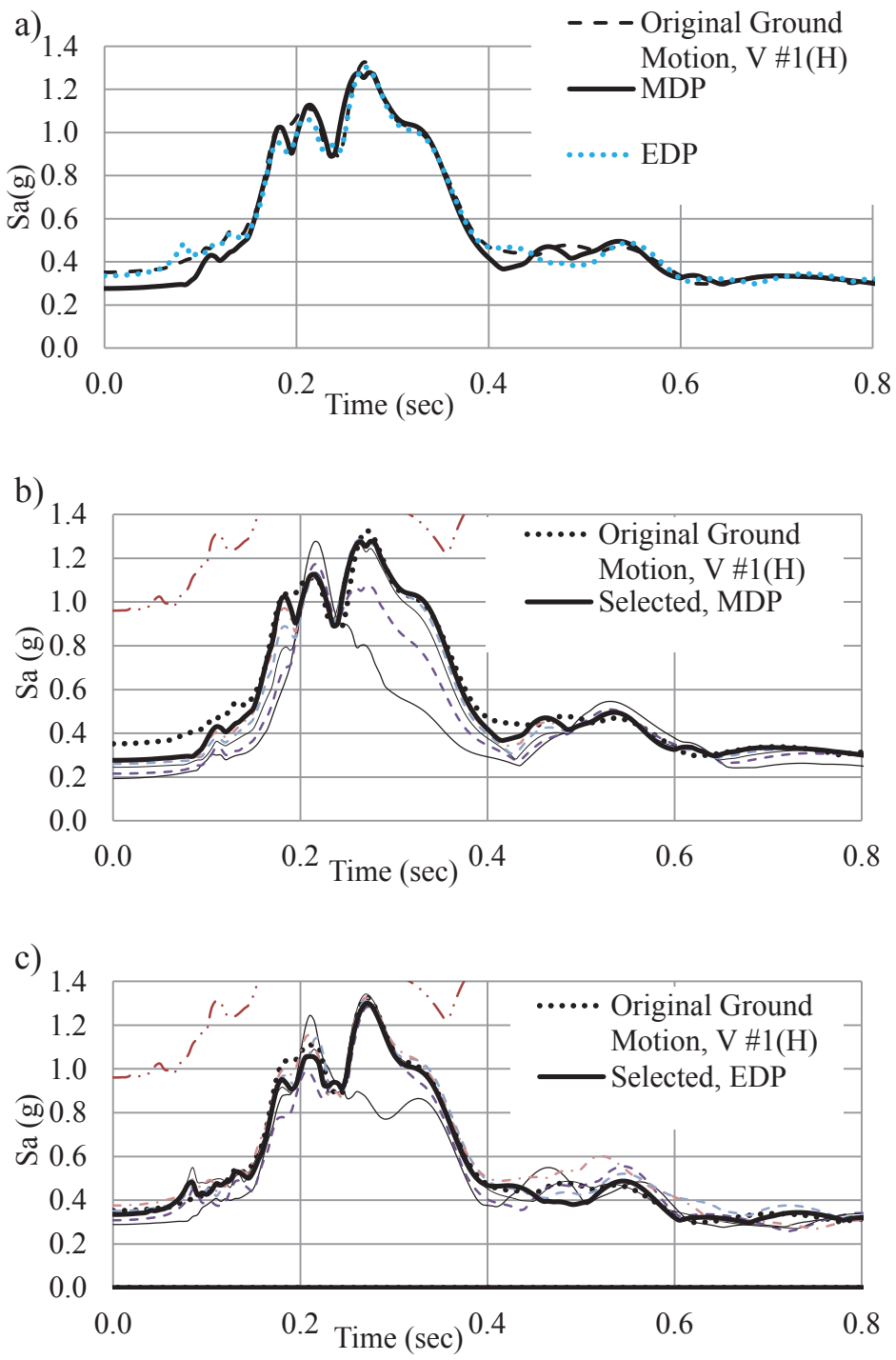

Figure A.7 Deconvolved ground motions: a) Original Ground Motion, V #1(H) with modified (MDP) and existing deconvolution procedure (EDP); b) V #1(H) with selected MDP and rest of iterations; c) V #1(H) with selected EDP and rest of iterations.

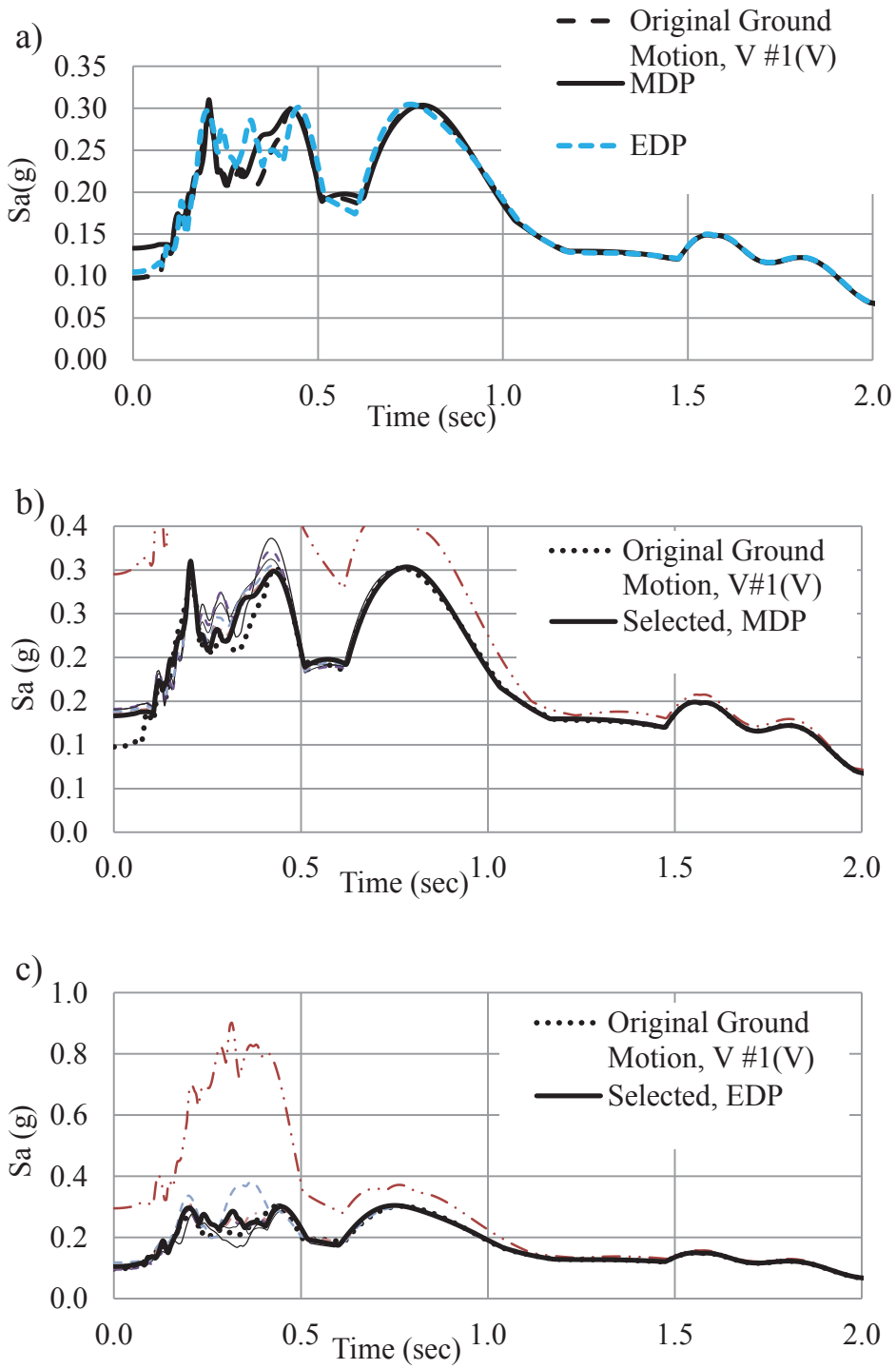

Figure A.8 Deconvolved ground motions: a) Original Ground Motion, V #1(V) with modified (MDP) and existing deconvolution procedure (EDP); b) V #1(V) with selected MDP and rest of iterations; c) V #1(V) with selected EDP and rest of iterations.

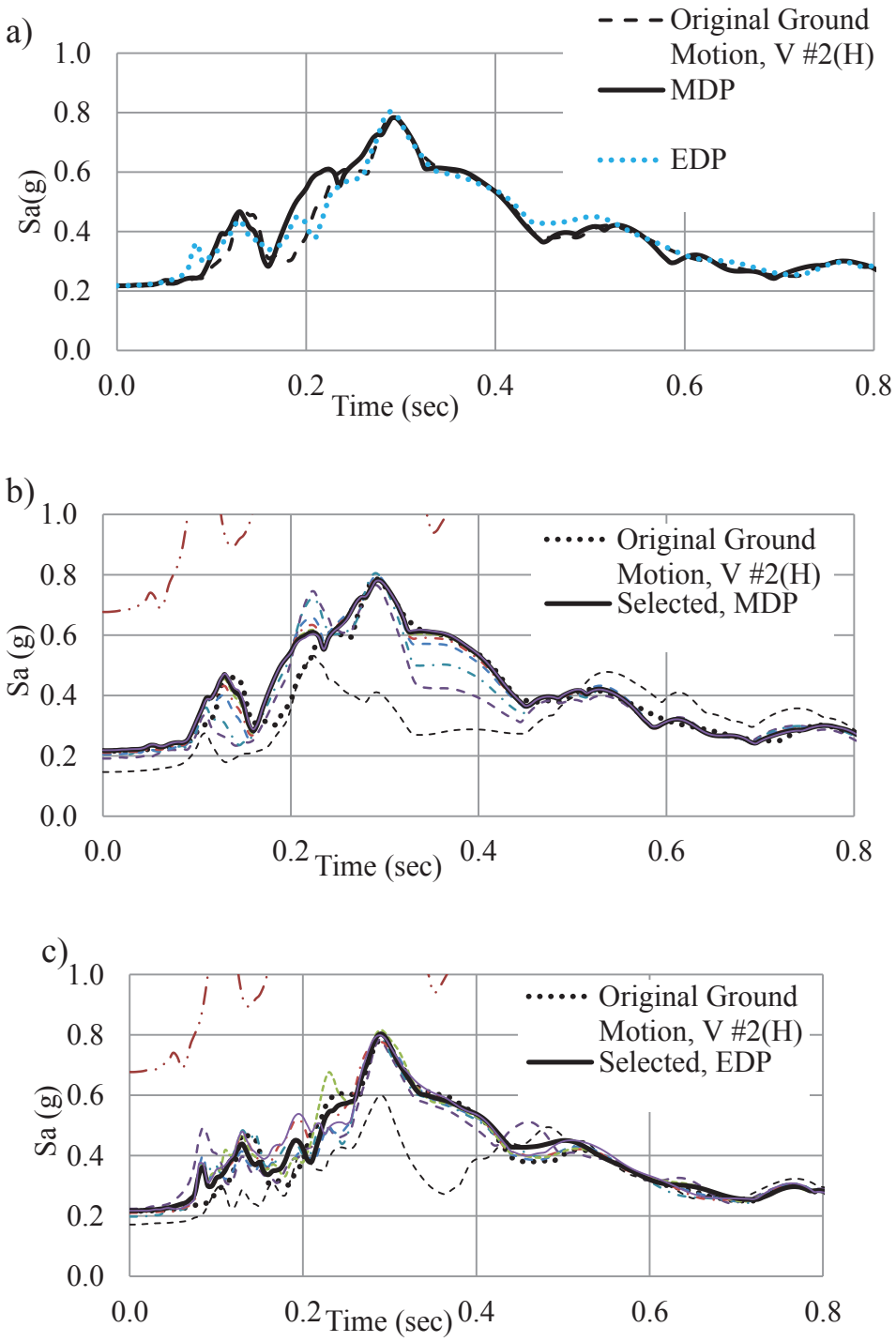

Figure A.9 Deconvolved ground motions: a) Original Ground Motion, V #2(H) with modified (MDP) and existing deconvolution procedure (EDP); b) V #2(H) with selected MDP and rest of iterations; c) V #2(H) with selected EDP and rest of iterations.

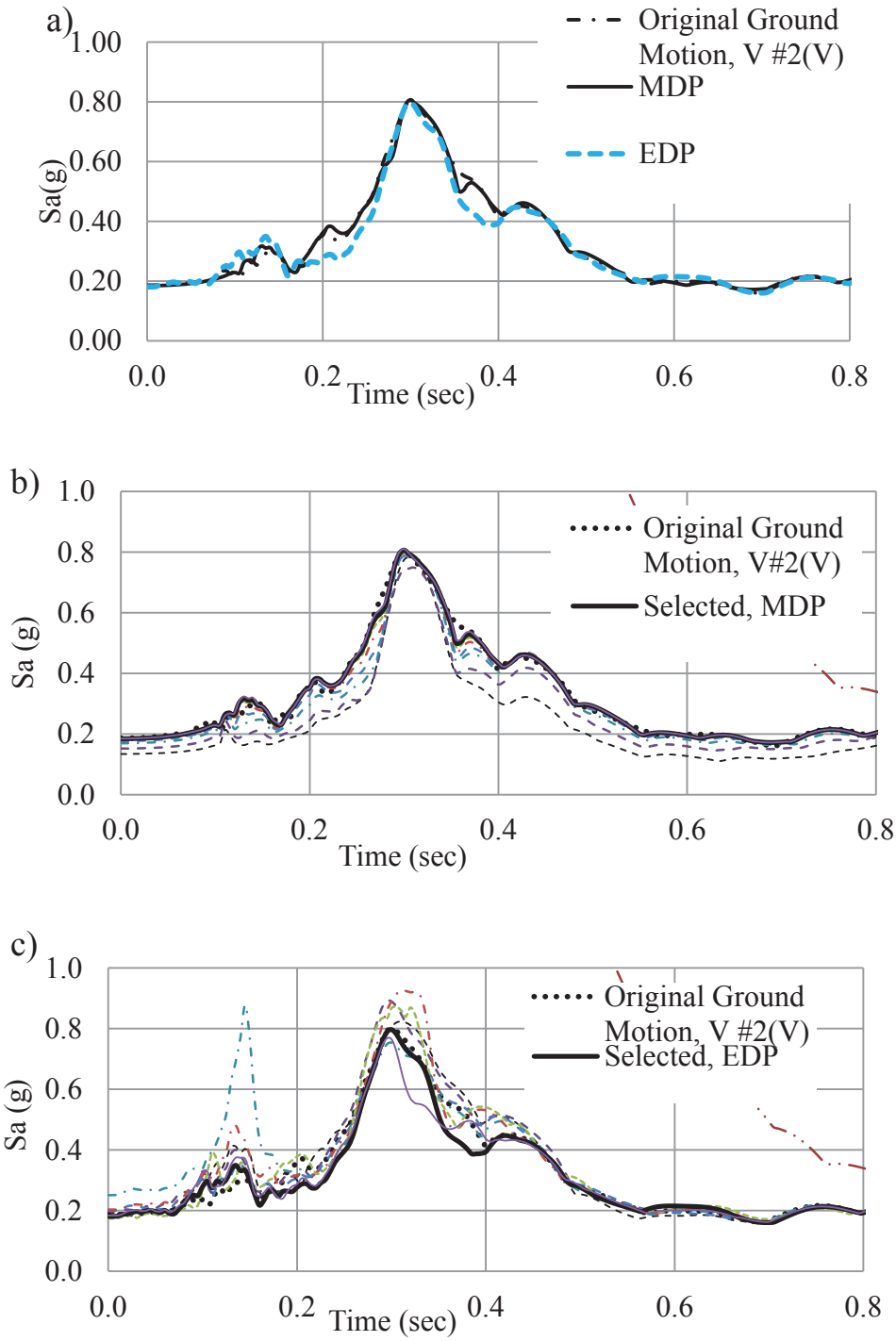

Figure A.10 Deconvolved ground motions: a) Original Ground Motion, V #2(V) with modified (MDP) and existing deconvolution procedure (EDP); b) V #2(V) with selected MDP and rest of iterations; c) V #2(V) with selected EDP and rest of iterations.

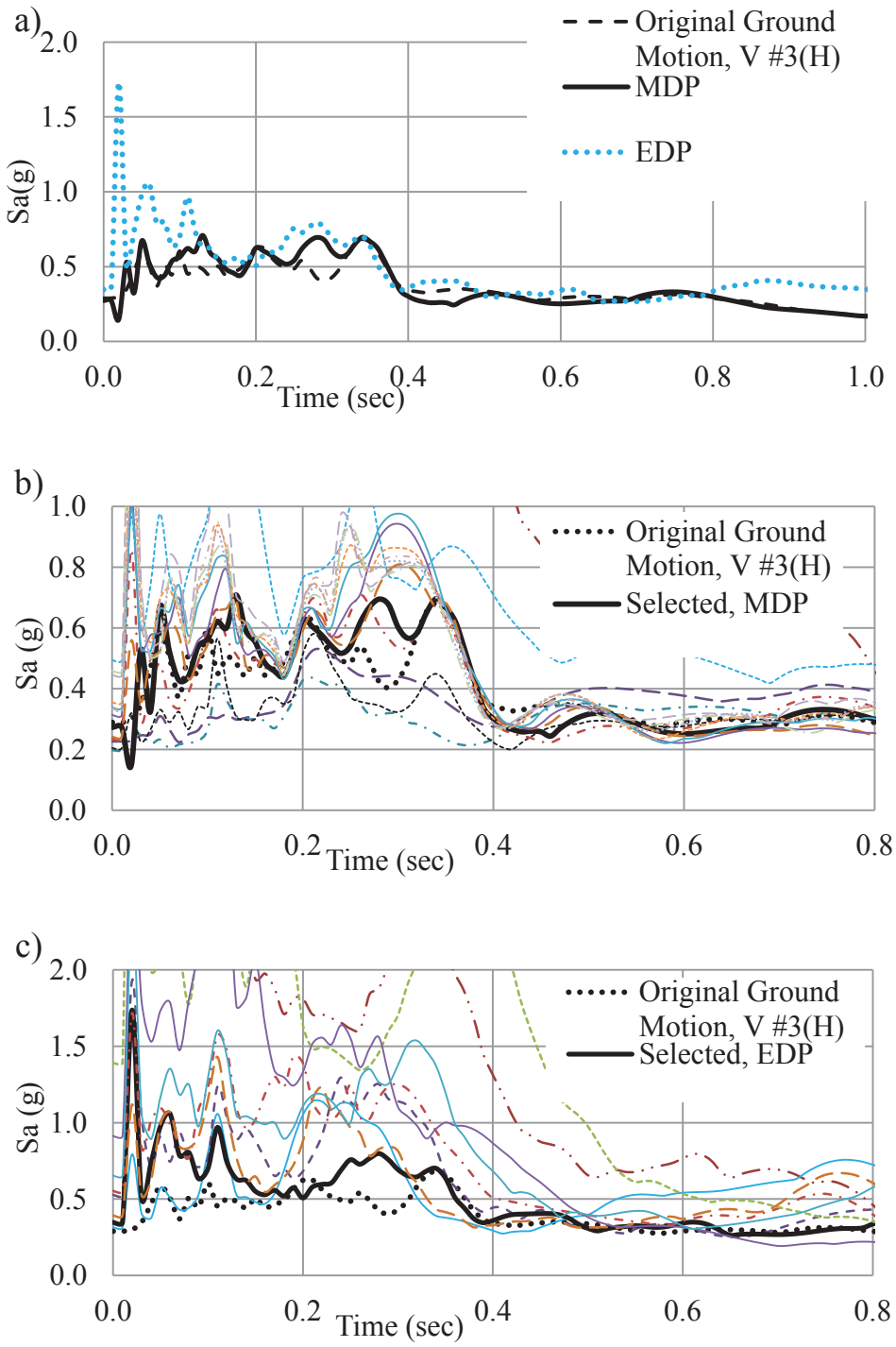

Figure A.11 Deconvolved ground motions: a) Original Ground Motion, V #3(H) with modified (MDP) and existing deconvolution procedure (EDP); b) V #3(H) with selected MDP and rest of iterations; c) V #3(H) with selected EDP and rest of iterations.

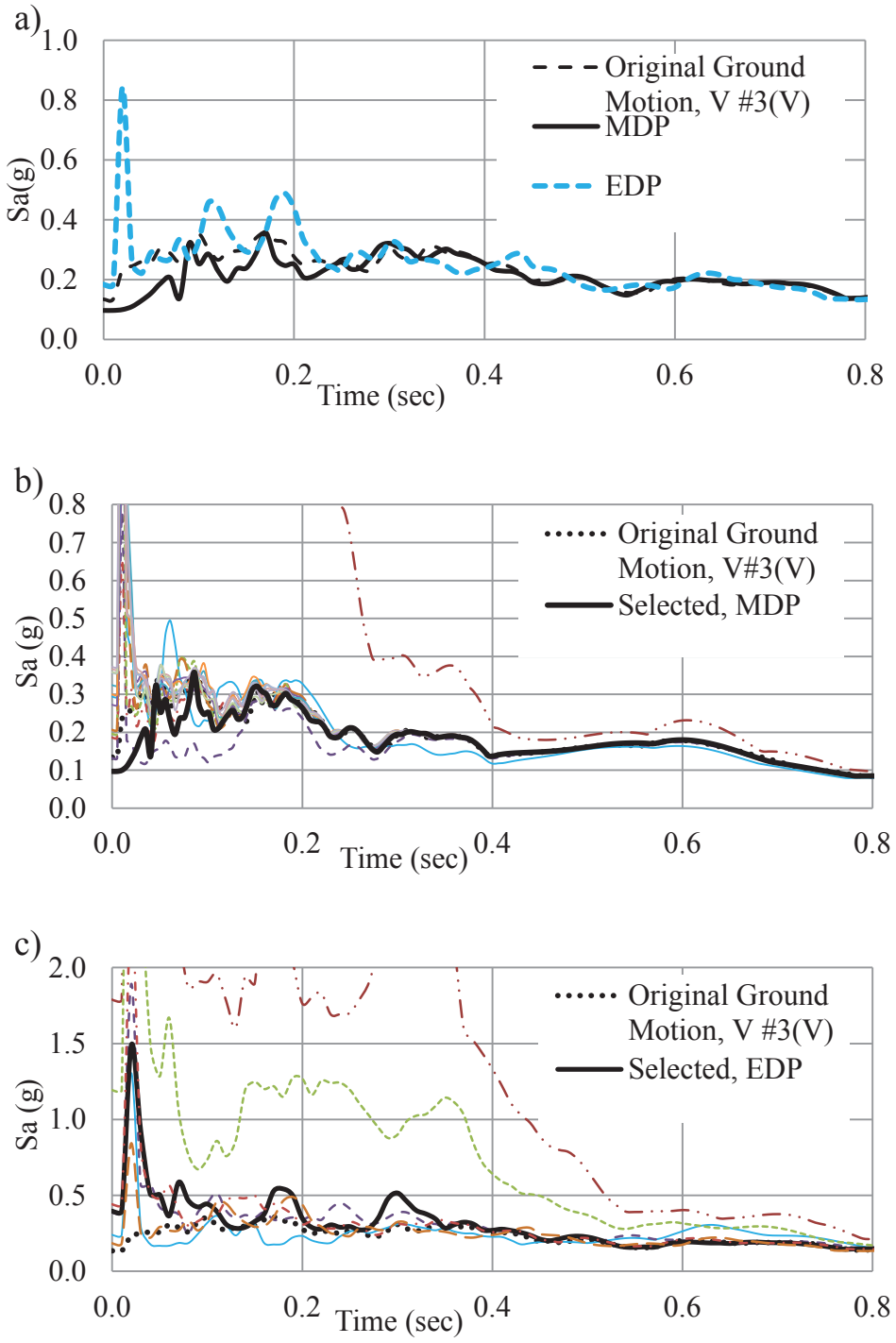

Figure A.12 Deconvolved ground motions: a) Original Ground Motion, V #3(V) with modified (MDP) and existing deconvolution procedure (EDP); b) V #3(V) with selected MDP and rest of iterations; c) V #3(V) with selected EDP and rest of iterations.

APPENDIX B : DECONVOLVED GROUND MOTIONS FOR DAM FOUNDATION SYSTEM, G-2

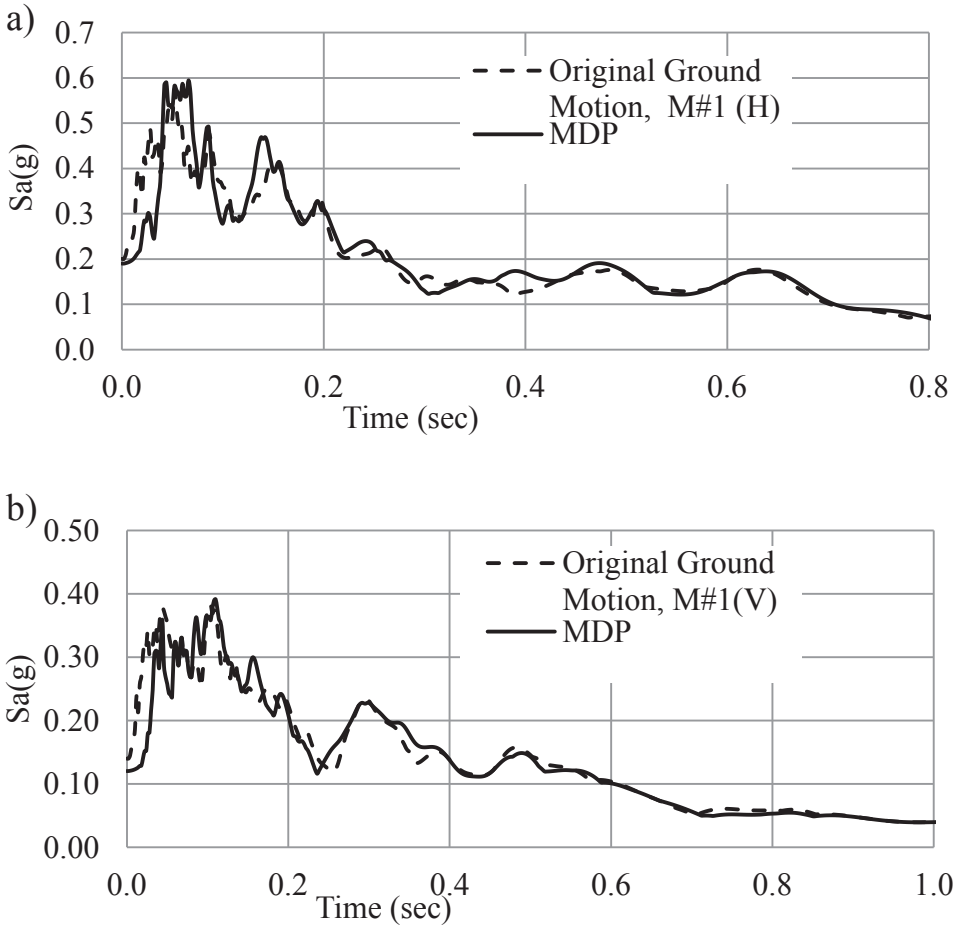

Figure B.1 Deconvolved ground motions: a) Original Ground Motion, M #1(H) with modified deconvolution procedure (MDP); b) Original Ground Motion, M #1(V) with modified deconvolution procedure (MDP).

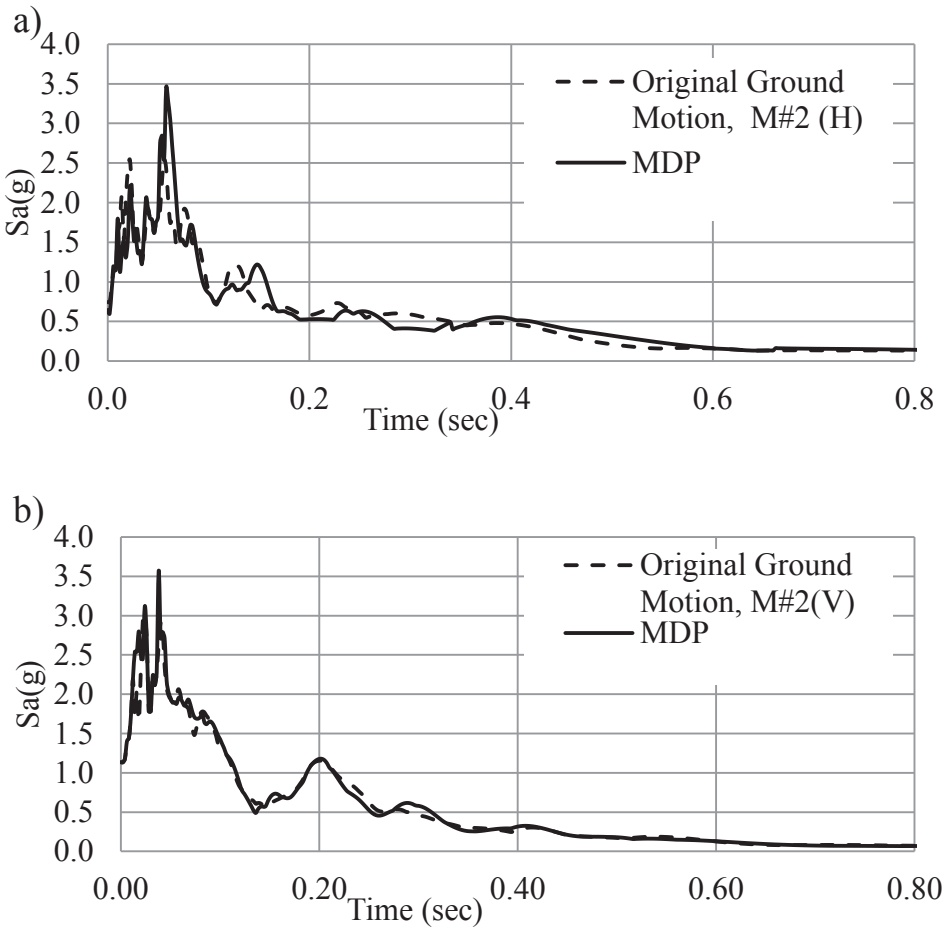

Figure B.2 Deconvolved ground motions: a) Original Ground Motion, M #2(H) with modified deconvolution procedure (MDP); b) Original Ground Motion, M #2(V) with modified deconvolution procedure (MDP).

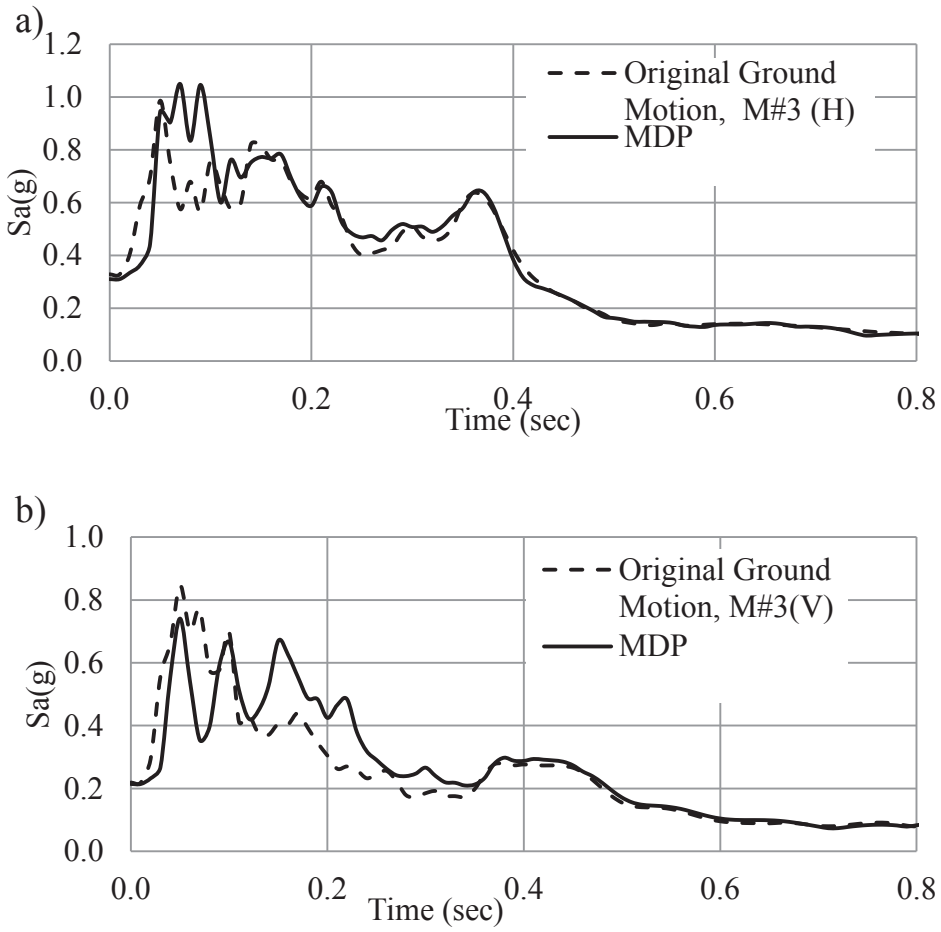

Figure B.3 Deconvolved ground motions: a) Original Ground Motion, M #3(H) with modified deconvolution procedure (MDP); b) Original Ground Motion, M #3(V) with modified deconvolution procedure (MDP).

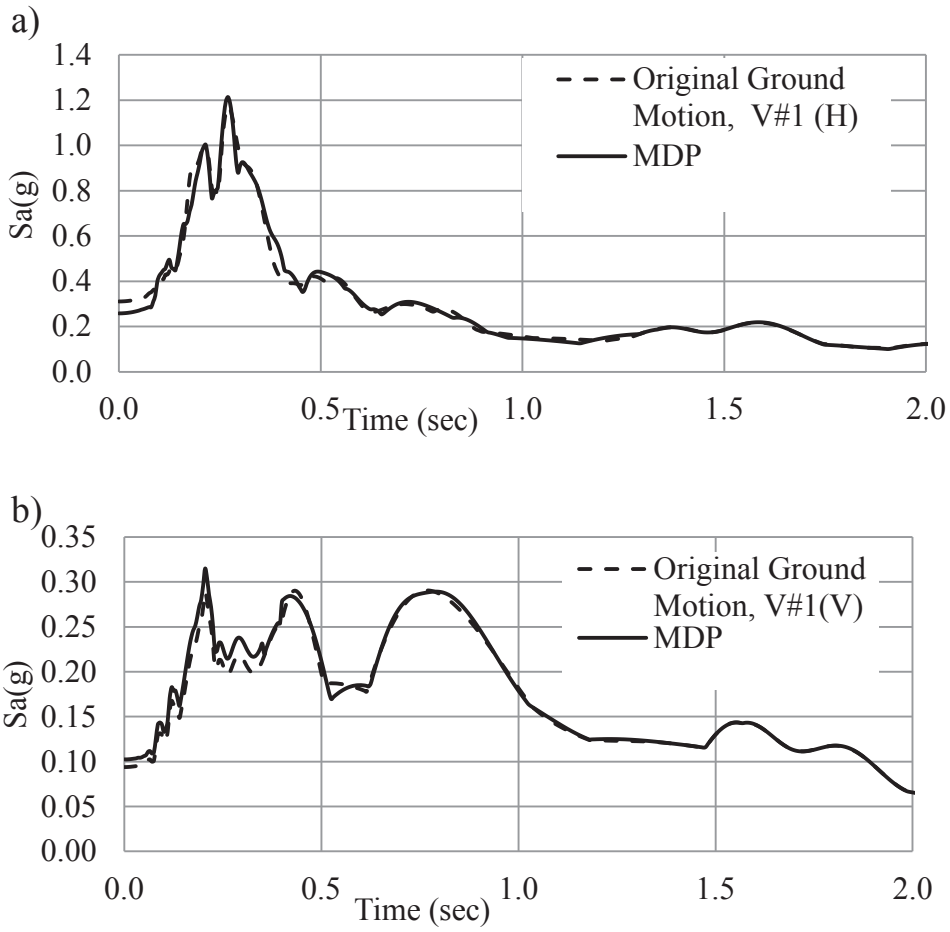

Figure B.4 Deconvolved ground motions: a) Original Ground Motion, V #1(H) with modified deconvolution procedure (MDP); b) Original Ground Motion, V #1(V) with modified deconvolution procedure (MDP).

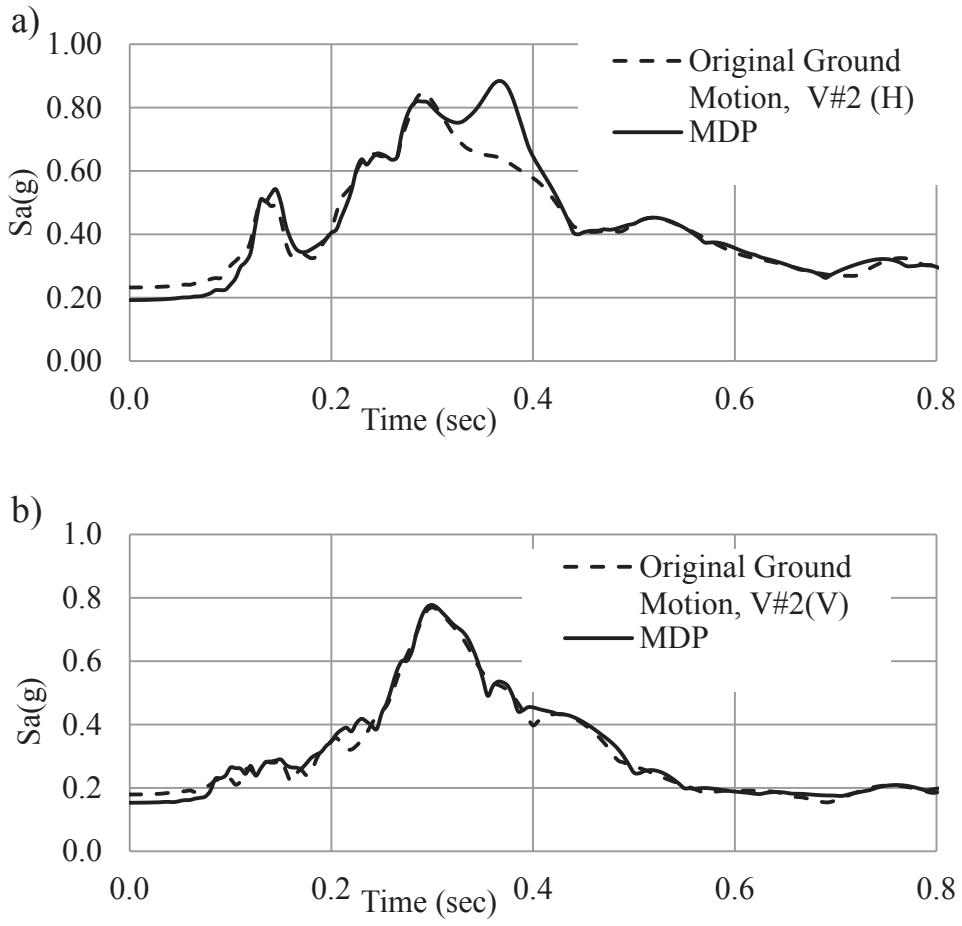

Figure B.5 Deconvolved ground motions: a) Original Ground Motion, V #2(H) with modified deconvolution procedure (MDP); b) Original Ground Motion, V #2(V) with modified deconvolution procedure (MDP).

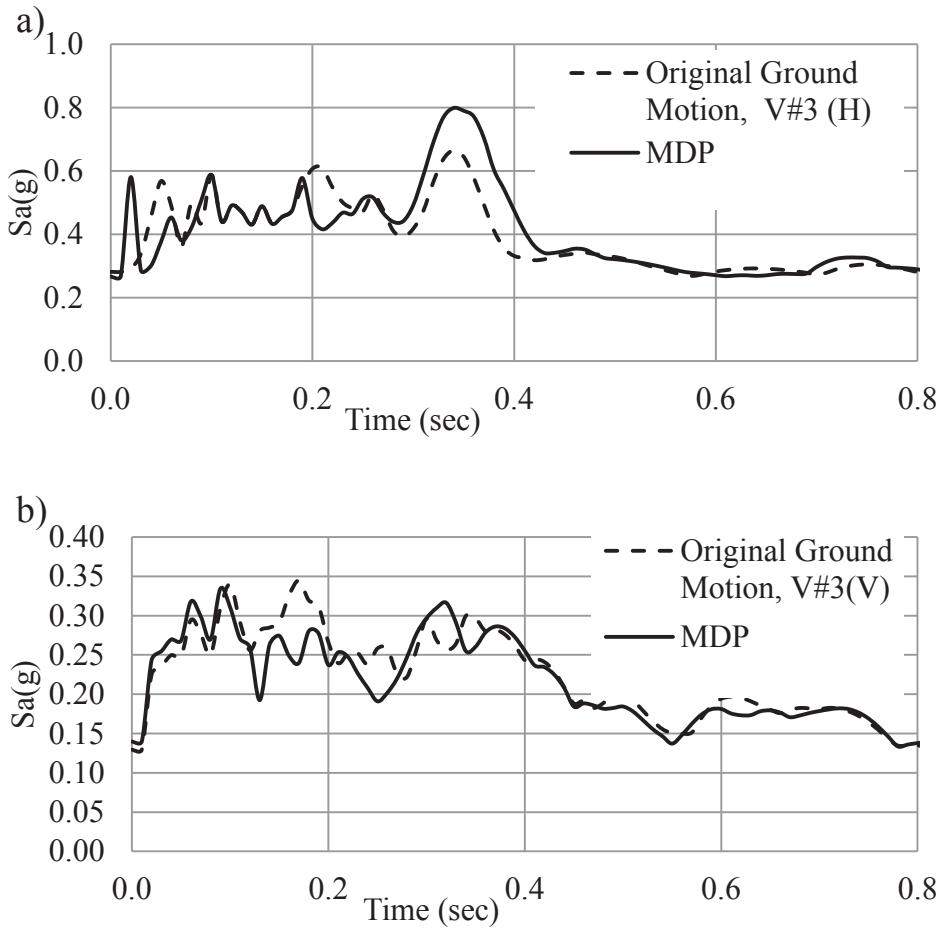

Figure B.6 Deconvolved ground motions: a) Original Ground Motion, V #3(H) with modified deconvolution procedure (MDP); b) Original Ground Motion, V #3(V) with modified deconvolution procedure (MDP).